UNIVERSITÀ
DI SIENA
1240

Dipartimento di Biotecnologie Mediche

Dottorato in Biotecnologie Mediche

38° Ciclo

Coordinatore: Prof. Francesco Iannelli

Evaluation of Piperazine-Based Compounds Against Flaviviruses and SARS-CoV-2, and *In Vitro*/*In Vivo* Selection of Benchmark Antivirals Against SARS-CoV-2

Candidato/a

Ilenia Varasi

Dipartimento di Biotecnologie Mediche

Firma digitale del/della candidato/a

Supervisore

Ilaria Vicenti

Dipartimento di Biotecnologie Mediche

Firmato digitalmente da Ilenia Varasi
Data: 26.03.2026 15:13:06 CET

Co-supervisore/i

Maurizio Zazzi

Dipartimento di Biotecnologie Mediche

Anno accademico di conseguimento del titolo di Dottore di ricerca

2024/25

INDEX:

1 My PhD activities

I began my PhD in Medical Biotechnologies at the University of Siena in 2023, continuing in the same institution where I had completed my Master's degree. My research took place at the Laboratory of Microbiology and Virology within the Department of Medical Biotechnologies, a department with a long-standing tradition in infectious disease research. Since 1990, it has housed the HIV Monitoring Laboratory which started as a public health service and gradually evolved into a hub for HIV research. In recent years, the lab expanded its focus to include emerging and re-emerging flaviviruses like Dengue, West Nile, and Zika viruses. When the COVID-19 pandemic hit, much of our work naturally shifted toward understanding SARS-CoV-2.

My PhD research centered largely on antiviral drug discovery, and I was fortunate to participate in several collaborative projects at the regional, national, and international levels. One of my first major involvements was in the APICE project (Antibodies and Peptides Inhibiting Coronavirus Entry), funded by the Tuscany Region. The goal was to develop entry inhibitors against SARS-CoV-2, and my role focused on testing phage-display derived peptides that targeted the viral Spike protein. Using cytotoxicity and live-virus assays, I evaluated whether these peptides could block viral entry into cells. Around the same time, I also joined TUSCAVIR.NET, another regional initiative aimed at building a strategic antiviral research platform to support Tuscany's healthcare system during and beyond the pandemic.

What really expanded my scientific horizons was an international collaboration with the Department of Organic and Medicinal Chemistry at the University of Seville. They were synthesizing novel piperazine-based compounds, and I was responsible for screening them against flaviviruses (Zika and Dengue) and SARS-CoV-2 using live-virus cell-based assays. This work was incredibly rewarding because several compounds showed genuine promise. Compound 21, for instance, inhibited both ZIKV and SARS-CoV-2, while compounds 6, 10, 12, and 13 demonstrated potent activity against ZIKV and DENV, with IC_{50} values that matched or even surpassed Sofosbuvir. These results were exciting because effective treatments for flaviviruses remain scarce, and broad-spectrum antivirals are desperately needed. I had the chance to present this work at the 52nd National Congress of the Italian Society for Microbiology in Pavia and at the INF-ACT meeting in 2024. But the highlight was definitely the 7th Innovative Approaches for Identification of Antiviral Agents Summer School in Pula, Sardinia, where I gave an oral presentation. That week was transformative, both scientifically and personally.

I also became involved in the AVITHRAPID consortium, an EU-funded initiative focused on developing broad-spectrum antivirals to tackle current and future pandemics. As part of Work Package 1, I evaluated the cytotoxicity and antiviral activity of compounds synthesized by partner institutions, testing them against

DENV, ZIKV, and WNV. The goal was to identify the most promising candidates for in vivo testing in the next phase of the project.

Through the INF-ACT consortium (Antiviral Strategies against Emerging Infectious Diseases), I contributed to the characterization of host-targeted antiviral compounds against multiple viral pathogens. I evaluated candidate small molecules targeting the ESCRT cellular machinery (specifically TSG101, Alix, and Nedd4 domains) for their potential anti-HIV activity using bicycle cell-to-cell transmission assays in H9 and TZM-bl cells. Unfortunately, about half of the compounds turned out to be highly cytotoxic with no antiviral effect. It was a reminder that not every experiment yields positive results, but that's part of the process. In parallel, I tested a different series of compounds against flaviviruses. While none were active against WNV or DENV, several showed promising activity specifically against ZIKV, with IC_{50} values ranging from 4.95 to 27.16 µM and selectivity indices up to 40. These results were encouraging and suggested that some of these molecules might be worth developing further.

Beyond drug discovery, a significant portion of my PhD involved monitoring SARS-CoV-2 evolution, particularly how the virus escapes immune responses and antiviral treatments. This work was split across two projects: EuCARE and ICOVA. In EuCARE, I investigated the neutralizing antibody response to the emerging Omicron subvariant BA.2.86 compared to the ancestral B.1 lineage. We studied a cohort of healthcare workers with different vaccination and infection histories. Using live-virus neutralization assays, we found that most individuals with multiple vaccine doses still developed detectable antibodies against BA.2.86, though titers were generally lower than those against B.1. This suggested that prior immunity continues to offer some level of protection, even against divergent variants. I presented these findings at the 16th ICAR Conference in Rome and at the 8th National Congress of the Italian Society for Virology in Bologna.

The ICOVA project (Impact of SARS-CoV-2 Variability on Antiviral Agents) was particularly engaging because it combined clinical and laboratory work. The goal was to detect potential resistance to monoclonal antibodies and direct-acting antivirals (DAAs) in treated patients. We analyzed paired nasopharyngeal swabs collected before and after treatment with either Remdesivir or Nirmatrelvir in hospitalized patients. Through genomic sequencing and *in vitro* experiments, we looked for resistance-associated mutations and assessed the genetic barrier to resistance in both the ancestral B.1 strain and the more recent Omicron KP.3 variant. While resistance was rare in patients, our *in vitro* resistance selection studies revealed that KP.3 was more resilient to drug pressure than B.1. However, combining Remdesivir and Nirmatrelvir effectively suppressed viral replication in both variants, suggesting that dual DAA therapy could be a valuable strategy to prevent resistance. I presented this work as an oral communication at the 23rd European Meeting on HIV & Hepatitis in Barcelona and at ICAR 2025 in Padua, and we're currently preparing the manuscript for publication.

Finally, I had the opportunity to collaborate with the University of Milan and Pio Albergo Trivulzio, Italy's largest long-term care facility, which resulted in my first first-author publication. We assessed the neutralizing

antibody response in a highly vulnerable population: SARS-CoV-2-naïve long-term care residents who had received four doses of the monovalent BNT162b2 mRNA vaccine. Using live-virus microneutralization assays, we measured their antibody responses against multiple predominant Omicron sublineages. To our knowledge, this was the first study of its kind in this specific population. While previous research had focused on clinical outcomes or breakthrough infections, our work provided direct serological evidence of humoral immune responses in this fragile group (Varasi *et al*., 2023). It was deeply meaningful to contribute data that could inform vaccination strategies for some of society's most vulnerable individuals.

2 INTRODUCTION

2.1 Arboviruses

Arthropod-borne viruses (arboviruses) are a diverse group of pathogens transmitted by hematophagous arthropods vectors such as mosquitoes, ticks, flies, and biting midges (Barzon, 2018; Brès, 2018; Sick *et al*., 2019). Although arbovirus transmission is most intense in tropical regions, infections also occur in temperate areas, albeit at lower rates. Environmental factors, including climate change, urbanization, and human migration, are altering the habitats and life cycles of arthropod vectors, thereby facilitating the geographical expansion of these viruses (Robert *et al*., 2020).

To date, over 500 arboviruses have been identified, and approximately 100 of those are recognized as human pathogens (Artsob *et al*., 2017; Brès, 2018). To survive, arboviruses must be able to replicate efficiently in both the arthropod vector and in the susceptible vertebrate hosts (mammals, birds, reptiles, and amphibians). Vertebrates with high viremia act as amplifying hosts, as they promote the propagation of the virus by infecting new vectors thereby maintaining the transmission cycle (Artsob *et al*., 2017)

Arboviruses are maintained in nature through different transmission cycles:

1) *Sylvatic (enzootic) cycle*: the virus circulates between wild animal reservoirs and arthropod vectors. Humans are not normally involved.
2) *Rural (epizootic) cycle*: domestic animals act as amplifying hosts, allowing the virus to circulate among them through vector transmission, with occasional spillover or reinfection events in humans.
3) *Urban (epidemic) cycle*: humans are the major reservoir, and peridomestic mosquitoes, particularly Aedes species, are the vectors able to transmit the virus among the population. (Artsob *et al.,* 2017; Brès, 2018; Weaver & Barrett, 2004) (Figure 1).

In some cases, animals or humans can be dead-end hosts, as they are infected but do not achieve sufficient viremia levels to infect new vectors (Artsob *et al*., 2017).

Transmission to a vertebrate host occurs when the virus reaches infectious titres in the salivary glands of the vector and is injected during blood feeding (Fong *et al*., 2018). After ingestion of viraemic blood, the virus migrates through the vector's digestive tract to the midgut, where it must avoid both physical and immune barriers (Artsob *et al*., 2017; Conway *et al*., 2014). Replication starts in the epithelial cells of the midgut, with subsequent spread to secondary tissues, and finally to the salivary glands, where the virus can be horizontally transmitted to new vertebrate hosts. In some cases, the virus can also infect the mosquito's reproductive tissues, which enables transmission from adult mosquitoes to their offspring (Artsob *et al*., 2017).

Most arboviruses that cause human disease belong to three main families: Togaviridae (genus *Alphavirus*), Flaviviridae (genus *Flavivirus*), and Bunyaviridae (genera *Bunyavirus*, *Orthobunyavirus*, *Nairovirus*, and *Phlebovirus*). Arboviruses from three additional families, *Rhabdoviridae*, *Orthomyxoviridae* and *Reoviridae* also cause human infections, though less frequently (Young, 2018).

***Figure 1**:The different arbovirus transmission cycles. Adapted from Cholleti et al. (2018).*

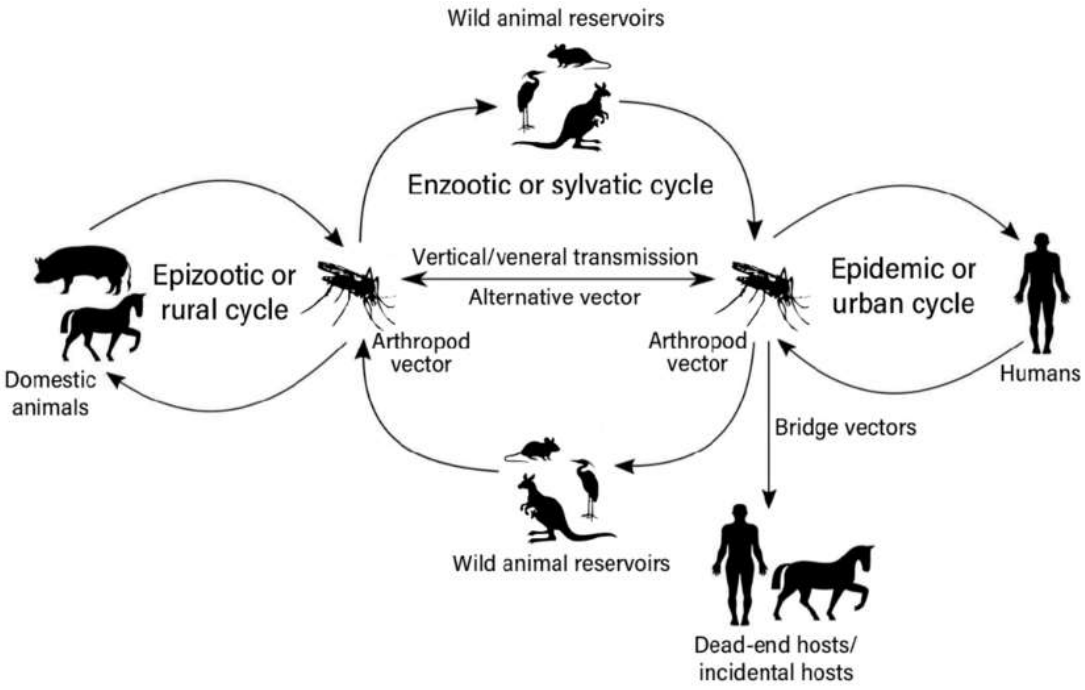

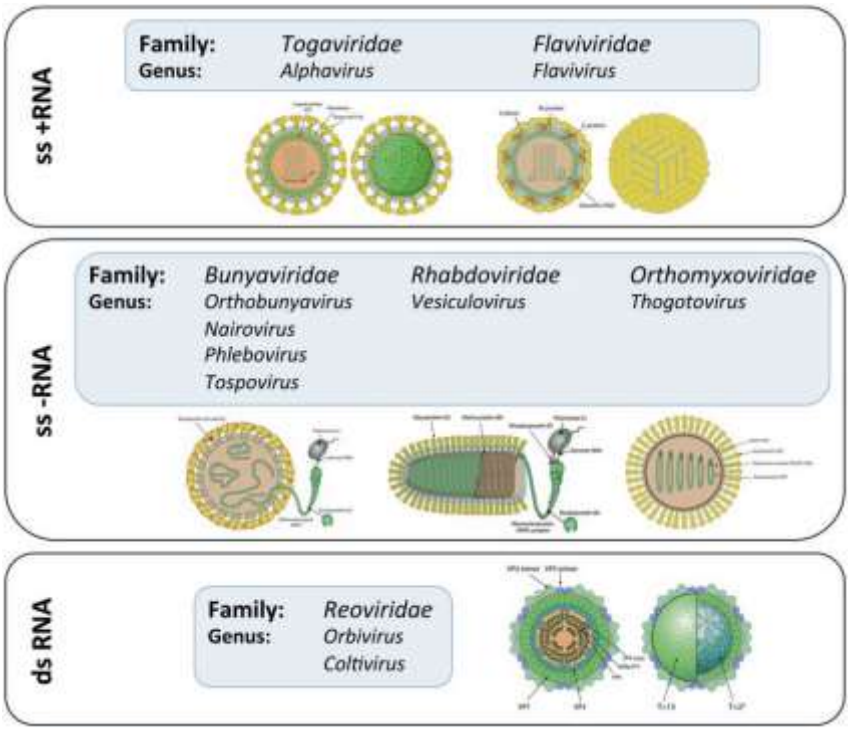

***Figure 2**: Biodiversity of arboviruses. Adapted from Young, 2018.*

Among them, flaviviruses are particularly important because of their wide geographical distribution, large number of human pathogens, and significant public health impact (Da Silva Queiroz *et al*.). Classic examples of them are Dengue virus (DENV), Zika virus (ZIKV), Yellow Fever virus (YFV), and West Nile virus (WNV). These viruses can cause enormous outbreaks and severe disease with a high mortality. Their primary vectors, *Aedes* mosquitoes (DENV, ZIKV) and *Culex* mosquitoes (WNV), are present in both tropics and temperate area, increasing the global risk of infection. Moreover, climate change and globalization have contributed to the expansion of their habitats, further increasing the risk of flavivirus transmission (Robert *et al*., 2020).

2.2 Flavivirus general overview and epidemiology

The Flaviviridae family comprises four distinct genera (Flavivirus, Hepacivirus, Pestivirus, and Pegivirus) of spherical, enveloped viruses with a non-segmented, positive-sense single-stranded RNA genome and an icosahedral capsid.

Flavivirus infections can be classified into two clinical phenotypes: viscerotropic, such as DENV and YFV, which cause systemic and haemorrhagic disease, and neurotropic, such as WNV and ZIKV, which can lead to severe neurological complications. Notably, ZIKV also exhibits a unique tropism for the reproductive tract, enabling sexual transmission and causing foetal malformations, of which microcephaly is a classic example (Liang & Dai, 2024).

DENV, WNV, ZIKV and YFV have emerged or over the past few decades as major human pathogens and continue to represent a persistent global threat to public health.

DENV is the most rapidly spreading mosquito-borne virus worldwide. It causes dengue fever, which has seen a dramatic rise in recent years. In 2024, more than 14.6 million cases and over 12,000 dengue-related deaths were reported globally, representing a historic high (World Health Organization [WHO], 2024). This represents a 2-fold increase compared to 2023 and a 12-fold rise compared to 2014 (WHO, 2024). Dengue is endemic in Southeast Asia and South Asia, where it creates substantial healthcare, economic, and social challenges. The Region of the Americas contributed significantly to the global burden, with over 13 million cases reported to WHO in 2024 (WHO, 2024). Dengue is spreading to new areas, including the European and Eastern Mediterranean regions, with 308 cases reported from three European countries (France, Italy and Spain) in 2024 (WHO, 2024). In Italy specifically, between 1 January and 23 September 2025, there were 166 confirmed dengue cases (162 travel-associated and 4 autochthonous), with no deaths (Istituto Superiore di Sanità [ISS], 2025a). Two distinct local transmission events were documented in the Emilia-Romagna and Veneto regions (ISS, 2025b). Predictive models suggest that climate change and urbanization will lead to further geographical spread. One modelling estimate indicates that 5.6 billion people are at risk of infection with dengue and other arboviruses (WHO, 2024), with estimates suggesting over 6 billion people could be at risk by 2080. Despite ongoing research, development of a dengue vaccine that is both safe and effective has been a major public health issue, with its long-term efficacy in endemic countries still uncertain (Liang & Dai, 2024).

ZIKV emerged as a public health threat in 2007 following an outbreak in Micronesia, which was succeeded by larger epidemics across the South Pacific and the Americas. In 2016, the Brazilian outbreak was declared a Public Health Emergency of International Concern by the World Health Organization (WHO), after infecting 440,000 to 1.3 million people. Although most infections are asymptomatic or mild, ZIKV epidemic raised concern due to the significant increase in cases of microcephaly and congenital Zika syndrome, both associated with high mortality rate. Currently, ZIKV transmission is largely confined to Latin America and the Caribbean, with sporadic cases reported elsewhere, however, climate models predict a potential expansion of ZIKV transmission zones into Europe, North America, and temperate Asia under future climate scenarios (Liang & Dai, 2024). In Europe, ZIKV sporadic travel-related cases continue to be reported. In 2024, Italy reported 7 imported Zika cases while from January 1 to September 23, 2025, Italy confirmed 4 Zika cases, all travel-associated with no deaths (ISS, 2025a).

WNV was first isolated in 1937 in Uganda (Smithburn *et a*l., 1940). For decades, human infections were uncommon and typically mild, occurring sporadically across Africa, the Middle East, Asia, and Australia. However, the situation changed in 1999, when a WNV strain caused a major outbreak in New York City, leading to severe neurological illness in several individuals and increased mortality among birds and horses. Following this event, WNV spread rapidly across North America and

subsequently became endemic in multiple continents, including Africa, Europe, Asia, North America, Australia, and the Middle East. In recent years, an increasing number of severe human cases have been reported (Clark & Schaefer, 2020; Pierson & Diamond, 2020;). In Europe, WNV has become an increasing concern. In 2024, approximately 1,200 annual cases were reported across Europe, with a focus in Mediterranean countries but also showing a spread to Germany and The Netherlands (Brüssow & Figuerola, 2025). In Italy, the ISS registered 460 cases of WNV infection in 2024, of which 272 were in the neuroinvasive form, with 20 deaths (ISS, 2025b). By September 3, 2025, Italy had confirmed 502 cases of WNV infection, including 226 neuroinvasive cases and 33 deaths, distributed across multiple regions including Piemonte, Lombardia, Veneto, Emilia-Romagna, Lazio, Campania, and Calabria (ISS, 2025b). To date, 9 WNV genetic lineages have been identified (Fall *et al*., 2017), of which lineages 1 and 2 are most frequently associated with human disease. Lineage 1 is further divided into three clades-1a, 1b, and 1c. Clade 1a isolates are distributed throughout Africa, Europe, the Middle East, and North America, while clade 1b, is found in Australia, and clade 1c includes isolates from India only (May *et al.* 2011). Lineage 1 strains are more likely to cause neuroinvasive disease, whereas lineage 2 strains, generally less virulent in humans, are mainly found in sub-Saharan Africa but have also been responsible for outbreaks in Central and Eastern Europe (Donadieu *et al*., 2013; Magurano *et al*., 2012).

2.3 Genome organization and structure

Flaviviruses are small (~50 nm) spherical virus particles containing a single-stranded RNA genome of positive-sense polarity that encoded three structural and seven non-structural proteins. The genome contains a single open reading frame (ORF) flanked by 5’ and 3’ untranslated regions (UTRs). The ORF encodes a large polyprotein (Figure 3) that is post-translationally cleaved by both host and viral proteases (Pierson & Diamond 2020). The 5’ UTR of flaviviruses is approximately 100 nucleotides in length (90-130 bp according to virus species) and contains a methyl-G-cap structure and two conserved stem-loop regions forming a secondary structure involved in regulating viral RNA synthesis and translation. The 3’ UTR varies in length (400–700 nucleotides) but contains conserved sequence motifs and RNA structural elements organized into three functional domains, which mediate interactions with both viral and host proteins (Ng *et al*., 2017).

The polyprotein is co- and post-translationally cleaved into three structural proteins, capsid (C), precursor membrane (prM), and envelope (E), located in the N-terminal region, and seven nonstructural (NS) proteins, NS1, NS2A, NS2B, NS3, NS4A, NS4B, and NS5, located in the C-terminal region. Although the NS proteins are not incorporated into the virion, they are essential for viral replication, assembly, protein processing, and immune evasion (Lindenbach *et al*., 2007; Morrison *et*

al., 2012; Laureti *et al*., 2018; Pierson & Diamond, 2020). The structural proteins form the virus particle and play a pivotal role in virus entry as well as assembly and release of progeny virions. The capsid protein binds the genomic RNA to form the nucleocapsid core, while the E and prM glycoproteins are viral surface proteins embedded in the host-derived lipid envelope. The non-structural proteins form the viral replication complex inside the host cell. NS3 and NS5 perform essential enzymatic functions: NS3 acts as a protease and helicase, whereas NS5 possesses RNA-dependent RNA polymerase and methyl/guanyltransferase activities. The remaining NS proteins primarily facilitate replication complex assembly and modulate host immune responses (Brand *et al*., 2017) [Figure 3].

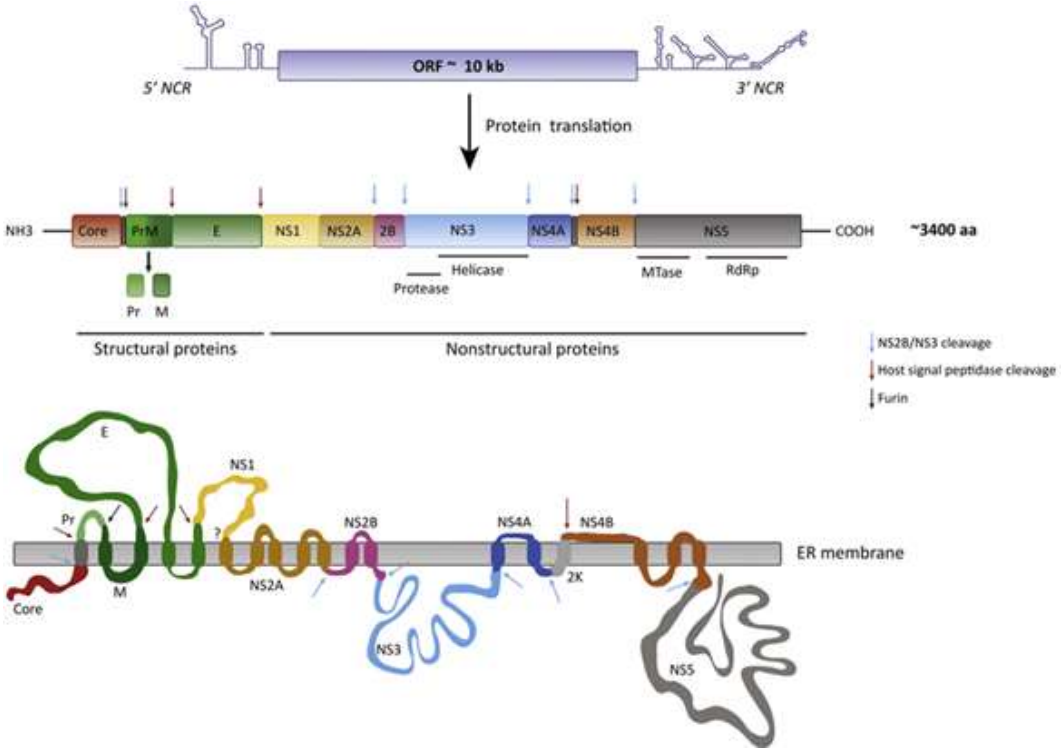

***Figure 3**: Genome organization and polyprotein of YFV as a flavivirus prototype. ORF, open reading frame; NCR, non-coding region (UTR). ER Membrane association of YFV proteins. Arrows indicate cleavage by different proteases. (Adapted from Elrefaey, 2019).*

2.4 Flavivirus replication cycle

The *flavivirus* replication cycle (Figure 4) occurs entirely within the cytoplasm of the infected cell and is closely associated with intracellular membranes, particularly those derived from the endoplasmic reticulum (ER) (Mukhopadhyay *et al.*, 2005). It begins when virions enter a susceptible cell, typically dermal fibroblasts, keratinocytes and Langerhans cells in the epidermis, via receptor-mediated endocytosis (Van Den Elsen *et al*., 2021). This process is initiated by interactions between the viral

surface E protein and the host receptor molecules (Neufeldt *et al*., 2018). Host protein receptors are essential for viral entry, catalyzing conformational changes that lead to membrane fusion. Additional surface molecules, known as attachment factors, facilitate virion binding to the host membrane but are insufficient on their own to induce the fusogenic conformational change (Pierson & Diamond, 2020). The best characterized attachment factor is the C-type lectin dendritic cell-specific ICAM-grabbing non-integrin (DC-SIGN), which is predominantly expressed on dermal macrophages and dendritic cells (Mukhopadhyay *et al*., 2005). Other attachment factors and receptors are highly sulfated glycosaminoglycans such as heparan sulphate proteoglycans, and TIM (T cell immunoglobulin and mucin domain) and TAM (TYRO3, AXL, and MER) family proteins. Following attachment, virions are internalized by clathrin-mediated endocytosis and transported to pre-lysosomal endocytic compartments. The acidic pH of this environment induces a major conformational change in the E protein, promoting fusion between the viral envelope and the endosomal membrane and thereby releasing the ribonucleocapsid into the cytoplasm (Van Den Elsen *et al*., 2021). Once in the cytoplasm, the nucleocapsid disassembles, releasing the viral RNA genome, which immediately serves as mRNA for translation. The capped, positive-sense RNA is translated by ribosomes on the rough endoplasmic reticulum (ER) into a membrane-associated polyprotein (Van Den Elsen *et al*., 2021). This polyprotein is subsequently cleaved by both host proteases (such as furin) and viral proteases, notably the NS3 protease, to yield the structural and non-structural viral proteins. The RdRp activity of NS5 initiates genome replication by synthesizing a full-length negative-sense RNA strand, which serves as a template to produce multiple positive-sense genomes. This process involves the formation of a double-stranded RNA intermediate, which is unwound by the NS3 helicase in coordination with NS5. Newly synthesized positive-sense RNA genomes are 5’ capped and methylated to generate a mature cap structure, enabling efficient translation and providing protection from exonucleolytic degradation.

Assembly begins when the capsid protein binds to the genomic RNA, forming the nucleocapsid, which subsequently buds into ER membranes containing the prM and E glycoproteins. These immature virions are transported through the secretory pathway in vesicles, where host furin-like proteases cleave prM to generate the mature M protein, thereby completing virion maturation. Finally, fully infectious virions are released from the cell via exocytosis, ready to initiate new rounds of infection (Van Den Elsen *et al*., 2021).

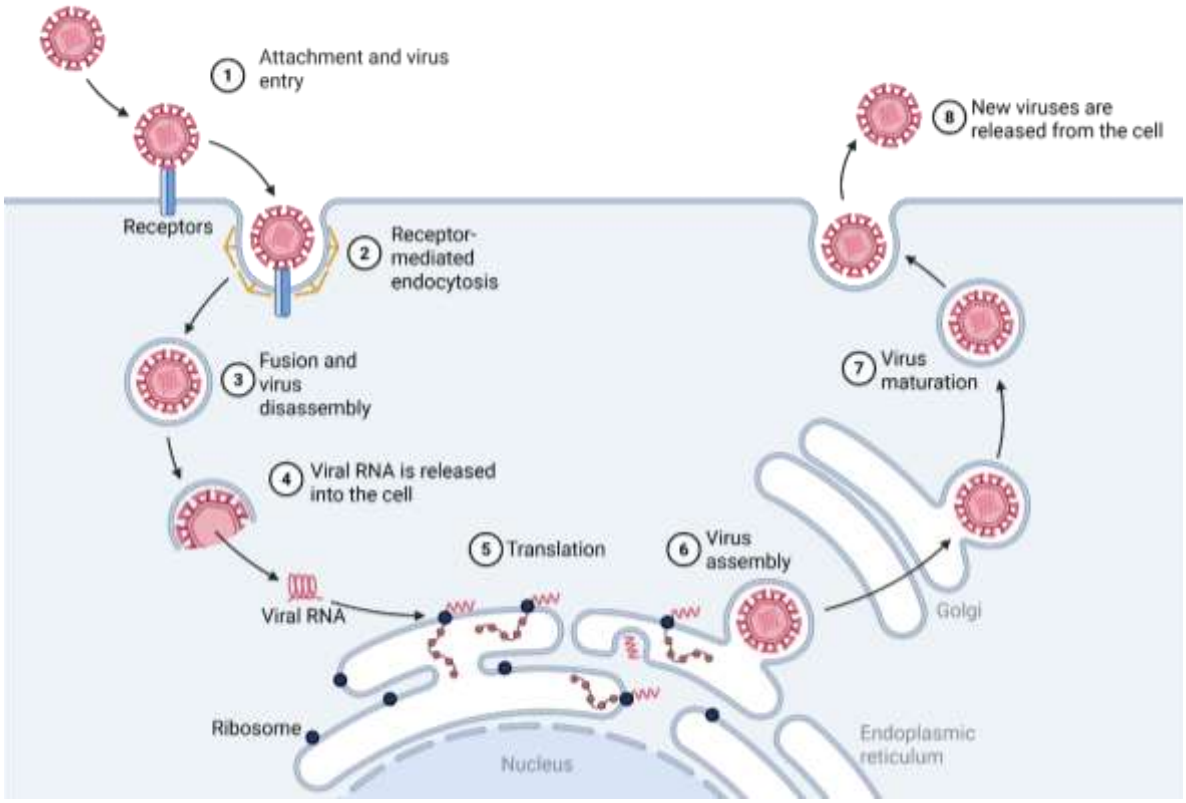

***Figure 4**: The flavivirus replication cycle (Created in https://BioRender.com).*

2.4.1 Dengue Fever Virus

2.4.1.1 General overview and epidemiology

The name "dengue" is believed to derive from the Swahili word "*dinga"*, which local populations used to describe an evil spirit thought to cause the symptoms now recognized as DENV infection («Etymologia», 2006). Globally, dengue is the most widespread mosquito-borne viral disease in humans (Bhatt *et al.,* 2013). The WHO estimates that there are approximately 390 million infections annually, primarily occurring in South-East Asia, the Western Pacific, the Americas, Africa and the Mediterranean region.

DENV consists of four antigenically distinct but highly similar serotypes (DENV-1 to DENV-4) with 60–75% amino acid sequence similarity, resulting in distinctive differences in viral fitness, epidemic potential, and virulence (Guzman & Harris, 2015; Weaver & Vasilakis, 2009). Infection with one serotype confers long-term immunity to that serotype but only temporary and partial cross-protection against others, increasing the risk of severe disease during secondary infections via antibody-dependent enhancement (ADE) (Halstead, 2007). ADE

occurs when antibodies generated from a previous dengue infection bind to, but fail to neutralize, a different serotype during a subsequent infection. Instead of blocking the virus, these sub-neutralizing antibodies help it enter immune cells more efficiently, increasing viral replication. As a result, the immune response becomes exaggerated and dysregulated, which can contribute to the development of more severe clinical manifestations such as dengue haemorrhagic fever (DHF) or and dengue shock syndrome (DSS) (Guzman & Harris, 2015). Among the 4 serotypes, DENV-2 has been most frequently associated with severe clinical outcomes, including DHF and DSS (Chen *et al*., 2007).

Over 13 million cases and more than 8,500 deaths caused by dengue were recorded in 2024 alone, according to the European Centre for Disease Prevention and Control (ECDC)**.** South America, dominated by Brazil, Peru, and Mexico, incurred the largest burden, followed by Southeast Asia, Africa (notably Burkina Faso), the Western Pacific (notably the Philippines and Vietnam), and the Eastern Mediterranean. Although not endemic in Europe, autochthonous cases have been reported in Italy, Spain, and France, mainly during summer months (ECDC, 2024; WHO, 2024). In Italy, between January 1 and August 5, 2025 (weekly update), the national surveillance system—led by the Istituto Superiore di Sanità (ISS)—reported 111 dengue confirmed cases, of which 107 were travel-related and 4 locally transmitted. The median age of the cases was 41 years, and 58% were males. There were no fatalities reported. Two events of autochthonous DENV transmission have been reported in Italy, specifically in the Emilia-Romagna and Veneto regions (https://www.epicentro.iss.it/arbovirosi/aggiornamenti). Since the beginning of 2025, over 4 million cases of DENV and more than 2,500 deaths caused have been reported in globally across 101 countries and territories spanning multiple WHO regions, including the Region of the Americas (PAHO), South-East Asia (SEARO), the Western Pacific (WPRO), the Eastern Mediterranean (EMRO), Europe (EURO), and Africa (ECDC, 2025). The marked increase in DENV transmission and mortality is driven by a combination of factors, with climate change playing a central role. Rising temperatures, high rainfall, humidity, and intermittent droughts create optimal conditions for *Aedes* vector proliferation. Peridomestic populations of mosquitoes, together with urbanization, inadequate water management, and increased human mobility, facilitate extended urban transmission cycles and transmission to new locations. Moreover, prolonged humanitarian crises and conflicts complicate health systems, making it difficult for diagnosis and treatment and producing more severe disease and death (Yu & Heng, 2022).

2.4.1.2 Transmission

DENV is transmitted primarily between humans through the bite of an infectious mosquito bite, most commonly *Aedes aegypti,* although other species such as *Aedes albopictus*, can also sustain transmission (CDC, 2024). *Aedes aegypti* is an urban, daytime-feeding mosquito with a strong preference for human blood, particularly in densely populated areas, and is found throughout tropical and subtropical regions (Chareonviriyaphap *et al.*, 2003). Conversely, *Aedes albopictus* is more aggressive day-biting species, typically found in outdoor environments, but still with a strong preference to feed on humans (Delatte *et al.*, 2010; Ponlawat & Harrington, 2005). It is adapted to a broader climatic range than *Aedes aegypti*, allowing DENV transmission to extend geographically into areas with a temperate climate.

Transmission of all four DENV serotypes occurs through two primary ecological cycles: a sylvatic (enzootic) cycle involving wild animals, and a human (urban) cycle (Chen & Vasilakis, 2011), as explained in Chapter 1.1. Even though the primary route of infection is through the bite of an infected mosquito, bloodborne exposure via infected blood, tissues, or organs such as bone marrow can occur, since DENV viremia often reaches high titres and persists for approximately seven days (CDC, 2024). Non-vector transmission is extremely rare, but perinatal and sexual transmission have been documented, with only a few sporadic cases reported to date (Chen & Wilson, 2016).

Finally, human-mediated factors, such as international travel and trade, amplify DENV spread. Travelers can introduce new serotypes or lineages into naïve regions, contributing to global expansion (Wilder-Smith *et al*., 2020).

2.4.1.3 Pathogenesis and symptoms

Following infection by the bite of an infected *Aedes* mosquito, DENV has an incubation period of 5-7 days, during which infectious virions disseminate systemically within the host's bloodstream (www.cdc.gov/dengue/training/cme/ccm). The virus primarily replicates in dendritic cells, monocytes, and macrophages. These infected cells then subsequently transport the virus to lymphoid tissues, where additional replication occurs while the virus evades immune clearance (Chauhan *et al*., 2024). The severity and duration of viremia levels in this early phase are predictors of clinical course and indicators of disease severity (Chauhan *et al*., 2024). It has been estimated that DENV infection is symptomatic only in a quarter of infections and most are an acute febrile illness of mild-to-moderate severity (www.cdc.gov/dengue/training/cme/ccm). Severe disease develops in approximately 5% of symptomatic infections and follows three phases: febrile, critical, and convalescence. The febrile phase, classically defined as dengue fever, is characterized by acute high fever onset,

headache, myalgia, arthralgia, and sometimes maculopapular rash. The critical phase occurs during defervescence and may coincide with the onset of DHF which can range from stage I to IV, with the last two stages classified as DSS (Rodriguez-Roche & Gould, 2013; Bhatt *et al*., 2021). DSS is characterized by plasma leakage, severe bleeding, shock, and potentially death. Severe outcomes are uncommon occuring in approximately 0.5–1% of cases even in secondary infections (Yu & Cheng, 2022; Chauhan *et al*., 2024).

Non-structural protein 1 (NS1) lies at the centre of dengue pathogenesis (Bhatt *et al*., 2021). NS1 exists in both a membrane-bound form (m-NS1) and a secreted form as a soluble lipoparticle (s-NS1) and serum levels of NS1 correlate with disease severity. NS1 contributes to vascular leakage through multiple mechanisms. First, NS1 can stimulate the immune system by activating Toll-like receptor 4 (TLR4) on macrophages and peripheral blood mononuclear cells, triggering an inflammatory response. It also activates the complement system, particularly the alternative pathway, leading to endothelial cell lysis, the release of pro-inflammatory cytokines, and the generation of anaphylatoxins such as C3a and C5a. Another key mechanism involves damage to the endothelial glycocalyx, where NS1 induces the shedding of heparan sulfate proteoglycans, particularly in the lungs, resulting in increased vascular permeability. Moreover, NS1 interacts with the immune system through antibody-dependent mechanisms. Anti-NS1 antibodies can modulate cytokine production by endothelial cells, causing elevated levels of monocyte chemoattractant protein 1 (MCP-1), IL-6, and IL-8, which are associated with haemorrhagic manifestations. In addition, molecular mimicry between NS1 and human proteins such as plasminogen and integrins may lead to autoimmune-mediated endothelial apoptosis and platelet dysfunction, further contributing to haemorrhage. Other viral proteins, including prM and E, have also been reported to participate in similar pathogenic processes (Bhatt *et al*., 2021; Pang *et al*., 2017). DENV infections can be divided in primary or secondary. Primary infections are most typically presented as mild or asymptomatic. Secondary infections with a different serotype are more prone to severe disease by ADE (Sinha *et al.* 2024). In ADE, non-neutralizing antibody from the first infection facilitates viral entry into Fcγ receptor-expressing cells, as well as viral replication, viremia, and increased disease severity (Bhatt *et al*., 2021). This must have been selected to prevent direct competition in a population between serotypes. Risk of severe disease is highest with secondary infection and decreases following repeated exposure (Yu & Cheng, 2022).

2.4.2 Zika Virus

2.4.2.1 General overview and epidemiology

ZIKV was first isolated in 1947 in Uganda from a Rhesus monkey. Two decades later, it was identified as a cause of human disease in Tanzania and Nigeria. By the late 1970s, the virus had spread to Asia, where human cases were reported in Indonesia, Malaysia, India, and Pakistan (Guarner & Hale, 2019). A significant epidemiological shift occurred in 2007, when an outbreak involving approximately 200 individuals was reported on Yap Island in Micronesia (Duffy *et al*., 2009). This was followed by a large epidemic in French Polynesia in 2013, affecting approximately 35,000 people and drawing attention to potential complications such as Guillain-Barré syndrome and congenital abnormalities, including microcephaly (Cao-Lormeau *et al*., 2014). The introduction of the virus into Brazil in 2014 subsequently triggered a large-scale epidemic across the Americas during 2015-2016, establishing a strong link between ZIKV infection, congenital Zika syndrome, and neurological sequelae in adults (Brasil *et al*., 2016). After this event, WHO declared ZIKV infection as a "Public Health Emergency of International Concern" in February 2016 (WHO, 2016). Nevertheless, by 2018 the number of new cases had strongly decreased, likely due to the development of herd immunity following the widespread circulation of both asymptomatic and symptomatic infection (Mlakar *et al*., 2016). Nonetheless, the risk of re-emergence remains, particularly since no licensed vaccine is yet available (Hasan *et al.*, 2019). In Europe, the majority of the reported ZIKV cases are associated with international travel, although some cases of local sexual transmission have been reported between 2016 and 2019 in France, Germany, Italy, and Norway. In 2019, three locally acquired cases of mosquito-borne transmission were also reported in Southern France, highlighting the potential for sporadic endemic circulation in locations with current competent vectors (Cataldo *et al*., 2024). In Italy, surveillance reports from the ISS indicate that all ZIKV infections detected up to October 2024, six in total, were imported and associated with travels to endemic regions (www.epicentro.iss.it/arbovirosi/aggiornamenti). The increasing number of imported cases in non-endemic countries with highly susceptible populations underscores the potential pandemic threat that ZIKV still poses.

Molecular epidemiological research has identified two predominant ZIKV lineages: the African and the Asian genotypes (Bernardo-Menezes *et al*., 2022). The African lineage is predominantly found in Central Africa, including countries such as Uganda, Senegal, and Nigeria, whereas the Asian lineage mainly circulates in Southeast Asia and the Pacific Region, for example in Micronesia, Cambodia, and French Polynesia. Phylogenetic analysis conducted during the large outbreak in the Americas in 2017 documented the emergence of a novel variant derived from the Asian lineage, now referred to as the American strain (Weaver *et al*., 2016). This isolate had a point mutation in the NS1 protein (A188V), a genetic mutation that

has been associated with increased pathogenicity and more severe clinical manifestations during and after the outbreak (Liu *et al*., 2017; Pierson & Diamond, 2020).

2.4.2.2 Transmission

ZIKV is primarily transmitted through the bite of infected *Aedes* mosquitoes, through the two distinct transmission cycles (sylvatic and urban cycles) already described in section 2.1.

Differently from DENV, in addition to mosquito-borne transmission, ZIKV can more commonly spread through non-mosquito routes, which include:

1) *Vertical and perinatal transmission*: Infection can occur during pregnancy or around the time of delivery, potentially causing neonatal fever, rash, conjunctivitis, and arthralgia;
2) *sexual transmission*: ZIKV can be transmitted sexually, even from asymptomatic individuals, at various stages of infection (before, during, or after symptomatic disease);
3) *blood transfusions and other biological exposure*: although transfusion-related cases have not been confirmed in the United States, several incidents were reported in Brazil (Guo *et al*., 2022).

Cases of transfusion-associated transmission have been reported, and the virus has also been detected in breast milk. However, it should be noted that breastfeeding transmission has not yet been confirmed (www.cdc.gov/zika/php/transmission/index.html).

2.4.2.3 Pathogenesis and symptoms

Following transmission, ZIKV replicates in the bloodstream and exhibits broad tissue tropism, infecting ocular, reproductive (testes, vagina, uterus), placental, and central nervous system cells (Miner & Diamond, 2017). Neurons are particularly susceptible, resulting in neurological sequelae in both adults as well as foetuses. The incubation period ranges from 3 to 14 days (Krow-Lucal *et al*., 2017), after which symptoms develop in only 20–25% of infected individuals.

ZIKV typically causes a mild, self-limiting illness characterized by fever, arthralgia, rash, conjunctivitis, myalgia, and headache. Additional manifestations such as retro-orbital pain, lymphadenopathy, vomiting, and brain edema have also been reported (*Guo et al., 2022*). Severe disease is uncommon but may include meningoencephalitis, acute myelitis, and thrombocytopenia. Notably, some patients develop Guillain–Barré syndrome (GBS) which appears to be mediated by an atypical immune response characterized by increased production of pro-inflammatory cytokines (CXCL10, IL-6, type I IFN), ultimately leading to

neuronal injury (Maucourant *et al*., 2019; Naveca *et al*., 2018). Vertical transmission of ZIKV during pregnancy is a major concern as the virus can cross the maternal–foetal barrier by infecting the endothelial cells of the decidua and chorionic villi, subsequently reaching the foetus (Guo *et al*., 2022).

ZIKV displays a strong tropism for embryonic neural stem cells, inducing apoptosis and impairing neurogenesis, processes that are further exacerbated by microglia-mediated inflammation (Giraldo *et al*., 2023). These mechanisms account for congenital ZIKV syndrome (CZS), which occurs in approximately 5–15% of affected infants and is characterized by microcephaly, cortical atrophy, seizures, ocular abnormalities, and motor impairment (Paixao *et al*., 2022). Vertical transmission has also been associated with spontaneous abortion and stillbirth (Guo *et al*., 2022). Additionally, ZIKV can persist in the male genitourinary tract by crossing the blood–testis barrier and infecting Sertoli cells, spermatogonia, and spermatozoa. Viral replication in semen accounts for its capacity for sexual transmission, a property that contributes to its unusual epidemiological pattern (Giraldo *et al*., 2023).

2.5 Current status of therapeutics against ZIKV and DENV infections.

Despite the extensive global burden imposed by flaviviruses, no specific antivirals have yet been approved for the treatment of DENV and ZIKV infections. Current management remains largely symptomatic, focusing on supportive care, fluid replacement, and the treatment of complications. The development of effective therapeutics faces major challenges, including high genetic variability, the emergence of quasispecies due to error-prone RNA polymerases, and the risk of ADE which complicates vaccine design (Boldescu *et al*., 2017; Diani *et al*., 2023; Côrtes *et al.,* 2023). Nevertheless, significant progress has been made in identifying potential antiviral drug classes and designing vaccine platforms that may provide extended protection.

2.5.1 Antivirals development

In recent years, extensive efforts have been directed toward the identification of antiviral compounds capable of inhibiting flavivirus replication. Given the absence of licensed specific treatments, research has focused on both viral and host cellular targets that are essential for the viral life cycle. Overall, these compounds can be broadly classified as *direct-acting antivirals* (DAAs) which interfere directly with viral proteins and *host-targeting agents* (HTAs), which disrupt cellular pathways exploited by the virus for replication. The main classes of DAAs investigated to date include the following:

(1) *Entry and fusion inhibitors* act by blocking the interaction between the viral envelope (E) glycoprotein and host receptors, thereby preventing viral attachment and internalization.

Peptides derived from viral fusion loops (e.g., DN59, P5) and monoclonal antibodies (mAb513, 2D22) have demonstrated inhibition of DENV and ZIKV replication *in vitro* and *in vivo* (Dejnirattisai *et al*., 2015; Deng *et al*., 2016). Small molecules such as prochlorperazine, palmatine, and nanchangmycin also reduce viral entry by interfering with clathrin-mediated endocytosis (Wang *et al*., 2009). Several neutralizing monoclonal antibodies against ZIKV, such as Tyzivumab, have reached phase I clinical trials (Fernandez *et al*., 2017).

(2) *Protease inhibitors* represent another promising DAA class. The NS3 serine protease, essential for polyprotein cleavage, shares similarities with the HCV protease. Repurposed HCV drugs, such as boceprevir and telaprevir, have shown activity against flaviviruses in preclinical studies (Boldescu *et al*., 2017; Lim *et al*., 2015). An example of innovative protease-targeting strategies is JNJ-64281802, a compound that blocks the interaction between NS3 and NS4B across all DENV serotypes. During the preclinical phase, it exhibited picomolar to nanomolar potency, with EC_{50} values ranging from 0.059 to 1.24 nM against DENV-2 laboratory strains (Goethals *et al*., 2023). It was also the first compound of its class to demonstrate safety and tolerability in a phase I clinical trial (Ackaert *et al*., 2023) and is now undergoing phase II evaluation.

(3) *Polymerase inhibitors* act on NS5 RNA-dependent RNA polymerase (RdRp), the essential enzyme for viral genome replication. Nucleoside analogues like sofosbuvir (SOF), originally developed and approved for HCV therapy, demonstrated activity against ZIKV and DENV *in vitro* and in mouse models (Sacramento *et al*., 2017, Vicenti *et al*., 2018). Other nucleoside analogs such as ribavirin and favipiravir have also been evaluated, though efficacy varies. Several compounds targeting the NS5 RdRp C-terminal domain are currently in clinical trials (Diani *et al*., 2023).

HTAs have also been explored. Inhibitors of lipid metabolism (e.g., statins, imipramine), autophagy modulators, cyclophilin inhibitors, and kinase inhibitors (erlotinib, sunitinib) showed activity against multiple flaviviruses (Boldescu *et al.,* 2017; Diani *et al*., 2023). These strategies aim to reduce the likelihood of viral resistance but raise concerns regarding host toxicity.

Overall, while a broad range of antiviral candidates has been identified, none have advanced to late-phase clinical approval. Combination therapies targeting multiple viral and host pathways are considered a promising future direction to overcome resistance and broaden efficacy.

2.5.2 Vaccines development

Vaccination remains the most effective long-term strategy for controlling flaviviral infection. YFV, Vaccine against Japanese encephalitis virus (JEV), and tick-borne encephalitis virus (TBEV) are currently available, produced as live-attenuated or inactivated formulations (Monath, 2012; Boldescu *et al*., 2017). The success of vaccines such as the YFV 17D, which provides lifelong immunity after a single dose, demonstrates that long-term protection can be achieved (Monath, 2012).

For DENV, two vaccines have now received regulatory approval: Dengvaxia (CYD-TDV) and Qdenga (TAK-003). Dengvaxia is a tetravalent live-attenuated chimeric vaccine based on a YFV backbone. Its efficacy varies substantially among serotypes and is higher in individuals with previous DENV exposure. In contrast, vaccination of seronegative individuals may increase the risk of severe dengue through ADE during subsequent infection (Hadinegoro et al., 2015). Consequently, current guidelines restrict its use to defined age groups and populations with confirmed prior DENV infection.

Qdenga (TAK-003), a live-attenuated tetravalent vaccine developed by Takeda, has demonstrated sustained protection in Phase 3 trials, particularly against DENV-1 and -2, with a favourable safety profile and efficacy in both seropositive and seronegative individuals, although performance varies by serotype and region (Tricou et al., 2024). Long-term effectiveness and durability of protection are still being evaluated (Biswal et al., 2019). In addition, other next-generation DENV vaccines, including purified inactivated candidates, remain in late-stage development.

For ZIKV, vaccine development accelerated after the 2015–2016 epidemic. Multiple platforms are being explored, including DNA, mRNA (following success of COVID-19 vaccines), viral-vectored (adenovirus- or vaccinia-based), and virus-like particles (VLPs) vaccines (Richner *et al*., 2017; Pardi *et al.*, 2018; Ostrowsky *et al.* 2025). Several candidates have reached Phase 1 or 2 clinical trials, showing encouraging safety and immunogenicity, but no ZIKV vaccine has yet been licensed as of 2025. Major hurdles include limited outbreak activity for large-scale efficacy trials, cross-reactivity with other flaviviruses, and the need for protection during pregnancy. Across flaviviruses, key challenges in vaccine development include the risk of ADE, the balance between serotype-specific and cross-protective immunity, and genetic variability among circulating strains. Structural studies have identified conserved epitopes on the E glycoprotein that may serve as targets for broadly neutralizing antibodies (Rouvinski *et al*.,

2017; Côrtes *et al*., 2023). Novel approaches, including mRNA vaccines and chimeric constructs, may increase safety and coverage breadth of protection in the coming years.

3 SARS-CoV-2 general overview and epidemiology

Over the past two decades, three coronaviruses have emerged as major human pathogens capable of causing severe and life-threatening disease: Severe Acute Respiratory Syndrome Coronavirus (SARS-CoV) in 2002, Middle East Respiratory Syndrome Coronavirus (MERS-CoV) in 2012, and Severe Acute Respiratory Syndrome Coronavirus 2 (SARS-CoV-2) in 2019. SARS-CoV-2 initially emerged in December 2019 in Wuhan, China, and rapidly spread around worldwide, causing millions of confirmed cases of Coronavirus Disease 2019 (COVID-19) and millions of deaths (Akkız, 2022). SARS-CoV-2 is an enveloped, spherical RNA virus belonging to the genus of *Betacoronaviruses*. It exhibits a characteristic crown-like shape due to the spike (S) glycoproteins protruding from the viral envelope. The S proteins play a significant role in viral entry by mediating attachment to the angiotensin-converting enzyme 2 (ACE2) receptor of human host cells (Ali & Vijayan, 2020).

On March 11, 2020, the World Health Organization (WHO) officially declared the COVID-19 a global pandemic (WHO, 2020). Since then, the virus has continued to circulate and evolve, leading to the emergence of numerous variants worldwide. To manage these developments, WHO classified SARS-CoV-2 variants according to their potential impact on public health. Variants under monitoring (VUMs) are those with genetic or epidemiological characteristics that warrant close observation to determine if they have the potential to become a new risk to global public health. Variants of Interests (VOIs) carry genetic changes that are known or suspected to affect viral transmissibility, disease severity or the response to vaccines and therapeutics, and may exhibit increased transmission compared to other circulating variants. Variant of Concerns (VOCs) represent a higher level of alert, in addition to meeting the criteria of VOIs, they have been associated with evidence of increased disease severity, reduced effectiveness of public health measures or decreased vaccine efficacy. To simplify communication, each VOC has been designated by a letter of the Greek alphabet. The most relevant VOCs include Alpha (B.1.1.7), Beta (B.1.351), Gamma (P.1), Delta (B.1.617.2), and Omicron (B.1.1.529), all of which carry mutations within the receptor-binding domain (RBD) of the S protein that enhance viral attachment, transmissibility, or immune evasion (Harvey *et al*., 2021; Tegally *et al*., 2021; WHO, 2022). Alpha demonstrated a 43–90% higher transmissibility compared to previous lineages (Davies *et al*., 2021). Delta exhibited even greater transmission potential, with the basic reproduction number (R_o), the average number of secondary infections generated by a single infected individual in a fully susceptible population, estimated at 5 to 8, and was associated with higher viral loads and longer duration of viral shedding (Liu & Rocklöv, 2021). Omicron subsequently replaced Delta globally due to its higher transmissibility, estimated to be more than twice that of Delta, even in highly vaccinated populations (Chen

et al., 2022). A comparative study ranked variant transmissibility as follows: Omicron > Delta > Alpha > Gamma > Beta. (Khan *et al*., 2023). Despite its increased transmissibility, Omicron has generally been associated with a lower risk of severe disease, hospitalization, and intensive care unit admission than Delta, likely reflecting reduced replication efficiency in lung tissue (Nyberg *et al*., 2022; Sheikh *et al*., 2022). This adaptive balance between virulence and transmissibility lies at the centre of SARS-CoV-2 epidemiology and underscores the continued importance of genomic surveillance, vaccination, and therapy.

3.1 Genome organization and life cycle of SARS-CoV-2

The genome of SARS-CoV-2 consists of a single-stranded, positive-sense RNA molecule approximately of 29.9 kilobases in length (Cevik *et al*., 2020). Like other coronaviruses, its genome (Figure 5) is highly conserved and displays a characteristic organizational pattern. The 5' region, which accounts for about two-thirds of the total genome, contains two overlapping open reading frames—ORF1a and ORF1b—that are translated into the large polyproteins pp1a and pp1ab. These polyproteins are subsequently cleaved by two viral proteases: the papain-like protease (PLpro, part of nsp3) and the main protease (Mpro or 3CLpro, corresponding to nsp5). Through these proteolytic processing events, sixteen non-structural proteins (nsps) are generated. The nsps then assemble into the replication–transcription complex (RTC), which directs both genome replication and the synthesis of subgenomic RNAs.

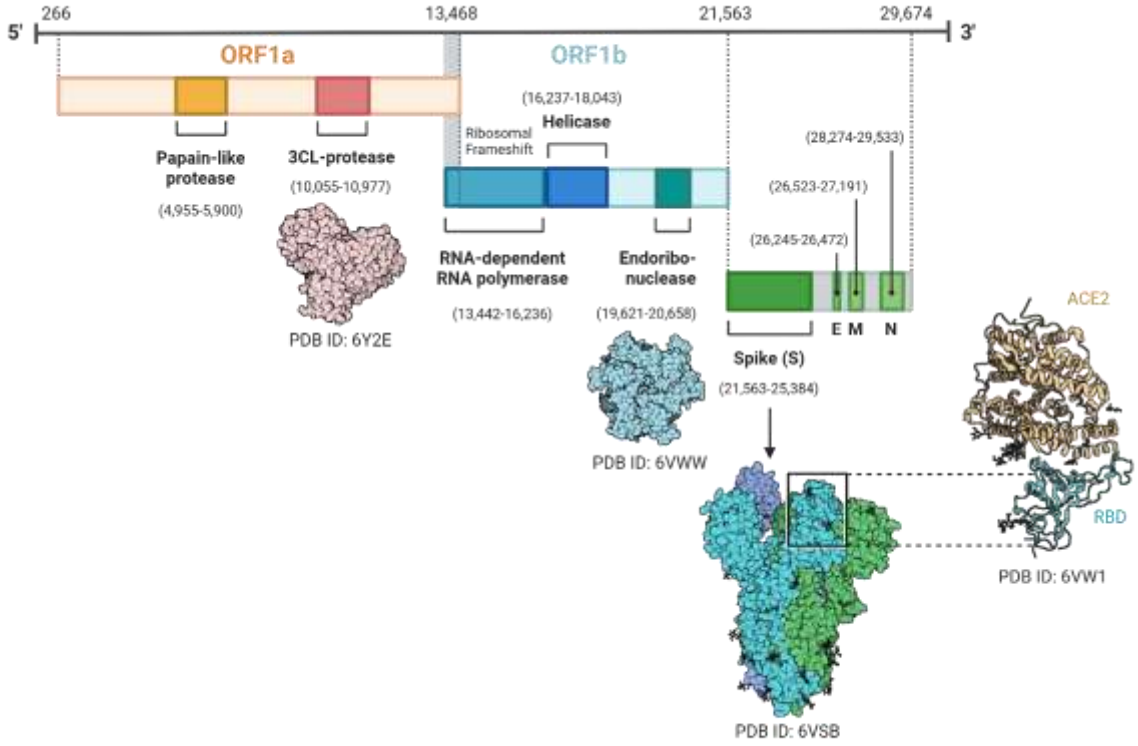

***Figure 5**: Genome organization of SARS-CoV-2 (Created in https://BioRender.com).*

A distinctive feature of coronaviruses, including SARS-CoV-2, is the presence of an RNA proofreading exonuclease (nsp14-ExoN). This enzyme enhances replication fidelity, which distinguishes coronaviruses from most other RNA viruses lacking such proofreading capacity (V'kovski *et al.,* 2021). The 3′ portion of the genome encodes the four principal structural proteins—spike (S), envelope (E), membrane (M), and nucleocapsid (N)—as well as several accessory proteins, including ORF3a, ORF6, ORF7a/b, and ORF8. Many of these accessory proteins contribute to immune evasion and viral adaptation. Among them, the trimeric spike (S) glycoprotein plays a key role in determining host specificity and pathogenic potential. The spike protein is divided into two main subunits: S1, which contains the receptor-binding domain (RBD) responsible for attachment to the ACE2 receptor, and S2, which mediates membrane fusion. Activation of the S protein requires proteolytic cleavage at the S1/S2 and S2′ sites by host proteases, notably TMPRSS2 and cathepsins, to facilitate viral entry (Hoffmann *et al*., 2020).

The viral life cycle (Figure 6) begins when the S protein binds to ACE2 receptors on the host cell surface, a process facilitated by host proteases such as TMPRSS2. Upon receptor engagement, the virus enters the host cell via membrane fusion or endocytosis. Once inside, the viral RNA genome is released into the cytoplasm and translated into non-structural proteins required for viral replication. The RTC subsequently guides both genome replication and the synthesis of subgenomic RNAs, which serve as templates for the production of structural and accessory proteins. New viral particles are assembled within the endoplasmic reticulum–Golgi intermediate compartment (ERGIC). Within this compartment, nucleocapsid (N) proteins encapsulate the genomic RNA, while the structural proteins integrate into budding viral membranes to form mature particles. The newly formed virions are then transported in vesicles and released through exocytosis, enabling infection of neighboring cells (Hoffmann *et al*., 2020; V'kovski *et al*., 2021).

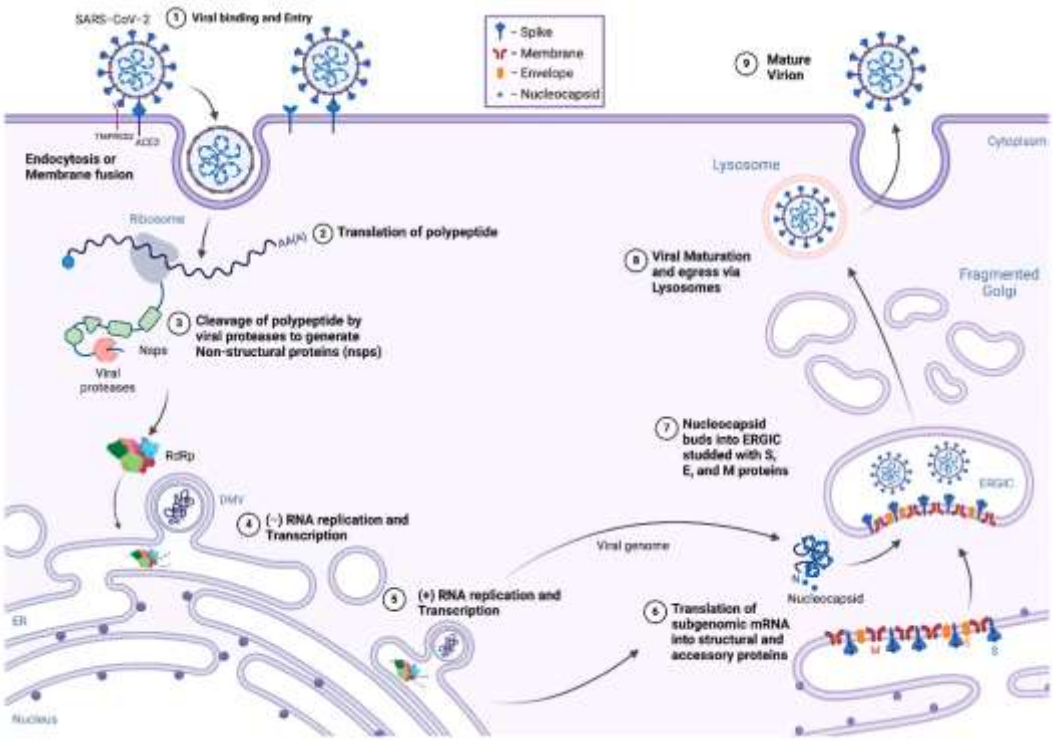

***Figure 6**: SARS-CoV-2 replication cycle (adapted from Katiyar et al. 2024).*

3.2 Transmission

SARS-CoV-2 spreads primarily through direct or indirect contact, aerosols, and large respiratory droplets. Direct contact occurs through close contact with an infected person, allowing viral particles to enter the body via the mucous membranes of the eyes, nose, or mouth. Indirect transmission, on the other hand, can occur through contaminated objects or surfaces (fomites); when these are touched and subsequently contact is made with the face, infection may result (Chung *et al.*, 2024). During the pandemic, these routes were particularly relevant among healthcare workers due to frequent close interactions with patients. Aerosol transmission plays a major role, especially in enclosed or poorly ventilated environments. Aerosols are tiny, virus containing particles, that can remain suspended in the air for prolonged periods, facilitating long-range airborne spread. Droplet transmission occurs when larger respiratory droplets are expelled by an infected individual during coughing or sneezing. Because such droplets typically travel only short distances, maintaining a physical distance of at least 1.5 meters helps reduce the risk of infection (Chung *et al.*, 2024). SARS-CoV-2 also exhibits broad tissue tropism, which contributes to its high transmissibility and the diverse range of clinical manifestations observed in infected individuals. The virus primarily targets epithelial cells of the respiratory tract, but the ACE2 and TMPRSS2 receptors can be also found in extrapulmonary tissues, including the gastrointestinal tract, kidneys, blood vessels, and central nervous system, facilitating systemic

infection (Puelles *et al*., 2020). Indeed, viral RNA and infectious particles have been found in faecal samples, suggesting that the virus can be shed through the gastrointestinal tract and potentially contaminate the environment, although faecal-oral transmission is considered uncommon (Xiao *et al*., 2020). The virus has also been detected in the olfactory epithelium and brain tissue, which may explain loss of smell and other neurological symptoms reported in COVID-19 patients (Meinhardt *et al*., 2021). Given that asymptomatic and pre-symptomatic individuals are estimated to account for up to half of all secondary infections, extensive testing and preventive public health measures are essential to control virus transmission (Buitrago-Garcia *et al*., 2022). Another valuable surveillance approach is wastewater-based epidemiology (WBE). As demonstrated by Agrawal et al., SARS-CoV-2 RNA can be detected in wastewater 30–60 days before clinical cases increase, highlighting its utility for early outbreak detection and the monitoring of emerging variants (Agrawal *et al*., 2023).

3.3 Pathogenesis and symptoms

SARS-CoV-2 infection can lead to a wide spectrum of clinical outcomes, ranging from asymptomatic or mild respiratory illness to severe pneumonia, acute respiratory distress syndrome (ARDS), multi-organ failure, and even death (Buitrago-Garcia *et al*., 2022; Li *et al*., 2024). The course of infection is often divided into three stages. The first stage corresponds to the incubation period, when the virus replicates without causing noticeable symptoms. The second stage, the symptomatic phase, is characterized by the onset of cough, fever, and pneumonia. In the most severe cases, a third stage emerges, marked by strong inflammation and multi-organ dysfunction (Chung *et al*., 2024).

As mentioned in chapter 2, SARS-CoV-2 infection begins when the viral S protein binds to the ACE2 receptor, which is expressed in multiple tissues, including the respiratory tract, blood vessels, heart, kidneys, and intestines. This broad tissue distribution contributes to the multi-organ manifestations of COVID-19 (Li *et a*l., 2024; Yan *et al*., 2020). Upon viral infection, the immune system recognizes the pathogen and triggers immune and inflammatory responses. In a subset of patients, this response becomes dysregulated resulting in a "cytokine storm" characterized by very high levels of pro-inflammatory cytokines, including IL-6, IL-1β, and TNF-α. These molecules can damage blood vessels and tissues, potentially leading to ARDS and multi-organ failure (Tay *et al*., 2020; Schurink *et al*., 2020). Individuals with comorbidities, such as hypertension, diabetes, obesity, or cardiovascular and renal disease, are at increased risk of developing severe COVID-19. These comorbid conditions can upregulate ACE2 expression, facilitating viral entry and increasing the severity of infection. Patients with multiple chronic diseases face approximately twice the risk of mortality, mainly due to the enhanced effects of inflammation and organ damage (Chung *et al*., 2024). Neurological symptoms such as loss of smell, headache, encephalitis, and cognitive difficulties are also common. They are thought to result from both direct viral invasion of the nervous system and immune-mediated damage (Bourgonje *et al*., 2020;

Liang *et al.*, 2020). After the acute phase, some people experience persistent symptoms known as post-COVID-19 condition, or long COVID. These symptoms typically manifest within three months of acute infection and persist for at least two months, often impacting daily functioning. Approximately 6% of individuals infected develop long COVID, although recent studies indicate that this prevalence may be declining. The most frequently reported symptoms include fatigue, dyspnoea, myalgia or arthralgia, trouble concentrating, and sleep disturbances (Soriano *et al*., 2024). Current evidence indicates that long COVID results from the persistence of viral particles, ongoing immune activation, and sustained vascular damage. Most patients experience gradual recovery within 4–9 months; however approximately 15% continue to exhibit symptoms after a year. The World Health Organization is developing guidelines to support the management of long COVID, focusing on self-care, pharmacological interventions when necessary, and access to multidisciplinary rehabilitation services (WHO, 2024).

3.4 Current measures to counteract COVID-19: vaccines, monoclonal antibodies and antivirals

During the COVID-19 pandemic, three main strategies that constituted the foundation for disease control were adopted: vaccination, monoclonal antibodies (mAbs), and antiviral drugs. Vaccines remain the cornerstone of prevention, as they stimulate the immune system to reduce both infection rates and disease severity. mAbs have been primarily employed for prophylaxis or early treatment, providing transient passive immunity through direct viral neutralization. However, their effectiveness has decreased over time as new variants have appeared. Antiviral drugs inhibit viral replication and help prevent severe disease, especially in high-risk groups. Together, these interventions provide a comprehensive and adaptable defence against SARS-CoV-2, integrating prevention and treatment.

3.4.1 SARS-CoV-2 active immunization: Vaccines approved

As of mid-2025, three vaccines remain the primary tools for immunization in North America and Europe: the mRNA vaccines BNT162b2 (Comirnaty, Pfizer-BioNTech) and mRNA-1273 (Spikevax, Moderna), and the protein-subunit vaccine NVX-CoV2373 (Nuvaxovid, Novavax). Their continued use is supported by robust safety and efficacy data, as well as the possibility to be updated for new variants, including Omicron sublineages such as JN.1 and KP.2 (WHO Technical Advisory Group on COVID-19 Vaccines, 2024).

The mRNA vaccines contain nucleoside-modified RNA encoding prefusion-stabilized, full-length S protein. The inclusion of two proline substitutions (K986P and V987P), first described by Pallesen *et al*., maintain the S protein in the prefusion conformation, ensuring a robust immune response (Polack *et al*., 2020; Baden *et al*., 2021). The RNA also incorporates N1-methylpseudouridine, a stabilizer which enhances translation efficiency and reduces excessive innate immune activation. Each mRNA

molecule is packaged in lipid nanoparticles (LNPs) composed of ionizable lipids (ALC-0315 for Comirnaty and SM-102 for Spikevax), cholesterol, DSPC, and PEG-lipids. These LNPs protect the RNA from degradation and facilitated cellular uptake, allowing intracellular production of the S protein. Once expressed, the S protein is presented on the cell surface, eliciting both antibody and T-cell responses. LNPs themselves can further enhance innate immune activation, promoting a strong Th1-type response. Overall, these vaccines continue to confer robust protection against severe COVID-19, and their updated formulations remain critical for addressing immune evasion by Omicron sublineages (Magalhães *et al*., 2025; Tseng *et al*., 2023).

Protein-subunit vaccines, such as NVX-CoV2373 (Nuvaxovid), work in a different way. They employ a stabilized prefusion trimeric S protein produced using recombinant technology in insect cells through a baculovirus expression system. The S protein assembles into nanoparticles and is combined with the Matrix-M adjuvant, which enhances antigen presentation and elicits both antibody and T-cell responce (Heath *et al*., 2021). This platform offers practical advantages, as it can be maintained at standard refrigerator temperatures and provides a non-mRNA alternative for individuals who prefer or require it. NVX-CoV2373 has demonstrated strong protection against severe COVID-19 (Heath *et al*., 2021).

Newer vaccine technologies have also emerged, including self-amplifying mRNA (saRNA) vaccines such as Zapomeran. These vaccines use RNA molecules derived from alphavirus replicons that encode both the SARS-CoV-2 spike and the nonstructural enzymes required for RNA replication within host cells. This self-replicating mechanism enables higher antigen expression from a lower initial dose. saRNA vaccines are generally delivered via LNPs, but also cationic nanoemulsions or polymer-based delivery systems can also be employed to enhance stability and immunological tolerance (Silva-Pilipich *et al.*, 2024).

Because the RNA can replicate inside cells, saRNA vaccines can sustain antigen production for longer periods, creating strong and durable immune responses. They can induce high levels of neutralizing antibodies and Th1-biased T-cell responses, even higher than those from traditional mRNA vaccines. Early trials suggest a good safety profile and high flexibility for rapid updates to new variants, including recent Omicron lineages (Moderna press release, 2025; WHO, 2024). Their low-dose requirement and extended antigen expression make saRNA vaccines a promising option for future booster programs.

Viral vector vaccines use a non-replicating adenovirus to deliver the gene encoding the SARS-CoV-2 spike protein into host cells, triggering the production of protective antibodies. Compared with mRNA vaccines, these platforms are more stable and do not require ultra-cold storage conditions, making them easier to handle and distribute. During the COVID-19 pandemic, two adenoviral vector vaccines received authorization: AstraZeneca's ChAdOx1 nCoV-19 (Vaxzevria) and Johnson & Johnson's

Ad26.COV2.S (Jcovden). However, both vaccines have since been largely phased out in high-income countries and were officially withdrawn from the European market in 2024. Their decline reflects several factors, including decreased public demand, a growing preference for mRNA and protein-subunit vaccines, limited flexibility in adapting to emerging viral variants, and safety concerns associated with rare cases of thrombosis with thrombocytopenia syndrome (TTS) (European Medicines Agency [EMA], 2024; Pearce, 2024).

3.4.2 Monoclonal antibodies (mAbs)

Neutralizing mAbs were the first targeted therapies developed against COVID-19. These antibodies bind to the SARS-CoV-2 S glycoprotein providing immediate passive immunity through viral neutralization and Fc-mediated effector functions. During the early phase of the pandemic, mAbs were widely used to treat mild-to-moderate COVID-19 in high-risk patients and as pre-exposure prophylaxis in severely immunocompromised individuals who could not reach an adequate vaccine-induced immune response (Taylor *et al*., 2021; Focosi *et al*., 2024). By 2025, however, their role has changed significantly. Ongoing viral evolution has led to a substantial loss of neutralization activity, resulting in the withdrawal or de-authorization of most products. Currently, pemivibart (Pemgarda) is the only monoclonal antibody authorized under Emergency Use Authorization (EUA) by the FDA for pre-exposure prophylaxis in immunocompromised patients who are unlikely to achieve a sufficient immune response to COVID-19 vaccination (FDA, 2024). However, it has not received full regulatory approval and remains unauthorized by the EMA.

All anti-SARS-CoV-2 mAbs are human IgG1 antibodies produced by recombinant techniques. Several were engineered with Fc-domain modifications: YTE substitutions (M252Y/S254T/T256E) or LS substitutions (M428L/N434S), which extend serum half-life, whereas TM substitutions (L234F/L235E/P331S) modulate Fcγ-receptor and complement binding to minimize the risk of ADE (Taylor et al., 2021). These antibodies were administered either by intravenous infusion (IV) (e.g., sotrovimab, bebtelovimab, REGEN-COV) or intramuscular injection (IM) (e.g., Evusheld®). Engineered mAbs provided protection for up to of six months (Focosi *et al*., 2024). Unlike vaccines, mAbs do not elicit adaptive immunity responses but confer temporary passive immunity. Their mechanism of action include (1) direct viral neutralization through blockade of the receptor-binding domain (RBD) and inhibition of ACE2 engagement, and (2) Fc-mediated effector functions such as antibody-dependent cytotoxicity, phagocytosis, and complement activation. Protection wanes as antibody titers decline or as viral mutation accumulate.

Table 1 summarizes key mAb products developed from 2020 to 2025, their targets, routes of administration, regulatory status, and withdrawal reasons. Early mAbs achieved strong results before Omicron emergence, but antigenic drift caused sequential loss of activity, leading regulators to revoke

emergency authorizations (FDA, 2022; Choudhary *et al*., 2022). Later agents such as bebtelovimab and Evusheld® initially retained efficacy but were eventually discontinued once resistance extended to BQ.1 and XBB variants (EMA, 2023; Focosi *et al.,* 2024). Sipavibart (Kavigale), a long-acting IgG1 mAb targeting the SARS-CoV-2 spike RBD, was developed for pre-exposure prophylaxis in immunocompromised patients; however, its activity was lost against emerging variants carrying the F456L mutation, leading to limited use or withdrawal from the market (EMA, 2024; Haidar et al., 2025; Focosi, 2025). Meanwhile, SA55, a broadly neutralizing mAb against sarbecoviruses, showed strong in vitro potency against multiple Omicron sublineages and is currently being investigated as an intranasal prophylactic agent in early-phase clinical trials (Hu *et al*., 2025; Cao *et al.,* 2022). Thus far in 2025, pemivibart (PEMGARDA™, VYD222) remains the only monoclonal antibody with US emergency use approval, limited to pre-exposure prophylaxis in those who are moderately to severely immunocompromised (FDA, 2024; EMA, 2024).

***Table 1**: Main anti-SARS-CoV-2 monoclonal antibodies: characteristics and regulatory status (update 2025).*

Antibody (brand name)	**Epitope target**	**Route of administration**	**Regulatory status (2025)**	**Reason for withdrawal / limited use**
Bamlanivimab/Etesevimab	Spike RBD	IV	EUA revoked (2022)	Loss of activity against BA.1/BA.2
Casirivimab/Imdevimab (REGEN-COV)	Spike RBD	IV	EUA revoked (2022)	Widespread resistance against BA.1/BA.2
Sotrovimab	Spike RBD	IV	De-authorized (2022)	Loss of efficacy against BA.2
Bebtelovimab	Spike RBD	IV	De-authorized (late 2022)	Resistance against BQ.1 and XBB
Tixagevimab/Cilgavimab (Evusheld®)	Spike RBD	IM	EUA revoked (2023)	Progressive loss of activity (BA.4/5, XBB)
Pemivibart (PEMGARDA™, VYD222)	Spike RBD (selected epitope)	IV	EUA active (US only, 2025)	Restricted use in susceptible immunocompromised patients
Sipavibart (Kavigale)	Spike RBD	IV	Limited/withdrawn (2025)	Loss of activity against variants carrying F456L mutation
SA55	Broad sarbecovirus epitope	Intranasal	Clinical trials (phase I)	Not yet authorized; investigational prophylaxis

3.4.3 Antivirals drugs

Antiviral drugs have played a key role in COVID-19 management since the beginning of the pandemic. Unlike vaccines, which stimulate long-term immunity, antivirals act directly on viral replication to reduce symptom severity, hospitalization, and death. Their importance has grown as neutralizing mAbs have lost their effectiveness due to viral evolution (Focosi *et al*., 2024). By 2025, the Infectious Diseases Society of America (IDSA), EMA and WHO guidelines suggest the early initiation of antiviral

therapy in non-hospitalized, high-risk patients, ideally within five days of symptom onset. Direct-acting antivirals (DAAs) such as nirmatrelvir/ritonavir (Paxlovid®), remdesivir (Veklury®), and molnupiravir (Lagevrio®) are the current treatments of choice, while host-targeting antivirals (HTAs) are under investigation.

3.4.3.1 Direct-Acting Antivirals (DAAs)

DAAs target viral enzymes essential for replication. Because the Mpro and the RdRp are highly conserved, these agents retain efficacy against all Omicron sublineages including JN.1 and KP.2 (Focosi *et al*., 2024). The major classes of DAAs currently authorized for COVID-19 treatment include protease inhibitors and nucleoside/nucleotide analogues, each acting on different steps of the viral replication cycle.

Protease inhibitors: Nirmatrelvir (NRM) covalently binds to the catalytic cysteine residue of Mpro, thereby preventing the cleavage of viral polyproteins and ultimately blocking viral replication (Owen *et al*., 2021). It is co-administered with ritonavir (RTV), a potent CYP3A4 inhibitor that prolongs NRM plasma exposure by reducing its metabolic clearance. In the Evaluation of Protease Inhibition for COVID-19 in High-Risk Patients (EPIC-HR) trial, early treatment with NRM/rtv resulted in a 89% reduction in hospitalization or death among high-risk, non-hospitalized adults (Hammond *et al*., 2022). Subsequent trials confirmed its efficacy against Omicron sublineages (Focosi *et al*., 2024). However, the extensive drug-drug interactions associated with ritonavir, make it use challenging, particularly in elderly patients with polypharmacy (Epling *et al*., 2022).

Nucleoside/nucleotide analogues: RdRp inhibitors such as remdesivir (RDV) and molnupiravir (MLN) have distinct mechanisms of action. RDV acts as a chain terminator, halting RNA elongation after incorporation (Beigel *et al*., 2020). The Adaptive COVID-19 Treatment Trial 1 (ACTT-1) showed faster recovery in hospitalized patients, and subsequent studies confirmed its benefit when administered early (Focosi *et a*l., 2024). However, the requirement for intravenous infusion limits its use outside hospital settings. MLN, on the other hand, induces an “error catastrophe” by introducing mismatched nucleotides, resulting in nonviable viral genomes (Painter *et al*., 2021). The Molnupiravir Outpatient Treatment for COVID-19 (MOVe-OUT) trial showed that MLN reduced hospitalization or death by approximately 30% in unvaccinated high-risk adults (Painter *et al*., 2021).

Current guidelines recommend NRM/RTV as the first-line treatment for eligible patients, with RDV considered when contraindications exist. MLN is reserved for cases where other options are unsuitable. Early initiation, within five days of symptom onset, is highly recommended to achieve optimal outcomes (IDSA, 2024; EMA, 2024).

3.4.3.2 Host-Targeting Antivirals (HTAs)

HTAs act on cellular processes exploited by SARS-CoV-2 and are theoretically more resistant to acquiring resistance (Focosi *et al*., 2024). Based on their mechanism of action, HTAs can be grouped according to the specific host pathways they modulate, including viral entry, innate immune activation, and cellular metabolism.

Entry inhibitors: TMPRSS2 inhibitors, such as camostat and nafamostat, block S protein priming and membrane fusion but have not demonstrated clinically effective. Similarly, drugs targeting endosomal acidification, including chloroquine and hydroxychloroquine, were ineffective and have been discontinued (WHO Solidarity Trial Consortium, 2022).

Innate immune modulators: Interferon-β inhalation was investigated to restore antiviral innate immunity in vulnerable patients. While a few studies showed increased viral clearance, benefits for clinical outcomes were inconsistent, excluding regulatory approval.

Metabolic inhibitors: Dihydroorotate Dehydrogenase (DHODH) inhibitors and other agents targeting nucleotide biosynthesis are currently undergoing early-phase clinical trials as of 2025.

At present, international guidelines do not recommend HTAs for standard treatment due to the lack of durable efficacy in randomized trials (IDSA, 2024; WHO, 2024). Their use remains confined to research.

3.5 SARS-CoV-2 genome evolution

The COVID-19 pandemic has offered a unique opportunity to observe viral evolution in real time. With millions of SARS-CoV-2 genomes sequenced, researchers have been able to track the emergence of different lineages noting changes in transmissibility, virulence and immune evasion. This unprecedented amount of genomic data has made SARS-CoV-2 a valuable model for studying RNA virus evolution at both the molecular and population levels (Markov *et al*., 2023).

Like many RNA viruses, SARS-CoV-2 mutates relatively rapidly. However, it possesses an error-correcting exonuclease, which lowers its mutation rate compared to most other RNA viruses. It's important to distinguish between two related concepts: the mutation rate, which refers to the number of errors introduced during replication, and the substitution rate, which reflects how many of those changes become fixed in the population. Early in the pandemic, the substitution rate was estimated at approximately 1×10^{-3} substitutions per site per year, similarly to that of other coronaviruses. This rate, however, is not uniform across the genome. Certain regions evolve faster than others due to selective pressures. Deleterious mutations are usually removed through purifying selection, while advantageous mutations tend to spread more rapidly (Markov *et al*., 2023).

The evolution of SARS-CoV-2 is shaped by a combination of molecular, epidemiological, and environmental factors. Molecularly, SARS-CoV-2 accumulates point mutations over time, with a strong predominance of cytosine-to-uracil (C→U) substitutions primarily induced by activity of host APOBEC enzymes. Most of the changes are deleterious or neutral and preferentially disappear by purifying selection. However, occasionally, some mutations are beneficial, increasing viral replication efficiency or reducing recognition by the host immune system (Markov *et al*., 2023). Natural selection subsequently operates on these mutations and selects for those that enhance viral fitness. The adaptive mutations that enhance transmissibility or immune evasion are particularly favorable. Substitution at N501Y, for instance, enhances S protein-ACE2 receptor binding affinity, while E484K and other mutations prefer antibody escape. Selective pressure acts both at individual hosts level, where the virus adapts to immune responses, and between hosts, favoring variants with enhanced transmissibility across populations. In addition to natural selection, stochastic processes such as genetic bottlenecks and genetic drift play important roles in driving SARS-CoV-2 evolution. Each new infection is typically initiated by only a few viral particles, creating a bottleneck in which chance determines which variants establish infection. Consequently, some lineages may become dominant not because they are better adapted, but due to random events such as founder effects or superspreading events. Prolonged infection in immunocompromised hosts represents another critical factor. While infections are usually cleared within weeks in most individuals, the virus can persist for months in these hosts, replicating under partial immune pressure. Such conditions favor the accumulation of adaptive mutations, including those conferring antibody resistance or enhanced receptor binding. It is widely hypothesized that major VOCs, including Alpha and Omicron, originated from long-term infections in immunocompromised individuals, which act as evolutionary incubators for viral diversification (Markov *et al.*, 2023). Recombination further contributes to SARS-CoV-2's genetic complexity. When an individual is co-infected with multiple viral lineages, RNA segments can be exchanged, generating hybrid viruses with novel combinations of mutations. This mechanism has been observed with the emergence of the recombinant lineage XBB, which combined immune-escape mutations from different Omicron subvariants and rapidly gained transmission advantage (Markov *et al.,* 2023).

Over the course of the pandemic, several VOCs have emerged. These lineages significantly changed the pandemic's trajectory due to higher transmissibility, immune escape, or increased severity.

- Alpha (B.1.1.7, UK, late 2020): acquired N501Y and P681H mutations, spread faster than earlier lineages, and quickly became dominant worldwide.
- Beta (B.1.351, South Africa, late 2020): acquired K417N, E484K, and N501Y mutations, which reduced vaccine-induced antibody neutralization.
- Gamma (P.1, Brazil, early 2021): shared several key mutations with Beta, leading to an increased rate of reinfections and immune escape.

- Delta (B.1.617.2, India, mid-2021): acquired L452R and P681R mutations, showing very high transmissibility, and causing more severe disease. It dominated globally before Omicron.
- Omicron (BA.1, South Africa, late 2021): acquired over 30 spike mutations, leading to strong immune evasion but generally milder disease. Its sublineages (BA.2, BA.5, XBB, JN.1, KP.*) continued to evolve, often converging on similar spike protein changes (Guo *et al*., 2024).

Omicron marked a significant shift in the pandemic. According to Guo *et al.* (2024), it combined strong immune escape with altered tissue tropism, replicating more efficiently in the upper airways rather than in deep lung tissue. This likely explain why Omicron spread more rapidly but generally caused less severe disease compared to Delta. The continual emergence of Omicron sublineages, many sharing similar immune escape mutations, shows how rapidly SARS-CoV-2 can adapt. These changes have rendered most mAbs therapies ineffective, emphasizing the need for more durable countermeasures, such as ACE2-based drugs that target conserved viral proteins less prone to mutations.

4 Evaluation of broad-spectrum piperazine-based compounds as inhibitors of flavivirus and/or SARS-COV-2 replication in a live virus assay.

4.1 Background

Despite extensive research efforts, no specific antiviral therapy is currently available for infections caused by ZIKV or DENV, both flaviviruses. Similarly, although the COVID-19 pandemic has prompted unprecedented global research activity, only two antiviral drugs, RDV and NRM, has been approved to date for the treatment of SARS-CoV-2 infection. The limited availability of existing antiviral drugs highlights the necessity to find new compounds with broad-spectrum activity against RNA viruses, including flaviviruses and coronaviruses, that remain a serious threat to world public health. In recent years, among the new antiviral scaffolds, the piperazine derivatives have been of great attention because they possess conformational flexibility as well as broad-spectrum biological activities. The piperazine scaffold, which consists of a six-membered heterocycle with two nitrogen atoms in opposite positions, is highly prone to chemical modification, with which pharmacokinetic and pharmacodynamic properties can be optimized. Originally found as antiparasitic agents, piperazine-based compounds have been altered for improving their bioactivity and specificity towards multiple viral targets. Their mechanism may involve inhibition of viral entry, replication, or assembly, often by binding to essential viral enzymes or cellular factors employed by the virus during its replication cycle. Studies have demonstrated antiviral activity of piperazine derivatives against different families of viruses. For example, Mazzotta *et al.* (2020) and Sánchez-Céspedes *et al.* (2016)

revealed that certain piperazine derivatives inhibited human adenovirus replication *in vitro* by interfering with viral processes, whereas Bassetto *et al.* (2017) reported HCV NS3 helicase subunit inhibition leading to defective viral replication. Additional studies by Kounde *et al.* (2017) demonstrated that piperazine derivatives can inhibit DENV replication by binding to non-structural viral proteins, while Gao *et al.* (2023) reported piperazine analogues targeting viral polymerases with broad-spectrum inhibitory activity. Later, Ji *et al.* (2024) developed ZIKV-active piperazine derivatives with the ability to cross the blood–brain barrier—a very important feature in the management of ZIKV neurological sequelae. In the framework of this field of research, in our laboratory of the Virology Unit of the University of Siena, we had already screened a library of 34 small molecules derived from piperazine for their potential to become *Flaviviridae* NS3 protease inhibitors (Del Rosario García-Lozano *et al*., 2023). Among them, two lead compounds exhibited broad-spectrum activity against both ZIKV and DENV in the low micromolar range, with good cytotoxicity profiles. Molecular docking analyses confirmed specific interactions within the active site of NS3 proteases. This protein represents a valuable antiviral target, being well conserved across flaviviruses and structurally preserved despite differences in cofactor usage (NS2B for ZIKV/DENV and NS4A for HCV) (Winkler, 2024). The antiviral activity of piperazine derivatives has also been described towards coronaviruses. Biochemical and computational studies have revealed piperazine derivatives that can target SARS-CoV-2 3CLpro and RdRp and accordingly interfere with key steps of viral replication (Choudhury *et al*., 2021; Sencanski *et al*., 2022). Other studies have shown that piperazine-containing molecules can disrupt spike-ACE2 interactions, thereby suppressing viral entry and infectivity (Kumar *et al*., 2023). These findings suggest that the piperazine scaffold represents a valuable platform for the design of cross-family antiviral agents targeting conserved viral processes shared by flaviviruses and coronaviruses. Based on these findings, a new collaborative project was initiated with the Chemical Unit of the University of Seville to further optimize the lead molecules through a privileged structure-based design approach (Cavallaro *et al*., 2023). The subsequent series of compounds retained the piperazine scaffold while introducing strategic modifications aimed at enhancing potency, selectivity, and drug-like stability. The aim of the present study was to evaluate the *in vitro* antiviral activity of this novel library of piperazine-derived compounds against ZIKV, DENV, and SARS-CoV-2 in live virus cell-based assays, in order to identify potential broad-spectrum inhibitors with activity against multiple clinical relevant RNA viruses.

4.2 Material and Methods

4.2.1 Candidate antivirals and reference compounds

The family of candidate molecular prototypes (CMPs) evaluated in this study was synthesized by our collaborators at the Department of Organic and Medicinal Chemistry, University of Seville (Spain). This work builds on our previous collaborative efforts which led to the identification of two piperazine-based lead compounds showing significant antiviral activity against flaviviruses.

Building on these leads, a new series of 22 related CMPs (CMP 1–22) was designed to investigate structure-activity relationships and to optimize antiviral potency while maintaining low cytotoxicity. The piperazine ring was preserved as the central structural core and selectively functionalized at both nitrogen atoms. To accomplish this, one nitrogen was temporarily protected with a tert-butyloxycarbonyl (Boc) group, a commonly used protecting group that prevents undesired side reactions, thus allowing selective modification of the second nitrogen. After the desired acylation step, the Boc group was removed to enable further functionalization of the molecule.

The synthetic route therefore comprised two key steps:

1. N-acylation of Boc-protected piperazine to introduce the acyl substituent;
2. Deprotection and subsequent functionalization of the free nitrogen with aromatic isocyanates or sulfonyl chlorides to yield urea and sulphonamide derivatives under room temperature conditions.

All compounds were obtained as purified powders and dissolved in dimethyl sulfoxide (DMSO) to prepare stock solutions at 10 mM or 20 mM, depending on their solubility. Sofosbuvir (SOF; MedChem Express, cat. HY-15005) and NRM (Sigma/Merck, cat: SML3313) were used as a reference antiviral compounds and prepared at a working concentrations of 20 mM and 10 mM in DMSO, respectively (Table. 2). The compounds investigated in this study were synthesized by the Chemical Unit of the University of Seville according to their previously established procedures and were provided to our laboratory for antiviral evaluation.

CMP	MW (g/M)	Suspended in DMSO (mM)
1	237.3	20
2	348.4	20
3	388.5	20
4	446.8	20
5	469.8	20
6	435.2	20
7	369.4	20
8	427.5	20
9	436.1	20
10	467.9	20
11	366.2	20
12	464.9	20

13	487.9	20
14	509.9	20
15	340.8	20
16	382.5	20
17	368.4	20
18	282.3	20
19	443.6	20
20	485.9	20
21	466.6	20
22	268.3	10
SOF	529.6	20
NRM	499.5	10

Table 2: *Molecular weight (MW) and working concentration of the resuspended CMPs tested*

4.2.2 Cell cultures

A549 ACE2-TMPRSS2 (A549-AT) cell line (National Institute for Biological Standards and Control [NIBSC] 101006) is an adherent human alveolar basal epithelial adenocarcinoma cell line. The parental A549 cells were transduced to express human ACE2, selected with hygromycin B, and subsequently cloned. Clone 8 was further transduced to express human TMPRSS2 and selected with hygromycin B and geneticin, resulting in a pool of hygromycin and neomycin resistant cells highly susceptible to SARS-CoV-2 infection. A549-AT cells were cultured in F-12K Nutrient Mix medium (Gibco™) supplemented with 10% heat-inactivated foetal bovine serum (FBS), 2 mM L-glutamine, 2 mg/ml geneticin (G418), 200 µg/ml hygromycin B, and 1% penicillin/streptomycin (PS, Euroclone). These selection antibiotics maintain stable expression of ACE2 and TMPRSS2, ensuring that only cells retaining these constructs survive, thereby maintaining a consistent culture suitable for SARS-CoV-2 infection assays. A549-AT cells were used for *in vitro* cytotoxicity assays and for the antiviral testing of CMPs. VERO E6 (ATCC® CRL-1586) is an adherent immortalized cell line derived from kidney epithelial cells of the African green monkey. This cell line was used for the propagation of DENV and SARS-CoV-2. Huh7, provided by the "Istituto Toscano Tumori, Core Research Laboratory" (Siena, Italy), is an adherent immortalized human hepatoma cell line originally estabilished in 1982. Huh7 cells were used for *in vitro* cytotoxicity assays, antiviral testing of candidate compounds, and for the expansion and titration of ZIKV. Both VERO E6 and Huh7 cells were cultured in DMEM High Glucose (Euroclone) supplemented with 10% FBS (Euroclone) and 1% PS (Euroclone). All cells were passaged at 70–90% confluence and maintained at 37°C in a humidified 5% CO_2 incubator.

4.2.3 Virus stocks expansion and titration

ZIKV H/PF/2013 Asiatic strain, and DENV New Guinea C, serotype 2 strain, were provided by the Istituto Superiore della Sanità (Rome, Italy) while the EU wild type (D614G) SARS-CoV-2 strain was provided by the Luigi Sacco Hospital (Milan, Italy). To expand the viruses, 2.5×10^5 cells of the appropriate cell line (VERO E6 for DENV or Huh7 for ZIKV) were seeded in T75 flasks (75 cm^2) with 20 mL of propagation medium one day prior to infection. This seeding density allowed cells to reach 50–80% confluence at the time of infection. Flasks were maintained in a humidified incubator at 37°C with 5% CO_2. The infection medium was the same as the propagation medium but supplemented with 1% FBS. The day of infection, after confirming 70–80% cell confluence, viral stocks were diluted in infection medium to a final volume of 5 mL and added to the cells. To promote virus adsorption, flasks were incubated for 1 h at 37°C with 5% CO_2, after which 15 mL of infection medium was added. Infected cells were incubated for 72 h, after which supernatants were collected and subjected to a freeze-thaw cycle to increase viral titer by lysing the cells, followed by centrifugation at 1,300 × g for 30 min to remove cell debris. Viral stocks were stored at –80°C until titration. SARS-CoV-2 was expanded in VERO E6 cells following the same procedure used for ZIKV and DENV. Viral titers were determined as tissue culture infectious doses per milliliter ($TCID_{50}$/mL), defined as the dilution of viral stock required to infect 50% of a given cell culture (Lei *et al*., 2020). For ZIKV and DENV, titration was performed by immunodetection assay (IA). Six replicates of 2-fold serial dilutions, starting from 1:50, were transferred to 96-well plates containing 6,000 pre-seeded Huh7 cells per well and incubated for 72 h at 37°C with 5% CO_2. Mock-infected wells were included to normalize results. Cells were fixed with 10% formaldehyde (Carlo Erba Chemicals) for 20 min, rinsed with PBS, permeabilized with 1% Triton X-100 (Carlo Erba Chemicals) for 20 min, and blocked with 3% Bovine Serum Albumin (BSA, Sigma-Merck) for 30 min. After washing with PBS containing 0.05% Tween 20 (Carlo Erba Chemicals), cells were incubated for 1 h with a monoclonal anti-flavivirus mouse antibody (clone D1-4G2-4-15; Novus Biologicals) diluted 1:400 in blocking buffer (PBS containing 1% BSA and 0.1% Tween 20), washed four times, and incubated for 1 h with a HRP-conjugated anti-mouse IgG secondary antibody (Novus Biologicals) diluted 1:10,000 in blocking buffer. Following five washes, 3,3',5,5'-tetramethylbenzidine substrate (TMB, Life Technologies) was added, incubated for 5 min in the dark, and the reaction was stopped with 0.5 M sulfuric acid (Carlo Erba). Absorbance at 450 nm (OD450) was measured with a GloMax Discover Multimode Microplate Reader and adjusted by subtracting the background (twofold the mean OD450 of mock wells). TCID50 values were calculated using the Reed and Muench method. For SARS-CoV-2, viral stocks were titrated in A549-AT cells. Six replicates of 5-fold serial dilutions, starting from 1:50, were added to 96-well plates containing 6,000 pre-seeded A549-AT cells per well and incubated for 96 h at 37°C with 5% CO_2. Uninfected cell controls were included in each plate. Cell viability and $TCID_{50}$ were assessed using the CellTiter-Glo 2.0 Luminescent Cell Viability Assay (Promega), an ATP-based method that quantifies metabolically active cells. This assay provides a sensitive

and reliable measure of virus-induced cytopathic effects. Briefly, the supernatant was removed from each well and a volume (60µl) of Cell-Titer-Glo 2.0 reagent was added. Plates were then placed on an orbital shaker at 400 rpm for 10 minutes at room temperature to induce cell lysis. The resulting lysates were transferred to white 96-well plates and luminescence was measured using the GloMax Discover Microplate Reader. The luminescent signal generated is directly proportional to the amount of ATP present, providing a quantitative and reproducible measure of cell viability and so giving a measure of virus-induced cytopathic effects. All virus propagation and infection procedures were carried out in BSL3.

4.2.4 Determination of CMPs cytotoxic concentration

To determine the cytotoxicity of each CMPs, Huh7 and A549-AT cells were seeded at 6,000 cells/well in tissue culture-treated 96-well plates and allowed to adhere overnight. Serial six-point 4-fold dilutions of CMPs in infection medium, starting from 200 µM, were then added to the cells. After 72 hours of incubation for Huh-7 cells and 96 hours for A549-AT cells at 37°C with 5% CO_2, cell viability was assessed using the Cell-Titer-Glo 2.0 Luminescent Cell Viability Assay (Promega) according to the manufacturer's protocol. The luminescent signal generated by cells treated with the tested CMPs was compared with that generated by cells treated with DMSO vehicle control to determine the half-maximal cytotoxic concentration (CC_{50}) and the concentration causing 10% cell death (CC_{10}). CC_{50} is defined as the compound concentration that reduces cell viability by 50% compared to untreated controls, while CC_{10} represents the concentration that causes 10% reduction in cell viability relative to controls. Results were normalized with a death control (100% DMSO, 0% cell viability) and a cell control (100% cell viability). The cytotoxicity assay was performed in duplicate across two independent experiments.

Raw data were analyzed using GraphPad Prism software version 10.4.0, generating dose-response curves that were used to extrapolate both the CC_{50} and CC_{10} of each CMP through non-linear regression analysis (Fig. 7).

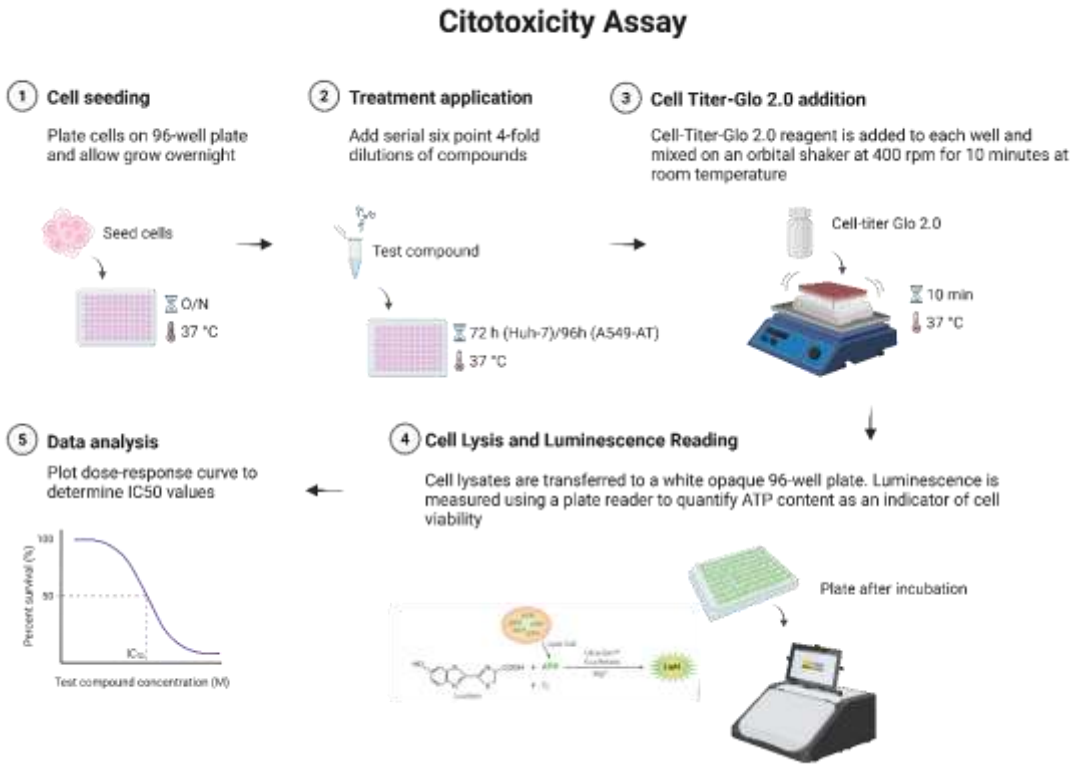

Figure 7: *Cytotoxicity assay workflow (Created in https://BioRender.com)*

4.2.5 Antiviral assay

The antiviral activity of the candidate CMPs was evaluated using a direct yield reduction assay, in which cells were infected in the presence of serial dilutions of each compound. For DENV and ZIKV, antiviral efficacy was determined by quantifying the inhibition of viral envelope protein production using the IA previously described for viral titration. For SARS-CoV-2, antiviral activity was assessed indirectly through cell viability measurements, used as a surrogate for the viral cytopathic effect (CPE). Infection assays were performed using Huh-7 cells for DENV and ZIKV (Figure 8) and A549-ACE2 cells for SARS-CoV-2.

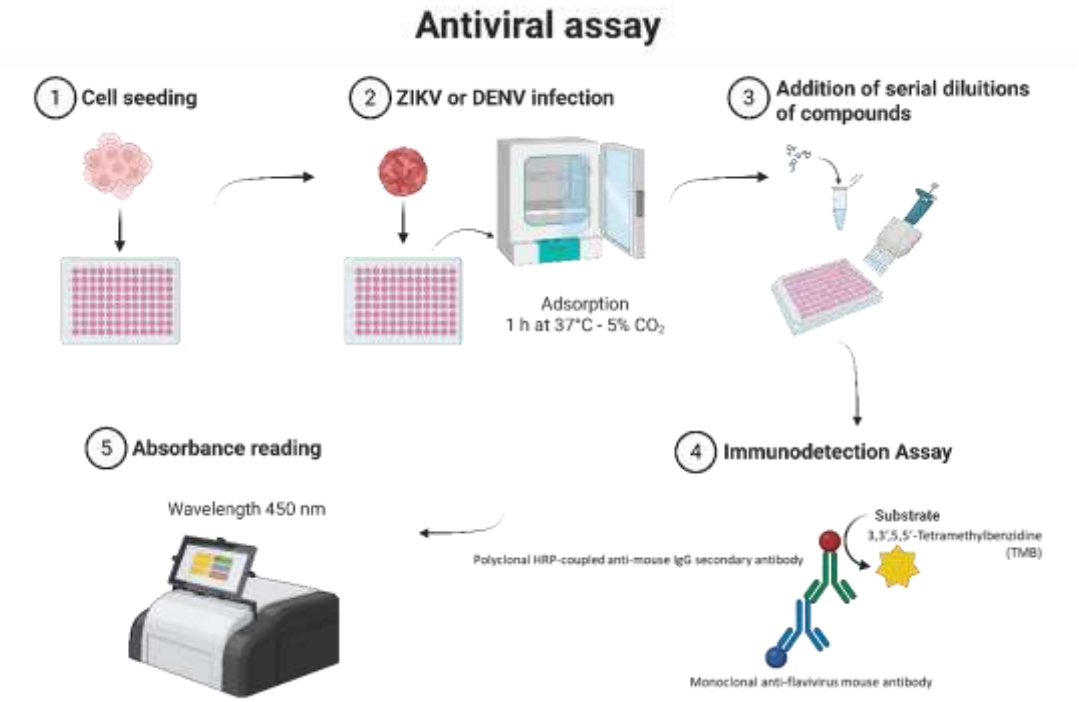

Figure 8: *Workflow of the anti-flavivirus assay (Created in https://BioRender.com)*

Cells were seeded at a density of 6,000 cells per well in tissue culture-treated 96-well plates and allowed to adhere overnight. Cells were then infected with DENV or ZIKV at a multiplicity of infection (MOI) of 0.02, corresponding to 200 $TCID_{50}$ per well, based on titers determined by the Reed and Muench method. Viral adsorption was carried out for 1 hour at 37°C in a 5% CO_2 atmosphere. After removing the inoculum, six-point, four-fold serial dilutions of each CMP were added, starting from the maximum non-toxic concentration determined in the cytotoxicity assay. The plates were incubated for 72 hours under the same conditions. At the end of the incubation period, cells were fixed, and the IA was performed as described in Section 4.2.3. To evaluate antiviral activity against SARS-CoV-2, a similar approach was followed using A549-AT cells. Cells were seeded at 6,000 cells per well in 96-well plates and allowed to adhere overnight. Cells were then infected with SARS-CoV-2 at an MOI of 0.005 (equivalent to 60 $TCID_{50}$ per well) in the presence of six-point, four-fold serial dilutions of each CMP, starting from the maximum non-toxic concentration previously determined. No viral adsorption step was included in this assay. After 96 hours of incubation at 37°C with 5% CO_2, cell viability was assessed using the CellTiter-Glo® 2.0 Luminescent Cell Viability Assay (Promega), as described in Section 4.2.3.

For all assays, a four-fold serial dilution of SOF was included as a reference antiviral compound for DENV and ZIKV, while NRM was used as the reference compound for SARS-CoV-2. Infected untreated cells (viral control) and uninfected cells (cell control) were included to represent 0% and 100% cell viability, respectively, for data normalization (Figure 9). Each compound concentration was tested in duplicate across two independent experiments. The half-maximal inhibitory concentration (IC_{50}) of each CMP was calculated through non-linear

regression analysis with a variable slope (four parameters) model of the dose-response curves generated

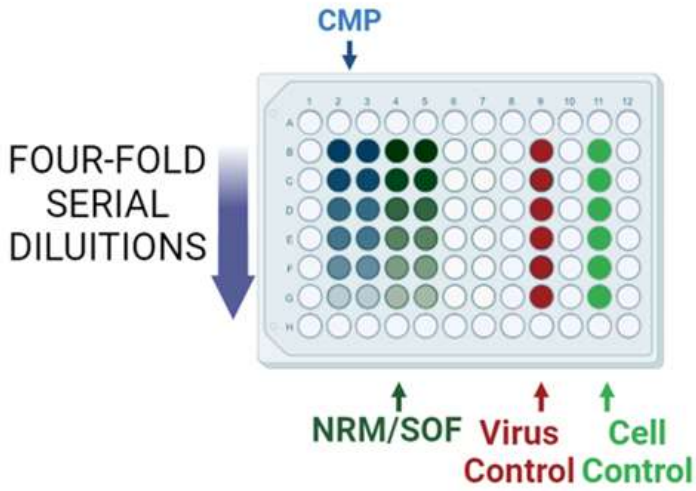

Figure 9: *Antiviral assay performed in 96 wells plate*

using GraphPad Prism software version 10.4.0. IC_{50} is defined as the compound concentration that inhibits viral replication by 50% compared to untreated infected controls.

4.3 Results and Discussion

4.3.1 CMPs cytotoxicity

Most of the tested compounds showed low cytotoxicity in both cell lines, with CC_{50} values above 200 µM. In particular, compounds 1, 2, 3, 8, 11, 14, and 15 exhibited CC_{50} > 200 µM in both cell lines, indicating a favorable safety profile, as summarized in Table 3.

Some compounds displayed moderate cytotoxicity with distinct profiles between the two cell lines. Compound 4 showed similar cytotoxicity in both lines (CC_{50} = 32 µM in HuH-7 and 30 µM in A549-AT), whereas compound 7 exhibited higher cytotoxicity in HuH-7 cells (CC_{50} = 15 µM) compared to A549-AT (CC_{50} = 133 µM).

Compounds 16 and 17 exhibited comparable CC_{50} values in both cell lines (52 vs. 57 µM and 51 vs. 91 µM, respectively).

Interestingly, several compounds displayed selective cytotoxicity toward one of the two cell lines. Compound 5 was more cytotoxic to A549-AT cells (CC_{50} = 109 µM) than to HuH-7 cells (CC_{50} > 200 µM). Similarly, compounds 12, 13, 20, 21, and 22 showed higher cytotoxicity toward the A549-AT cell line.

CC_{50} (µM)		
CMP	**HUH-7**	**A549-AT**
1	> 200	> 200
2	> 200	> 200
3	> 200	> 200
4	32	30
5	> 200	109
6	182	95
7	15	133
8	> 200	200
9	53	21
10	156	84
11	> 200	> 200
12	> 200	188
13	> 200	29
14	> 200	> 200
15	> 200	> 200
16	52	57
17	51	91
18	182	125
19	133	127
20	> 200	151
21	> 200	170
22	> 200	118
SOF	> 200	-
NRM	-	40

***Table 3**: Cytotoxicity results*

Among the tested compounds, CMP 7 exhibited marked cytotoxicity, and was therefore excluded from subsequent antiviral assays. As illustrated in Figure 10, dose–response analysis revealed a CC_{50} of 15 µM and a CC_{10} of 3 µM in HuH-7 cells, indicating substantial toxicity even at relatively low concentrations. In contrast, when tested in A549-AT cells, CMP 7

displayed a milder cytotoxic profile, cell viability remained above 80% up to 10 µM and decreased to approximately 40% at 100 µM (CC_{50} = 133 µM). Conversely, CMP 14 exhibited no evident cytotoxicity and demonstrated a favorable safety profile, as shown in Figure 11. Across the entire concentration range tested, cell viability remained above 80–90% in both HuH-7 and A549-AT cells, with only minor reductions observed at the highest concentrations (200 µM). Throughout all experiments, DMSO vehicle control maintained cell viability close to 100% at the different concentration tested, confirming that no cytotoxic effects were associated with the solvent.

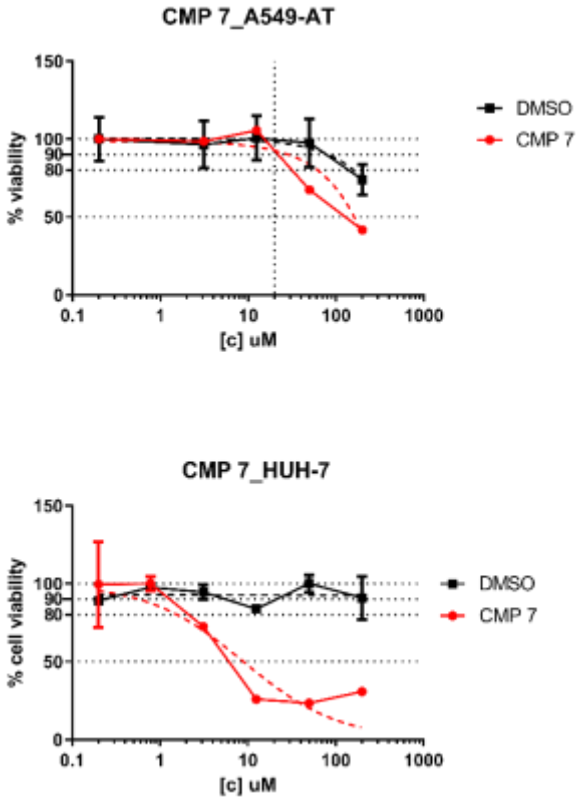

***Figure 10**: Dose-response cytotoxicity curves of CMP 7 in A549-AT and HuH-7 cell lines*

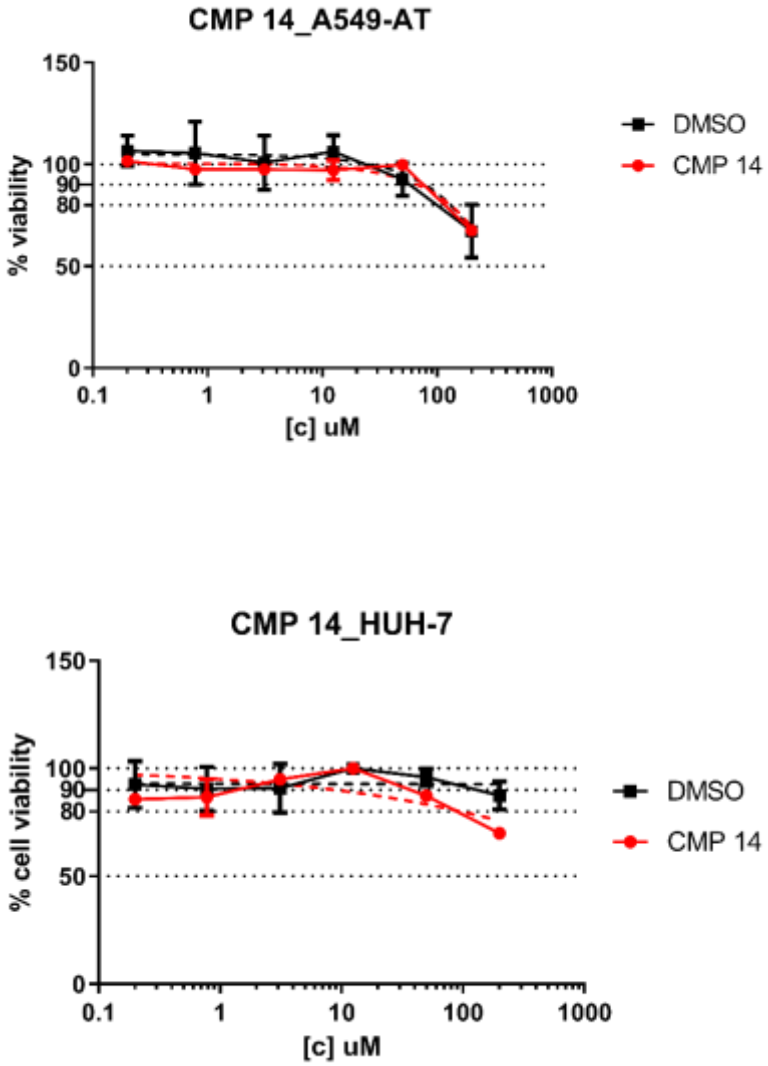

***Figure 11**: Dose-response cytotoxicity curves of CMP 14 in A549-AT and HuH-7 cell lines*

4.3.2 CMPs antiviral activity

The antiviral activity of the synthesized compounds was evaluated against three viruses: ZIKV, DENV and SARS-CoV-2. The IC_{50} reported in the table (Table 4) was calculated as an average between two independent experiments. Among the 22 compounds tested, several displayed promising antiviral activity against at least one of the target viruses. Compounds active against ZIKV displayed IC_{50} values ranging from 1.6 to 48.1 µM; only these ZIKV-active compounds were subsequently evaluated against DENV, where several retained comparable inhibitory effects. Notably, a single compound (CMP 21) showed measurable activity against SARS-CoV-2, while also being active against ZIKV, suggesting a potential broad-spectrum antiviral profile. The reference compounds NRM and SOF were included as positive controls to validate the experimental setup.

A considerable number of compounds (1–4, 16–19, 22) were not active (NA) toward any of the tested viruses.

Table 4: *CMPs activity results against ZIKV, DENV and SARS-CoV-2 expressed as micromolar concentration (μM). Abbreviations; NA: non active, NT: not tested, SD: Standard deviation.*

	ZIKV		DENV		SARS-CoV-2	
CMP	**Activity**	**IC50 (μM) ± SD**	**Activity**	**IC50 (μM) ± SD**	**Activity**	**IC50 (μM) ± SD**
1	NA		NT		NA	
2	NA		NT		NA	
3	NA		NT		NA	
4	NA		NT		NA	
5	Active	27.9 ± 5.3	NA		NA	
6	Active	48.1 ± 0.3	Active	67.9 ± 5.4	NA	
7	NT		NT		NA	
8	Active	38.7 ± 0.7	NA		NA	
9	Active	5.1 ± 0.0	NA		NA	
10	Active	13.2 ± 0.4	Active	33.8 ± 3.3	NA	
11	NA		NT		NA	
12	Active	4.6 ± 0.7	Active	11.7 ± 2.2	NA	
13	Active	1.6 ± 0.0	Active	3.8 ± 0.7	NA	
14	Active	125.3 ± 0.6	NA		NA	
15	Active	43.7 ± 3.6	NA		NA	
16	NA		NT		NA	
17	NA		NT		NA	
18	NA		NT		NA	
19	NA		NT		NA	
20	Active	3.2 ± 0.9	NA		NA	
21	Active	2.7 ± 0.7	NA		Active	22.5 ± 1.5
22	NA		NT		NA	
SOF	Active	3.7 ± 5.5	Active	4.3 ± 1.4	NT	
NRM	NT				Active	0.04 ± 0.00

4.3.3 Activity against ZIKV

Ten compounds exhibited significant anti-ZIKV activity with IC_{50} values ranging from 1.6 to 48.1 µM. CMP 13 was the most potent compound (IC_{50} = 1.6 ± 0.0 µM), showing superior activity compared to the reference compound SOF (IC_{50} = 3.7 ± 5.5 µM). As illustrated in Figure 12, CMP 13 exhibited consistent dose-dependent inhibition across both independent experiments, with viral replication decreasing progressively to near-complete inhibition at 10 µM.

CMP 20 (IC_{50} = 3.2 ± 0.9 µM), CMP 21 (IC_{50} = 2.7 ± 0.7 µM), CMP 12 (IC_{50} = 4.6 ± 0.7 µM), and CMP 9 (IC_{50} = 5.1 ± 0.0 µM) also showed potent anti-ZIKV activity comparable to SOF (Figure 12).

Compounds with moderate activity included CMP 10 (IC_{50} = 13.2 ± 0.4 µM), CMP 5 (IC_{50} = 27.9 ± 5.3 µM), CMP 8 (IC_{50} = 38.7 ± 0.7 µM), CMP 15 (IC_{50} = 43.7 ± 3.6 µM), and CMP 6 (IC_{50} = 48.1 ± 0.3 µM). CMP 14 showed weaker activity, with an IC_{50} of 125.3 ± 0.6 µM. Notably, compounds 1-4, 16-19, and 22 displayed no detectable anti-ZIKV activity, while compound 7 was not evaluated due to excessive cytotoxicity.

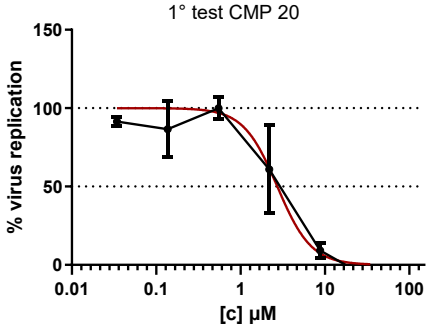
1° test CMP 20
% virus replication
150
100
50
0
0.01
0.1
1
10
100
[c] µM

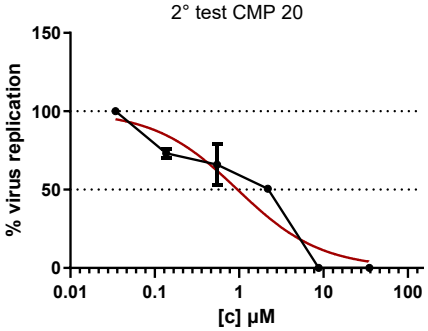
2° test CMP 20
% virus replication
150
100
50
0
0.01
0.1
1
10
100
[c] µM

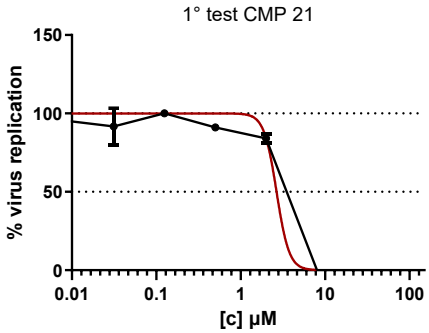
1° test CMP 21
% virus replication
150
100
50
0
0.01
0.1
1
10
100
[c] µM

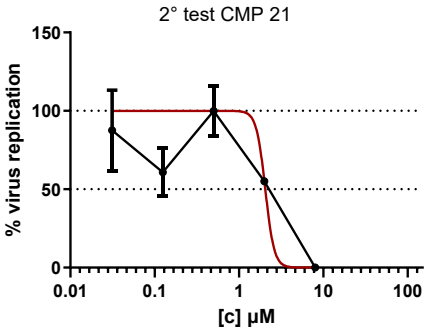
2° test CMP 21
% virus replication
150
100
50
0
0.01
0.1
1
10
100
[c] µM

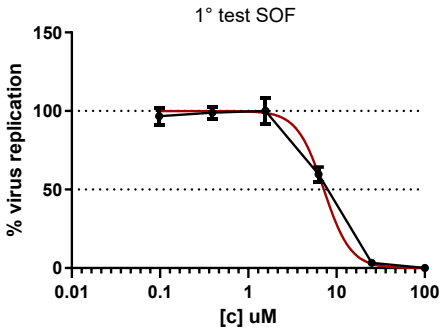
1° test SOF
% virus replication
150
100
50
0
0.01
0.1
1
10
100
[c] uM

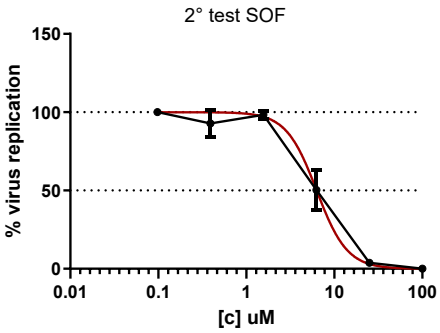
2° test SOF
% virus replication
150
100
50
0
0.01
0.1
1
10
100
[c] uM

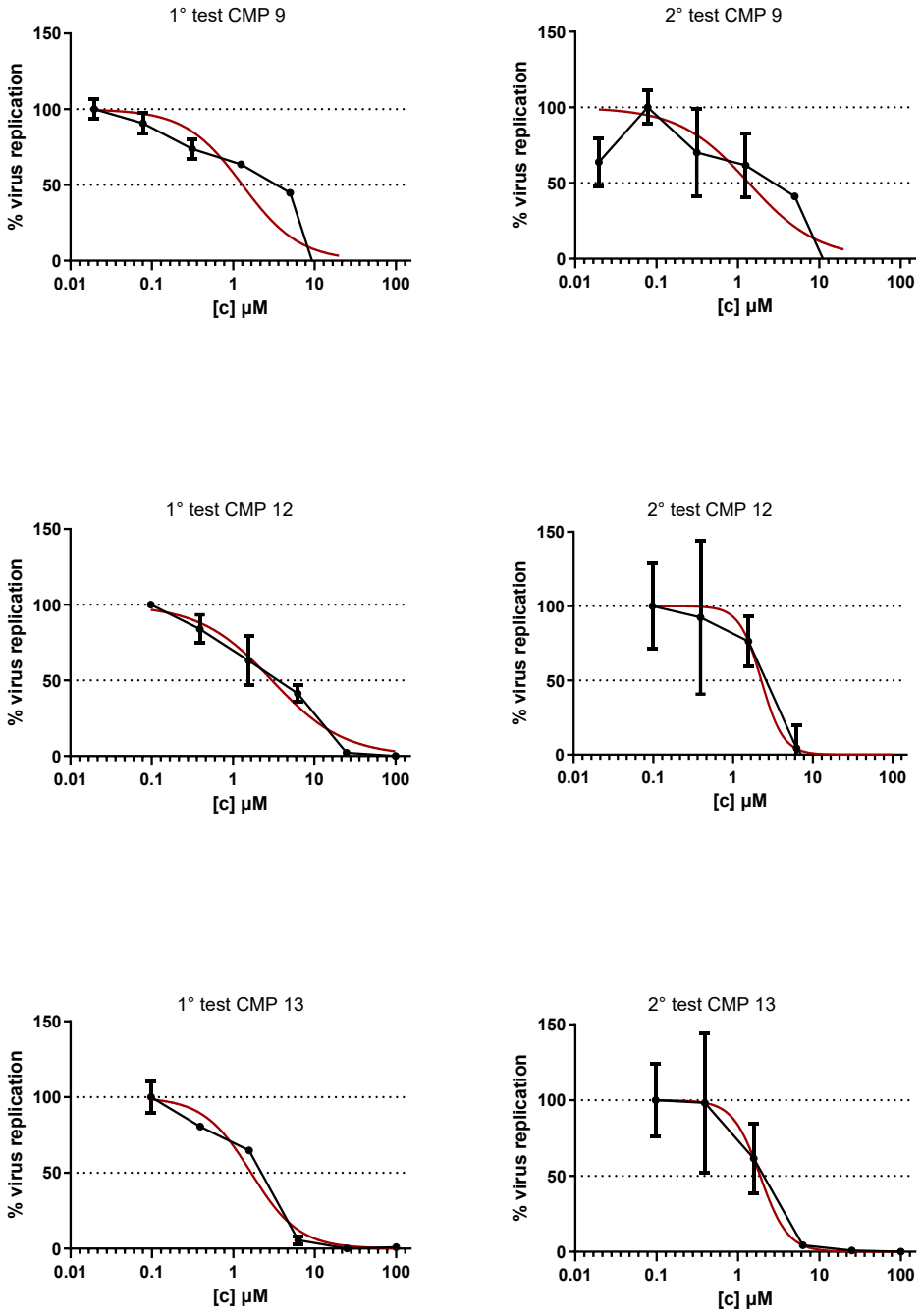

***Figure 12**: CMPs and SOF activity against ZIKV. Each CMP was tested in 2 independent experiments (left and right). Dose response curves were generated using the largest value of each dataset as the 100% of virus replication. Dose response fitting curves are indicated in red.*

4.3.4 Activity against DENV-2

Only CMPs previously identified as active against ZIKV were evaluated against DENV due to the high genetic and structural similarity between the two flaviviruses. Among the 11

tested compounds, four (CMP 6, CMP 10, CMP 12, and CMP 13) showed inhibitory activity against DENV, with dose-dependent effects confirmed in two independent experiments.

CMP 6 displayed modest antiviral activity, with measurable inhibition only at higher concentrations. CMP 10 showed a clearer dose-response trend, although with slightly reduced potency in the second experiment. CMP 12 demonstrated a more consistent and reproducible inhibitory profile across both assays.

Notably, CMP 13 emerged as the most potent compound in the series, with IC_{50} values in the low micromolar range, comparable to the SOF reference compound. This makes CMP 13 a promising candidate for further investigation. Overall, these results confirm that part of the CMP chemical series retains antiviral activity against DENV. The IC_{50} values are summarized in Table 4, and the dose-response curves of SOF and active CMPs are shown in Figure 13.

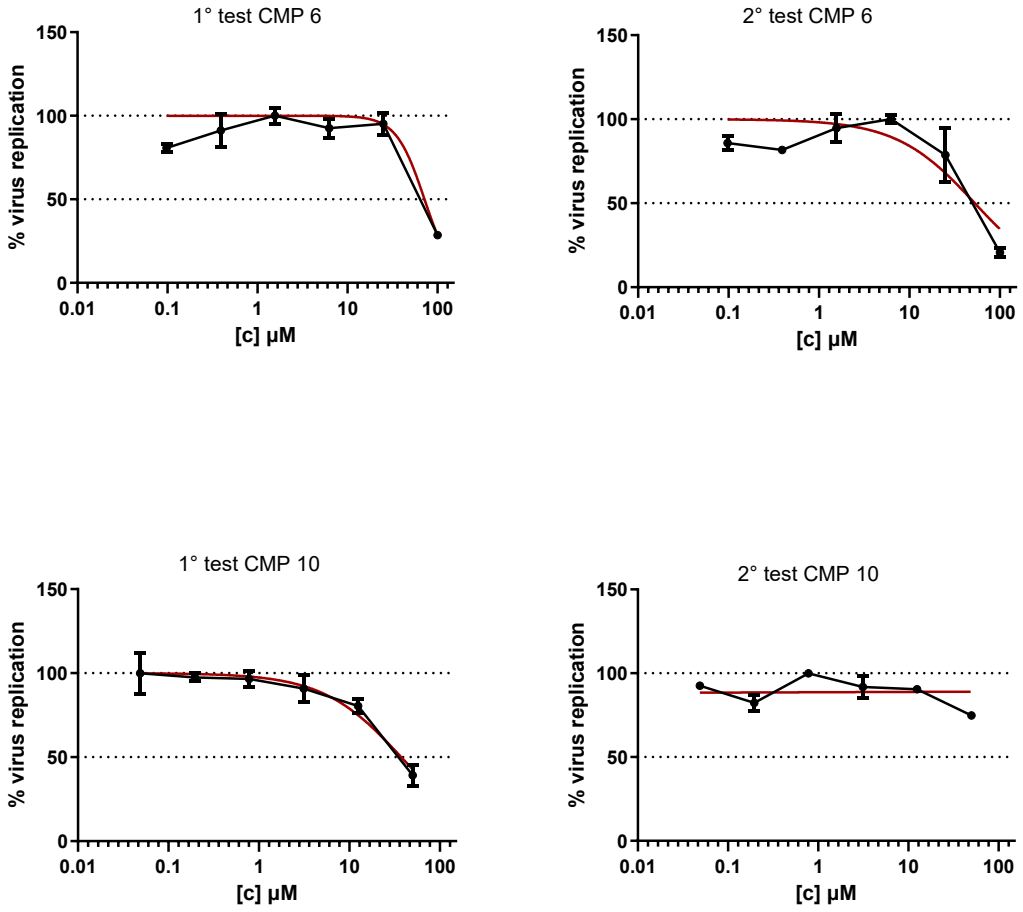

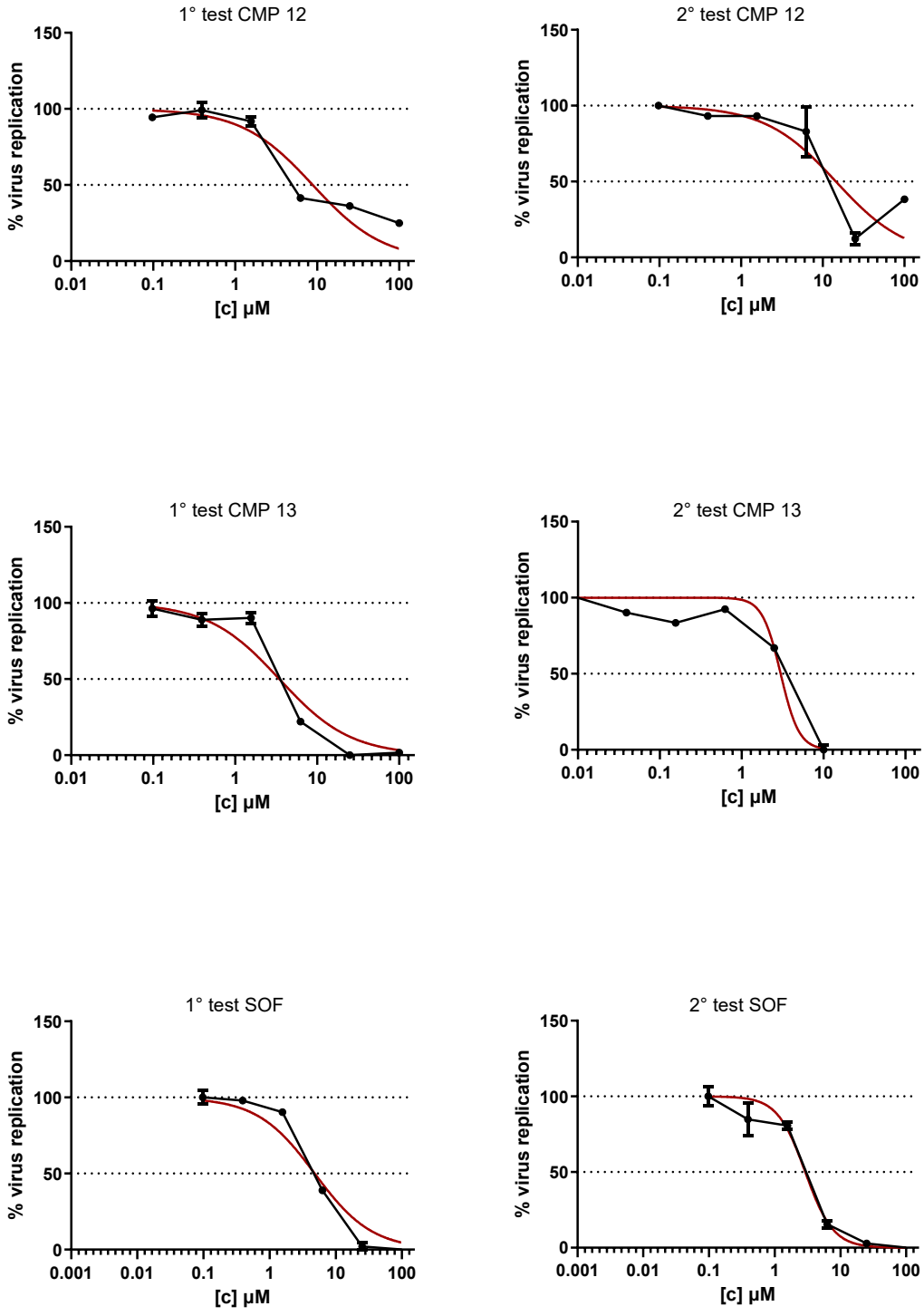

Figure 13: *CMPs activity against DENV. Each compound was tested in 2 independent experiments (left and right). Dose response curves were generated using the largest value of each dataset as the 100% of virus replication. Dose response fitting curves indicated in red.*

4.3.5 Activity against SARS-CoV-2

CMP 21 exhibited antiviral activity with an IC50 of 22.5 µM as shown in Figure 14. The compound showed a selectivity index (SI) of 7.6.

The reference compound NRM displayed markedly superior potency, with an IC_{50} of 0.04 µM (500-fold lower than the active concentration of CMP 21) while maintaining 100% cell viability across a broader concentration range, indicating significantly better potency and selectivity.

These results indicate that CMP 21 has limited antiviral activity at concentrations approaching cytotoxic levels, suggesting modest selectivity. Despite these limitations, CMP 21 could serve as a starting point for structural optimization to improve both potency and selectivity.

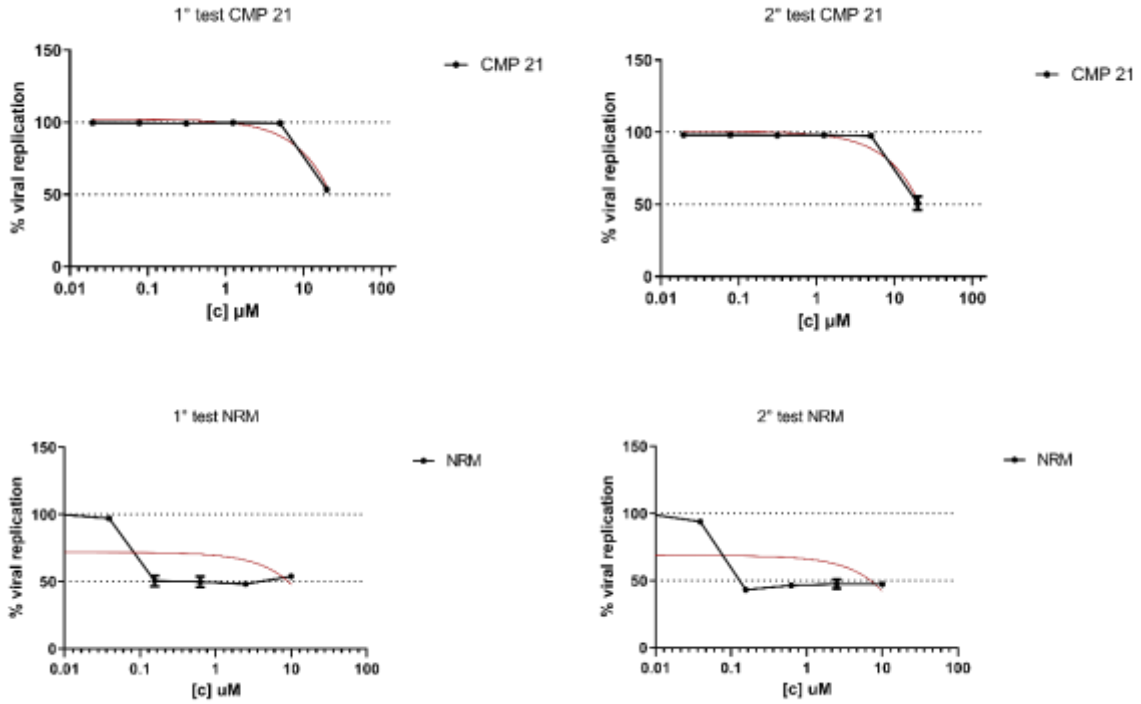

Figure 14: *Dose-response curves of CMP 21 and NRM against SARS-CoV-2.*

4.3.6 Selectivity index

The Selectivity Index (SI), defined as the ratio between CC_{50} and IC_{50}, is a key parameter for identifying promising antiviral candidates; indeed, a higher SI indicates a wider therapeutic window and a more favorable balance between efficacy and safety. Generally, SI values above 10 suggest compounds worthy of further optimization. Among the 22 CMPs tested, six (CMP 9, 10, 12, 13, 20,

and 21) showed good selectivity against ZIKV, accounting for 27.3% of the library. Notably, CMP 20 and CMP 21 exhibited very high SI values (>63.5 and >104.8, respectively), outperforming the reference drug SOF. CMP 13 also displayed a strong SI (>21.3), confirming both potency and low cytotoxicity. Against DENV, only CMP 12 and CMP 13 maintained SI values above the relevance threshold (>17.1 and >52.7, respectively). This highlights that antiviral activity against one flavivirus does not necessarily translate to another. Importantly, CMP 13 was the only compound with an SI higher than SOF against both ZIKV and DENV, making it the most promising broad-spectrum anti-flaviviral lead. In contrast, for SARS-CoV-2, only CMP 21 showed a borderline SI (7.6), remaining well below the threshold of relevance and not comparable to the reference compound NRM, which displayed a markedly higher SI. These findings indicate that CMP 21's antiviral effect against SARS-CoV-2 is limited and would require further optimization before it can be considered a viable lead.

CMP	SI ZIKV	SI DENV	SI SARS-CoV-2
1	-	-	-
2	-	-	-
3	-	-	-
4	-	-	-
5	-	-	-
6	3.8	2.7	-
7	-	-	-
8	>5.2	-	-
9	10.4	-	-
10	11.8	4.6	-
11	-	-	-
12	>43.8	>17.1	-
13	>125.0	>52.7	-
14	>1.3	-	-
15	>4.6	-	-
16	-	-	-
17	-	-	-

18	-	-	-
19	-	-	-
20	63.5	-	-
21	>104.8	-	7.6
22	-	-	-
SOF	>44	>46.5	-
NRM	-	-	1,000

***Table 5**: CMPs and reference compounds selectivity index. The symbol "-" indicates compounds that were either inactive or not tested for cytotoxicity; therefore, the selectivity index could not be calculated.*

4.4 Conclusions

The lack of specific antiviral therapies for ZIKV and DENV, together with the limited treatment options available for SARS-CoV-2, highlights the urgent need for new broad-spectrum agents targeting RNA viruses. In this study, we evaluated a library of 22 piperazine-derived compounds, designed through a privileged structure-based approach, for their antiviral activity against ZIKV, DENV, and SARS-CoV-2 using a live virus cell-based assays.

Among these molecules, 11 compounds displayed notable anti-ZIKV activity, with CMP 9, 13, 20, and 21 showing inhibition in the low micromolar range, comparable to or surpassing that of the reference compounds. Several molecules also demonstrated dual activity against both ZIKV and DENV, with CMP 13 exhibiting particularly strong cross-reactivity. This broad-spectrum effect likely reflects the high structural conservation of the NS3 protease within the Flaviviridae family, supporting the rationale for targeting conserved viral enzymes as an effective strategy for developing multi-pathogen antivirals.

In contrast, activity against SARS-CoV-2 was limited. CMP 21 exhibited only borderline antiviral activity (SI = 7.6) with efficacy detectable at 22.5 µM, approximately 500-fold less potent than the reference compound NRM (IC_{50} = 0.04 µM). These results indicate that, while the piperazine scaffold demonstrates promising activity against flaviviruses, its effectiveness against coronaviruses remains modest and will require substantial structural optimization to enhance both potency and selectivity.

The structural optimization performed by our collaborators at the University of Seville, together with molecular docking analysis revealing specific interactions with NS3 protease active sites, validates the design strategy employed. Nevertheless, cytotoxicity remains a critical concern, for example, CMP 7 was excluded due to high toxicity, underscoring the necessity of balancing antiviral efficacy with safety during compound development. Future studies should prioritize *in vivo* validation of lead compounds, particularly CMP 13 and CMP 14, which combine potent antiviral activity with favorable toxicity profiles. For neurotropic ZIKV

infections, assessment of blood-brain barrier permeability will be essential. Additionally, given the high mutation rates of RNA viruses, resistance profiling and exploration of synergistic combination therapies should be pursued to ensure long-term efficacy. For SARS-CoV-2 activity, more extensive scaffold modifications will be required to achieve clinically relevant activity.

In conclusion, this study highlights piperazine-based molecules as a valuable platform for the development of targeted antivirals against flaviviruses, with potential for broader application to other RNA viruses through rational structural optimization and a deeper mechanistic understanding of conserved viral targets.

5 Evaluation of the SARS-CoV-2 virus genetic barrier to Remdesivir and Nirmatrelvir *in vitro* and *in vivo*

5.1 Background

Since the emergence of SARS-CoV-2, the development of DAAs has represented a cornerstone in the therapeutic response to COVID-19. Among the available DAAs, RDV, an RdRp inhibitor, and NRM, a selective Mpro or 3CLpro inhibitor, are the two principal agents used in clinical practice. These compounds act by blocking essential viral enzymes involved in replication and transcription, thereby reducing viral load and disease severity when administered early during infection (Beigel *et al*., 2020; Owen *et al*., 2021). As these proteins are evolutionarily highly conserved among coronaviruses and play a crucial role in viral replication, they represent ideal targets for antiviral intervention. Although RDV and NRM have demonstrated consistent clinical efficacy and a low propensity for resistance development, the selective pressure exerted by these drugs may facilitate the emergence of mutations that decrease viral susceptibility, particularly in cases of prolonged infection or suboptimal drug exposure. The likelihood of resistance emergence depends on the so-called genetic barrier, that is, the number and nature of genetic changes that virus must accumulate to develop clinically meaningful resistance, often at the cost of its replicative capability (Dinata *et al*., 2025). Drugs with high genetic barrier require multiple simultaneous or sequential mutations, each potentially detrimental to viral fitness, making resistance events rare and often transient. In the case of RDV, *in vitro* studies have demonstrated that prolonged viral exposure can lead to the selection of specific substitutions in the RdRp, namely V792I and E802D, which are associated with reduced drug susceptibility (Vangeel *et al*., 2021). These mutations have also been sporadically observed *in vivo*, particularly in immunocompromised patients undergoing long-term RDV therapy (Martinot *et al*., 2022; Ling-Hu *et al*., 2025). However, their emergence is rare and typically associated with

impaired replication competence, indicating a substantial fitness cost that limits their persistence in circulating viral strains.

Similarly, the development of NRM resistance appears to require multiple coordinated alterations within the Mpro active site. Experimental selection studies have identified mutations such as L50F, E166A/V, and L167F which reduce NRM binding affinity and consequently increase IC_{50} values (Moghadasi *et al*., 2023). These same substitutions have been detected at low frequency in treated patients (Hu *et al*., 2023; Deschenes *et al*., 2025), suggesting that although the virus can evolve under protease inhibitor pressure, such variants exhibit reduced overall fitness and rarely sustain transmission. Structural analysis further indicated that these mutations destabilize the hydrogen-bond network implicated in NRM–Mpro interactions, thereby limiting drug binding while simultaneously compromising enzymes stability (Moghadasi *et al.*, 2023).

Overall, both *in vitro* and *in vivo* evidence indicates that SARS-CoV-2 maintains a relatively high genetic barrier to resistance against both RDV and NRM. The emergence of resistance remains uncommon and is typically confined to immunocompromised individuals with chronic viral replication, in whom prolonged drug exposure enables the gradual accumulation of adaptive mutations. Notably, most of these drug resistance mutations carry a measurable fitness cost, suggesting that, in the absence of selective drug pressure, wild-type viruses are likely to outcompete them.

The aim of this study was to evaluate the genetic barrier of SARS-CoV-2 to RDV and NRM by integrating *in vitro* resistance selection experiments with *in vivo* analysis of treated patients. Specifically, the study investigated the emergence and persistance of resistance-associated mutations and their effects on drug susceptibility and viral replication. Experiments were performed using both the ancestral B.1 lineage and the Omicron KP.3 subvariant, enabling comparison between early pandemic and currently circulating strains with distinct mutational profiles and replication dynamics.

The integration of *in vivo* longitudinal genomic data from treated individuals with *in vitro* selection experiments provides a comprehensive framework to investigate how viral mutations emerge, stabilize, or disappear under therapeutic pressure.

5.2 Materials and Methods

5.2.1 Workflow for the detection of resistance in vivo

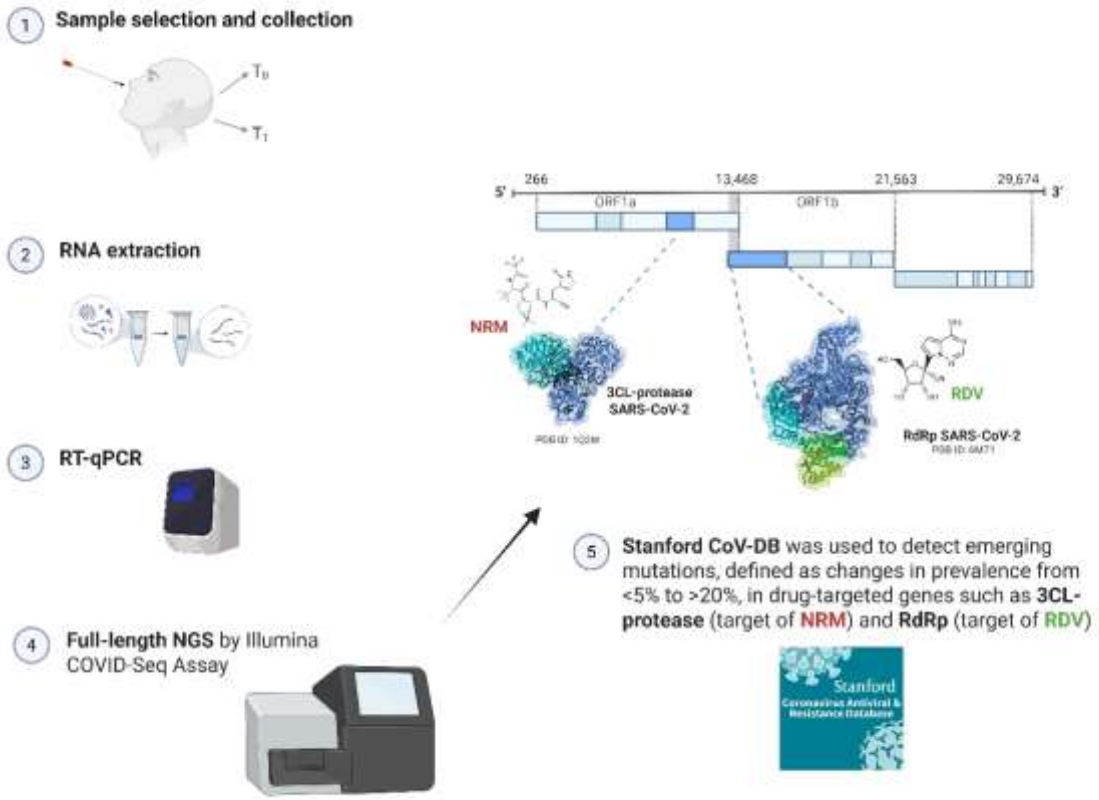

Figure 15: *Workflow for the detection of resistance in vivo. Created with https://BioRender.com*

5.2.2 Selection of patients and collection of clinical samples

Nasopharyngeal swab samples from SARS-CoV-2 positive subjects were collected at the University of Milan (UNIMI), Legnano Hospital, and at the University of Perugia (UNIPG) between March 2022 and February 2025. A total of 101 paired nasopharyngeal swabs were obtained from 98 subjects undergoing treatment with DAAs. Most patients received RDV (RDV, n = 92) while a few were treated with NRM (NRM, n = 6). Two patients received both drugs, one as a combination therapy and the other sequentially. Samples were collected at two time points: baseline (T0, prior to treatment initiation) and after about five days of therapy (T1, 5 [3–6] days). This paired sampling strategy allowed us to monitor the possible emergence of drug resistance mutations during antiviral treatment. After collection, all samples were sent from UNIMI, Legnano Hospital, and UNIPG to the Department of Medical Biotechnologies at the University of Siena (UNISI). During transport, the swabs were kept on dry ice and stored at -80 °C until processing. The viral transport medium contained in the swabs stabilized the nucleic acids, lysed the cells, and inactivated both nucleases and infectious agents, ensuring that the samples remained suitable for molecular analyses.

5.2.3 Extraction of viral RNA

Viral RNA extraction from nasopharyngeal swabs was performed in a biosafety level 3 (BSL3) laboratory using the Quick RNA™ Viral Kit (Zymo Research, USA). This kit employs silica membrane-based spin column technology for efficient RNA purification. The extraction workflow began with a lysis and a binding step: 200 µL of each nasopharyngeal swab sample was mixed with Viral RNA Buffer at a 1:2 ratio and transferred to a spin column containing a silica membrane. After centrifugation at 14,000 × g for 2 minutes, viral RNA bound to the silica matrix, while cellular debris, proteins and other contaminants were removed in the flow-through. The column membrane was then washed twice with Viral Wash Buffer to remove contaminants and enzymatic inhibitors, each wash performed at 14,000 × g for 30 seconds with the flow-through discarded after each wash. Finally, the purified RNA was eluted by adding DNase/RNase-free water directly onto the membrane, followed by centrifugation at 14,000 × g for 30 seconds. The eluted RNA was either used immediately for cDNA synthesis or stored at -80°C to preserve RNA integrity.

5.2.4 Viral load quantification by Real-Time (qPCR)

RNA reverse transcription

Extracted viral RNA was converted to cDNA using the LunaScript RT SuperMix Kit (E3010L, New England Biolabs). RNA samples were first denatured at 70°C for 10 minutes to disrupt secondary structures and ensure efficient access of the reverse transcriptase to the RNA template. Following denaturation, after cooling the samples briefly on ice, LunaScript RT SuperMix containing the enzyme and nuclease-free water was added to achieve a final reaction volume of 20 µl. The samples were then placed in a thermal cycler and subjected to a three-step program optimized for the LunaScript enzyme:

Step	Temperature	Duration
Primer annealing	25°C	2 minutes
Reverse transcription	55°C	10 minutes
Enzyme inactivation	95°C	1 minute

The resulting cDNA represented the complete viral genome in a stable DNA form suitable for quantitative analysis.

Real-Time quantitative PCR

Quantitative PCR (qPCR) was carried out using a TaqMan probe-based approach. In this system, each probe binds to an internal region of the target sequence and is labeled with a reporter dye at the 5' end and a quencher at the 3' end. When the probe is intact, the quencher suppresses fluorescence from the reporter. During amplification, the 5'→3' exonuclease activity of Taq polymerase cleaves the probe, releasing the reporter dye and producing a measurable fluorescence signal in real time. cDNA synthesized from the reverse transcription reaction was quantified by qPCR using the Luna Universal Probe qPCR Master Mix (M3004, New England Biolabs). Each 20 µL reaction contained 10 pmol/µL of forward and reverse primers (P990 and P991), 2.5 pmol/µL of the 5'-6FAM-3' MGBNFQ probe (P992), Master Mix, and nuclease-free water (Table 6). Two microliters of cDNA from each sample were added to the reaction mix, which was then distributed into 0.2 mL PCR tubes.

Name	Type	Sequence (5' → 3')	Labels
P990	Forward primer	GGCACGTAGTGTAGCTAGTC	—
P991	Reverse primer	TGGGTATGGCAATAGAGTTATTAG	—
P992	TaqMan probe	ACTATGTCACTTGGT	6FAM (5') – MGBNFQ (3')

***Table 6**: Oligonucleotide sequences used in the assay, including forward and reverse primers and the TaqMan probe with corresponding fluorescent labels*

Amplification was performed on a Rotor-Gene Q thermal cycler (Qiagen) under the following conditions: an initial denaturation at 95 °C for 60 seconds, followed by 45 cycles of 95 °C for 15 seconds and 60 °C for 30 seconds. Fluorescence signals were acquired at each cycle by the Rotor-Gene Q software, which automatically determined the cycle threshold (Ct) based on the exponential phase of amplification, a key quantitative parameter inversely proportional to the initial amount of target nucleic acid in the sample (lower Ct values indicate higher viral loads). Relative quantification was obtained by comparing sample Ct values to a standard curve generated from serial dilutions of samples with known concentrations (Table 7).

STANDARD CURVE
p258 $2x10^0$
p258 $2x10^1$
p258 $2x10^2$
p258 $2x10^3$

***Table 7:** Standard curve derived from serial dilutions of samples at known concentrations*

5.2.5 Viral genome sequencing

To assess the genetic evolution of SARS-CoV-2 during antiviral treatment and to identify potential resistance-associated mutations, we performed whole-genome sequencing on all paired samples

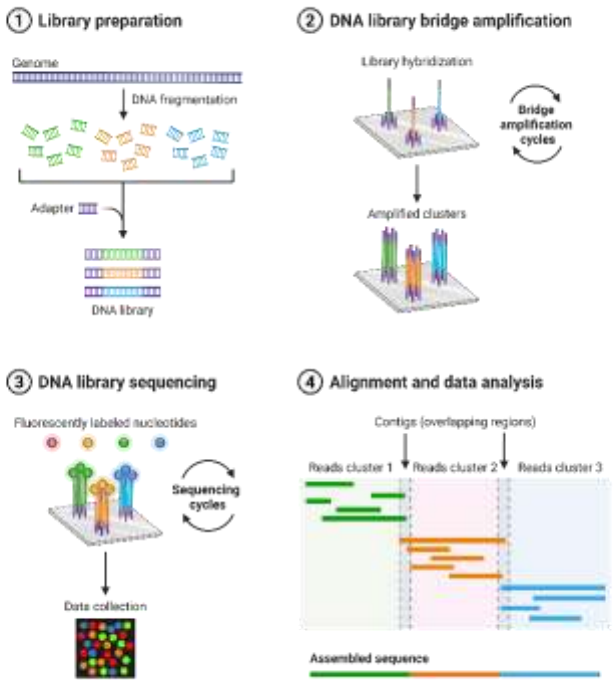

Figure 16: *Next Generation Sequencing (Illumina) workflow*

(T0 and T1) using Next-Generation Sequencing (NGS) technology with the Illumina COVIDSeq™ Assay (Illumina, Cat. No. 1000000126053) [Figure 16].

Not all collected samples were subjected to whole-genome sequencing. To ensure high-quality sequencing results and reliable variant calling, we applied a selection criterion based on viral load. Only paired samples with cycle threshold (Ct) values ≤ 29 at both time points (T0 and T1) were included in the sequencing workflow. This threshold was established because samples with Ct values above 29 typically contain insufficient viral RNA to generate adequate genome coverage and sequencing depth, potentially leading to incomplete genome assemblies, gaps in coverage, and unreliable mutation detection. By restricting our analysis to samples with Ct ≤ 29, we ensured that each sequenced genome would have sufficient viral material to achieve the minimum read depth necessary for confident variant identification across the whole SARS-CoV-2 genome. This selection criterion is particularly important in the context of antiviral treatment studies, as treated patients often experience significant viral load reduction by T1. Consequently, while all 101 paired samples underwent viral load quantification by qPCR (5.2.4), only those having the Ct ≤ 29 at both time points were processed for NGS analysis.

cDNA Synthesis

RNA extracted from nasopharyngeal swabs was reverse transcribed into complementary DNA (cDNA) using random hexamer primers. During the fragmentation and priming step, Elution Prime Fragment reagent was added, and the samples were incubated at 65 °C for 3 min. Reverse transcription was then carried out by adding reverse transcriptase and First Strand Mix, reaching a final reaction volume of 25 µL. The thermal cycler program was set as follows: 25 °C for 5 minutes, 50 °C for 10 minutes, 80 °C for 5 minutes, and a final hold at 4 °C.

cDNA Amplification

The synthesized cDNA was amplified in two independent PCR reactions using primer pools C4P1 and C4P2, designed to generate overlapping amplicons of approximately 400 bp that span the whole viral genome. Each reaction contained the corresponding Master Mix and nuclease-free water. Amplification was performed for 35 cycles under the following conditions: 98 °C for 15 seconds, 63 °C for 5 minutes, followed by a final hold at 4 °C. After amplification, the two reactions for each sample were pooled together.

Library Preparation and Tagmentation

Pooled PCR amplicons were subjected to enzymatic tagmentation, a transposase-mediated process that simultaneously fragments DNA and ligates adapter sequences necessary for Illumina sequencing. These adapters (P5 and P7) enable fragment attachment to the flow cell surface and provide priming sites for cluster generation and sequencing. Tagmentation reactions were incubated at 55°C for 5 minutes to achieve optimal fragmentation and adapter insertion.

Purification and Amplification of Tagmented Amplicons

Following tagmentation, excess reagents and short fragments were removed using paramagnetic beads. Samples were placed on a magnetic rack for approximately 3 min, until the solution became clear, allowing removal of the supernatant. Beads containing DNA fragments were washed twice with Tagmentation Wash Buffer. Adapter extension and indexing were then performed using Enhanced PCR Mix and Index Adapters, which also introduced sample-specific barcodes for downstream bioinformatic analysis. Amplification was carried out according to the following thermal profile: 72 °C for 3

minutes, 98 °C for 3 minutes, followed by 7 cycles of 98 °C for 20 seconds, 60 °C for 30 seconds, and 72 °C for 1 minute, with a final extension at 72 °C for 3 minutes and a final hold at 10 °C.

Pooling, Quantification, and Normalization of Libraries

After amplification, individual libraries were pooled in a single tube and purified with paramagnetic beads. Beads were washed twice with 80% ethanol, air-dried, and resuspended in elution buffer. DNA concentration was measured using the Qubit dsDNA HS Assay Kit (Thermo Fisher, Q32851), which employs a fluorescent dye selective for double-stranded DNA.

Library molarity (nM) was calculated using the formula:

$$\text{Molarity} = \frac{\text{Concentration (ng/µL)}}{660 \times 400} \times 10^6$$

where 400 bp represents the average fragment size. The pooled library was diluted to 4 nM, denatured with 0.2 N NaOH (Euroclone), and further diluted to a final loading concentration of 9 pM.

Sequencing and Data Processing

Libraries were loaded onto a MiSeq instrument (Illumina) using the MiSeq V2 300-cycle reagent kit (Cat. No. 15033624). Sequencing-by-synthesis was performed, during which fluorescently labeled nucleotides were incorporated and detected in real time. The instrument generated thousands of reads per sample, which were stored as FASTQ files for downstream analysis.

Bioinformatic Analysis

Raw FASTQ reads were processed for quality control, adapter trimming, and reference-based genome assembly. Consensus FASTA sequences were uploaded to the Stanford Coronavirus Antiviral & Resistance Database (CoVDB) [https://covdb.stanford.edu/] and compared with the SARS-CoV-2 Wuhan-Hu-1 reference genome (GenBank accession NC_045512.2) to identify mutations potentially associated with antiviral resistance. To ensure reliable mutation calling, a minimum read depth of greater than 50 was applied, so that each nucleotide position analyzed was supported by a sufficient number of reads. The CoVDB was

used to detect emerging mutations, defined as changes in prevalence from less than 5% to more than 20%, focusing on drug-targeted genes such as the 3CLpro (target of NRM) and the RdRp (target of RDV). This approach allows monitoring of low-frequency variants that may expand rapidly under antiviral pressure, providing insights into potential resistance mechanisms. Additionally, consensus FASTA sequences were analyzed using Illumina® DRAGEN COVID Lineage to assign each sequence to a known SARS-CoV-2 variant. This tool compares the detected mutations with known reference profiles and assigns each sequence to the most likely PANGO lineage.

5.2.6 Workflow for the selection of resistance in vitro

5.2.6.1 Cell line used for the assays

VERO E6 cells (ATCC® CRL-1586™), derived from African green monkey kidney epithelial cells, were used to assess the *in vitro* susceptibility to DAAs and to evaluate the genetic barrier to resistance development.

Cells were routinely cultured in DMEM with high glucose content (Euroclone), supplemented with 10% FBS and 1% PS (Euroclone). Cells were subcultured upon reaching 70–90% confluence. For infection experiments, the same medium was used with FBS concentration reduced to 1% (infection medium). All cultures were maintained in a humidified incubator at 37°C with 5% CO_2.

Uninfected cell culture maintenance was performed under biosafety level 2 (BSL2) conditions, whereas all infection experiments were carried out in BSL3 containment.

5.2.6.2 Antiviral drugs

RDV and NRM were dissolved in 100% DMSO (Sigma/Merck) at stock concentrations of 20 mM and 10 mM, respectively. To enhance intracellular uptake of the antivirals, the P-glycoprotein (P-gp) inhibitor CP-100356 was employed. This strategy was necessary as VERO E6 cells exhibit high expression levels of P-gp, an ATP-dependent efflux transporter that actively exports antiviral compounds, significantly limiting their intracellular bioavailability and therapeutic efficacy.

5.2.6.3 Cytotoxicity assay and determination of cell viability

The cytotoxicity assay was performed to determine the CC_{50}. Briefly, 6,000 VERO E6 cells per well were seeded in 96-well adherent plates (Euroclone) and incubated for 24 hours at 37°C in a humidified atmosphere with 5% CO_2. Four-fold serial dilutions of the antivirals were prepared in duplicate in an empty plate, including DMSO alone to assess potential cytotoxic effects of the solvent

used for compound resuspension. A fixed concentration (0.5 µM) of the P-glycoprotein inhibitor CP-100356 was added to each dilution. After removing the culture medium from the pre-seeded plates, the antiviral compound dilutions containing CP-100356 were transferred onto the VERO E6 cells and incubated for 72 hours at 37°C with 5% CO_2.

To determine cell viability, cells were treated with the CellTiter-Glo® 2.0 Luminescent Cell Viability Assay (Promega), as described in Chapter 3, Section 4.2.3. Luminescence values were measured using a GloMax® Discover Multimode Microplate Reader (Promega) and analyzed with GraphPad Prism version 9.0 software. Each plate included a cell control (CC, untreated cells), a DMSO dilution curve, and a maximum toxicity control (100% DMSO).

5.2.6.4 Viral titration assay

Viral stocks were titrated on VERO E6 cells in BSL3 to determine the $TCID_{50}$/mL representing the dilution of viral stock required to productively infect 50% of the cell culture.

VERO E6 cells (6,000 cells/well) were seeded in 96-well plates (Euroclone) and incubated for 24 hours at 37°C with 5% CO_2. Five-fold serial dilutions of each viral stock, starting at 1:250, were prepared in six replicates and added to the pre-seeded cells. Following 72 hours of incubation at 37°C with 5% CO_2, cell viability was assessed using the CellTiter-Glo® 2.0 assay (Promega; Chapter 3, Section 4.2.3). Each plate included uninfected cell controls for data normalization.

Luminescence readings were converted to binary outcomes (positive/negative) using a threshold derived from uninfected controls. The $TCID_{50}$/mL was calculated according to the Reed and Muench method, which applies the Spearman-Kärber algorithm to interpolate between two consecutive dilutions flanking the 50% endpoint. Specifically, the proportional distance (PD) between a dilution yielding >50% positive wells and the adjacent dilution yielding <50% positive wells was calculated as:

PD = (% positive above 50% − 50%) / (% positive above 50% − % positive below 50%)

The $TCID_{50}$/mL was then determined by applying the PD to the $\log_{10}$ dilution factor.

5.2.6.5 Antiviral activity assay

The antiviral activity of RDV and NRM against SARS-CoV-2 was evaluated by infecting VERO E6 cells in the presence of serial dilutions of each compound.

VERO E6 cells were seeded at 6,000 cells per well in 96-well tissue culture plates and incubated for 24 hours at 37°C in a humidified atmosphere with 5% CO_2. Serial dilutions of RDV and NRM were

prepared in duplicate in separate plates, and the P-glycoprotein inhibitor CP-100356 was added to each dilution at a fixed concentration of 0.5 µM. The compound dilutions were then transferred onto the pre-seeded VERO E6 cells and incubated for 60 minutes at 37°C with 5% CO_2 to allow drug uptake.

Following the pre-treatment step, plates were transferred to the BSL3 facility for viral infection. Cells were infected with SARS-CoV-2 at MOI of 0.005, corresponding to 50 $TCID_{50}$/mL per well. Each experiment included both a CC and a VC, both treated with CP-100356. After 72 hours of incubation at 37°C with 5% CO_2, antiviral activity was assessed using the CellTiter-Glo® 2.0 Luminescent Cell Viability Assay, as previously described.

The IC_{50} was determined by nonlinear regression analysis of dose-response curves using GraphPad Prism version 9.0 software. The VC and CC controls were used to define 100% and 0% viral replication, respectively, and all luminescence values were normalized accordingly. The selectivity index (SI) for each compound was calculated as the ratio of CC_{50} to IC_{50}.

5.2.6.6 In vitro selection of resistance

In vitro resistance selection experiments (IVRS) were performed to identify potential resistance-associated mutations emerging under antiviral selective pressure. One day prior to infection, VERO E6 cells were seeded at 1.2×10^6 cells per T25 flask (Euroclone) in complete growth medium and incubated at 37°C with 5% CO_2. On the day of infection, the culture medium was removed and cells were inoculated with a mixture containing SARS-CoV-2 and the respective antiviral compound at defined starting concentrations. For the B.1 lineage, RDV and NRM were initially added at 2× IC_{50}, while for the KP.3 variant, selection was initiated at 1× IC_{50}. The use of 2× IC_{50} for B.1 and 1× IC_{50} for KP.3 was chosen to harmonize the effective selective pressure across the two lineages. Because B.1 and KP.3 differ in replication dynamics and baseline drug susceptibility, adjusting the multiplicative factor of the IC_{50} allowed us to initiate the selection experiments under comparable conditions, ensuring sufficient viral replication while maintaining consistent antiviral pressure. The P-glycoprotein inhibitor CP-100356 was included at 0.5 µM in all conditions to enhance intracellular drug accumulation. The MOI was maintained at 0.01 throughout all passages.

Flasks were incubated at 37°C with 5% CO_2 and monitored daily for virus-induced CPE, characterized by cell rounding and detachment from the flask surface. When 80% CPE was observed, cells and supernatant were harvested and subjected to one freeze-thaw cycle to release intracellular virus. Following thawing, the lysate was transferred to a 15 mL conical tube and clarified by centrifugation

at 1,300 × g for 30 minutes at 4°C to remove cellular debris. The clarified supernatant containing infectious virus was collected for subsequent passage.

For each passage, 500 µL of viral supernatant was used to infect a freshly seeded T25 flask in the presence of increasing drug concentrations. Specifically, the antiviral concentration was doubled at

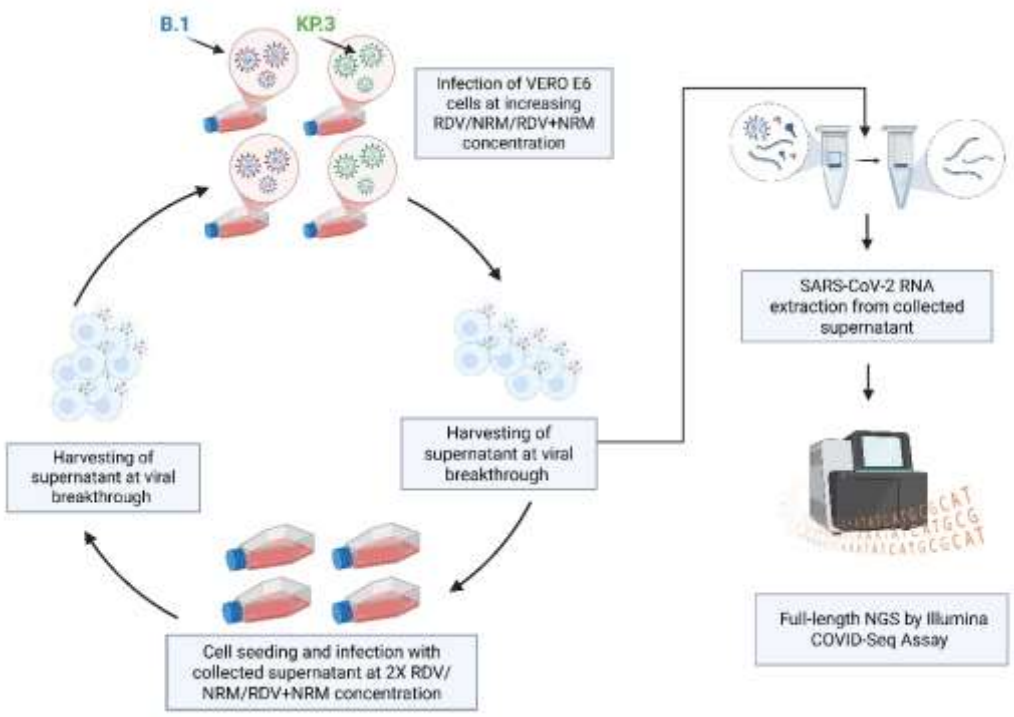

***Figure 17**: In vitro selection of resistance workflow*

each passage to progressively increase selective pressure. The remaining viral stock was aliquoted and stored at −80°C for subsequent titration and sequencing analyses. In cases where CPE was not observed upon reaching cell confluency, cells were trypsinized and subcultured into a new T25 flask containing fresh infection medium supplemented with the same drug and CP-100356 concentrations, allowing additional time for viral replication under selective pressure *(*Figure 17*).*

Each passage included a VC consisting of infected cells cultured without antiviral compounds, and a CC consisting of uninfected cells treated with the corresponding antiviral concentrations tested at each passage.

IVRS experiments were terminated if no CPE was observed for three consecutive weeks, indicating stable suppression of viral replication by the antiviral agent and the absence of viable resistant variants under the tested conditions. Conversely, experiments were continued until either a CPE emerged at drug concentrations significantly higher than the initial IC_{50}, suggesting resistance development, or a predetermined maximum concentration threshold was reached.

Viral stocks from each passage were stored at −80°C for subsequent determination of viral titers by $TCID_{50}$ assay (Section 4.2.3), phenotypic susceptibility to antivirals (Section 5.2.6.8), and genotypic characterization by NGS to identify emerging mutations (Section 5.2.6.7).

5.2.6.7 Sequencing of the viral genome

Resistance-associated mutations emerging during IVRS experiments were identified by whole-genome sequencing of viral stocks collected at the end of each selection passage. Viral RNA was extracted from clarified cell culture supernatants and subjected to NGS using the Illumina COVIDSeq™ Assay, following the protocol described in Section 5.2.5.

Sequence data were analyzed to identify single nucleotide variants (SNVs) and amino acid substitutions within antiviral target regions, including RdRp gene for RDV and the Mpro gene for NRM. Mutations were considered significant when present at >20% frequency in the viral population, reflecting positive selection under drug pressure. Reference sequences from passage 0 (pre-selection) and virus controls were used to distinguish drug-associated mutations from background genetic variability.

5.2.6.8 Antiviral activity assay on selected mutants

To confirm that genotypic changes corresponded to functional resistance phenotypes, viral stocks harboring resistance-associated mutations (identified by NGS) were subjected to phenotypic susceptibility testing. This assay assessed whether mutations in drug target sites resulted in measurable reductions in antiviral susceptibility, thereby validating the genotype-to-phenotype correlation for viral escape.

The phenotypic assay was performed following the antiviral activity protocol described in Section 5.2.6.5, with minor modifications. Briefly, VERO E6 cells were infected with either mutant viruses (selected under drug pressure) or the parental wild-type strain at an MOI of 0.005, in the presence of serial dilutions of RDV or NRM supplemented with 0.5 µM CP-100356. After 72 hours of incubation, cell viability was measured using the CellTiter-Glo® 2.0 assay, and IC_{50} values were determined by nonlinear regression analysis.

The fold-change as calculated as the ratio of the IC_{50} of the mutant virus to that of the wild-type reference strain:

$$FC = IC_{50}(\text{mutant}) / IC_{50}(\text{wild-type})$$

5.3 Results and discussion

5.3.1 In vivo selection

5.3.1.1 Clinical sampling

The study cohort included 100 patients with a median age of 80 years [68-85]. Among the participants, 43% were women, and 47% had a high comorbidity index, defined as the presence of three or more concurrent comorbidities. The comorbidity profile included hypertension (n = 60), cardiovascular disease (n = 50), chronic obstructive pulmonary disease (COPD; n = 43), diabetes mellitus (n = 30), chronic kidney disease (n = 20), non-hematologic malignancies (n = 14), hematologic malignancies (n = 11), autoimmune disorders (n = 9), and obesity (BMI > 35; n = 6).

Regarding clinical outcomes and patient characteristics, HIV-1 infection was documented in 3% of subjects. Most patients (94%) required hospitalization, and among these, 74% received supplemental oxygen therapy. The in-hospital mortality rate was 4%. With respect to SARS-CoV-2 vaccination status, 44% of patients had received at least one dose of an mRNA vaccine, whereas vaccination data were unavailable for the remaining 56%, as detailed in Table 8.

Age: 80 [68-85] years
Sex (F): 43%
Comorbidities*: • 0: 9% • 1-2 (low comorbidities score): 44% • ≥3 (high comorbidities score): 47%
Hospitalized: 94% • 74% required oxygen support • 4% died
Vaccinated**: 44%
HIV positive: 3%
Pneumonia: 64%

* Comorbidities include: hypertension, cardiovascular disease, diabetes, chronic kidney disease, COPD, non-hematopoietic cancer, hematopoietic cancer, autoimmunity, BMI > 35
** Data about vaccination status was missing for the rest of the population

Table 8: *Study population*

5.3.1.2 Viral load quantification

Viral load was assessed using RT-qPCR at two time points (T0 and T1) to track changes in viral levels over the course of treatment. Because RT-qPCR provides accurate quantification of

viral RNA, it offered a reliable method to determine whether patients achieved viral suppression or still harbored virus after therapy.

An adequate viral load is a fundamental prerequisite for successful whole-genome sequencing, as insufficient template material can compromise sequencing depth and coverage, ultimately leading to incomplete or fragmented genomic data. By restricting NGS analysis to samples with Ct ≤ 29, we ensured optimal sequencing quality, thereby facilitating comprehensive variant characterization and accurate lineage assignment according to established phylogenetic classification systems.

NGS was selectively performed on a subset of 33 specimens that tested positive for SARS-CoV-2, all with Ct values ≤ 29 at T0 and T1 timepoints (Figure 18).

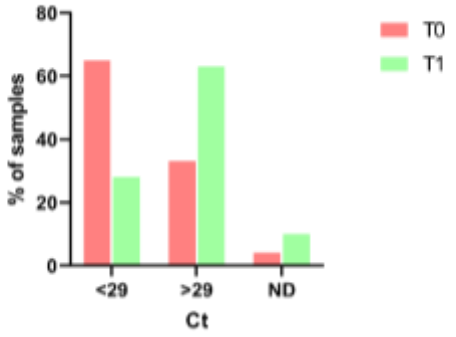

	T0	T1
<29 Ct	65	28
>29 Ct	32	63
ND	4	10

ND= Not detectable

Figure 18: *Percentage and absolute distribution of samples analysed via RT-qPCR, divided into three categories based on the Ct value at both T0 and T1: Ct ≤ 29 (high viral load), Ct > 29 (low viral load) and ND (not detectable).*

5.3.1.3 Variant attribution and sequence analysis

Following NGS completion, viral lineage assignment and phylogenetic classification were performed utilizing the Nextstrain bioinformatic platform (www.nextstrain.org), a widely recognized tool for real-time tracking of pathogen evolution and epidemiological surveillance. Longitudinal genomic analysis was conducted on samples from 33 patients who met the predefined Ct threshold of ≤ 29, with mean Ct values of 24 ± 8 at T0 and 26 ± 2 at T1. Phylogenetic reconstruction revealed that the identified viral sublineages were predominantly derived from two major circulating variants during the study period: XBB.1

and JN.1 (Table 9). The predominance of JN.1, in particular, reflects the epidemiological landscape of late 2023 and early 2024, when this variant rapidly displaced earlier Omicron sublineages worldwide due to its marked growth advantage and extensive spike protein modifications.

Variant	Sub-lineage	Lineage	WHO Label	Frequency (n)
BA.1	BA.1	Omicron	Omicron	1
BA.2	BA.2	Omicron	Omicron	4
BA.5	BA.5	Omicron	Omicron	4
JN.1	JN.1	Omicron (BA.2.86)	Omicron	2
JN.1	JN.1.4	Omicron (BA.2.86)	Omicron	1
JN.1	JN.1.8	Omicron (BA.2.86)	Omicron	1
JN.1	JD.1.1	Omicron (BA.2.86)	Omicron	1
JN.1	JG.3	Omicron (BA.2.86)	Omicron	2
JN.1	KP.3.1.1	Omicron (BA.2.86)	Omicron	4
XBB.1	XBB.1	Omicron (BA.2)	Omicron	1
XBB.1	FL.1.5.1	Omicron (BA.2)	Omicron	1
XBB.1	EG.5.1	Omicron (BA.2)	Omicron	1
XBB.1	HK.3	Omicron (BA.2)	Omicron	1

Variant	Sub-lineage	Lineage	WHO Label	Frequency (n)
XBB.1	HV.1	Omicron (BA.2)	Omicron	1
XBB.1	MC.16	Omicron (BA.2)	Omicron	1
XBB.1	BQ.1	Omicron (BA.5)	Omicron	1
XBB.1	BQ.1.18	Omicron (BA.5)	Omicron	1
XBB.1	KP.3.1.1	Omicron (BA.2.86)	Omicron	1
XEC	XEC	Omicron recombinant	Omicron	2
XEC	XEC.2	Omicron recombinant	Omicron	2

Table 9: *SARS-CoV-2 variants and sub-lineages detected during the study period with their phylogenetic classification. The table shows all SARS-CoV-2 variants and sub-lineages identified through whole-genome sequencing of 33 positive samples collected at baseline (T0) and follow-up (T1). Variants are grouped by their main lineage and further categorized by specific sub-lineages detected. All identified variants belong to the Omicron lineage or its recombinant forms. The phylogenetic classification includes the ancestral lineage in parentheses: BA.2.86 for JN.1-derived variants, BA.2 for most XBB.1 sub-lineages, and BA.5 for BQ.1 variants. XEC and XEC.2 represent Omicron recombinant variants. The frequency column (n) indicates the number of samples in which each variant was detected, with JN.1-related variants (n=11) and XBB.1-related variants (n=9) being the most prevalent.*

To identify and characterize emerging resistance-associated mutations, genomic sequences were compared with the Stanford CoV-DB, a curated database developed by Stanford University that compiles experimental data on SARS-CoV-2 mutations, including variant classification and neutralization susceptibility. This resource facilitates the analysis of how these mutations affect viral transmissibility, immune evasion, and the effectiveness of therapeutic interventions. Emerging mutations were defined as amino acid substitutions that increased in prevalence from <5% to >20% within genes encoding the DAAs targets, the 3CLpro and RdRp, providing an indication of potential drug resistance development.

Sequence analysis of the 3CLpro gene revealed no amino acid variations across the treatment course in any patient whereas the examination of the RdRp gene identified notable mutations in three patients who received RDV therapy, each reaching a prevalence greater than 20% (highlighted in bold in table 10). Specifically, subject 6 developed a mixed population harboring M794MI (methionine/isoleucine at position 794 with 60%/40% distribution), subject 31 exhibited V792VI (valine/isoleucine at position 792 at 50%/49% frequencies), and subject 96 showed an almost complete replacement with M794I (98% prevalence) (Table 10).

Subject	Pre-treatment AA Mutations	Post-treatment AA Mutations	RdRp Prevalence >20%
6	D63N (100%), P323L, G671S (100%)	D63N (100%), P323L, G671S (100%), M794MI (M/I = 60/40%)	**M794MI** (M/I =60/40%)
31	Y294YH (Y/H = 92/7.9%), P296PL (P/L =85/14%), P323L	P296PL (P/L = 93/6.6%), P323L, C464CY (C/Y = 86/14%), V792VI (V/I = 50/49%)	**V792VI** (V/I = 50/49%)
96	**P323L**	**P323L, M794I (98%)**	**M794I (98%)**

Table 10: *Emergent amino acid mutations detected in the RdRp gene. The table summarizes mutational profiles observed in subjects 6, 31, and 96 at T0 and T1 timepoints. Mutations highlighted in* ***bold*** *in the RdRp column represent those achieving >20% prevalence.*

These mutations fall within a functionally critical region of the RdRp catalytic domain that directly interacts with RDV's active triphosphate metabolite. Both V792I and M794I mutations have been extensively characterized in the literature as resistance-associated substitutions that compromise RDV efficacy through multiple mechanisms. The V792I mutation, in particular, has been documented across numerous studies involving both *in vitro* selection experiments and clinical cases of immunocompromised patients undergoing extended antiviral courses. Structural modeling studies have demonstrated that the V792I substitution alters the geometry of the nucleotide binding pocket, reducing the enzyme's affinity for RDV while maintaining sufficient polymerase activity for viral replication. This mutation has been observed to confer approximately 2-6-fold resistance in cell culture systems and has been associated with viral rebound in patients with persistent infections (Ling-Hu *et al*. 2025, Stevens *et al.* 2022)

The M794I mutation, although less frequently reported in the literature than V792I, is emerging as a potential concern in the setting of prolonged antiviral exposure. Iriyama *et al.* provided evidence of its clinical relevance in immunocompromised patients with hematologic malignancies experiencing persistent SARS-CoV-2 infections. In their cohort, M794I emerged after extended RDV treatment in a patient with lymphoma, and *in vitro* characterization confirmed that this substitution reduces RDV susceptibility while preserving viral fitness. The proximity of residue 794 to the RdRp catalytic active site suggests that replacement with isoleucine could sterically hinder RDV incorporation or promote excision from the nascent RNA chain, however the precise molecular mechanism remains to be fully elucidate (Iriyama *et al.*,2025). Phenotypic evaluation of the in vivo-derived SARS-CoV-2 isolate (patient 96B) revealed only a modest change in RDV IC_{50} (0.09 ± 0.001 µM) compared with the B.1 strain (0.06 ± 0.05 µM), indicating a markedly lower fold-change increase than that observed under prolonged in vitro RDV selection. This limited reduction in susceptibility is noteworthy given the presence of mutations located within this functionally critical region of the RdRp catalytic domain.

5.3.2 In vitro selection

5.3.2.1 Cytotoxicity and activity of DAAs

The cytotoxicity profile of NRM and RDV was initially evaluated to establish nontoxic working concentrations for subsequent antiviral assays. As shown in Figure 19, both compounds exhibited low cytotoxicity in VERO E6 cells. The CC_{50} values obtained for each DAA were used to define non-toxic doses corresponding to 90-100% cell viability. Based on these data, the concentrations selected for antiviral assays in combination with the efflux pump inhibitor CP-100356 were 1 µM for NRM and 2 µM for RDV. At these concentrations, NRM maintained cell viability close to 100%, while RDV resulted in approximately 90% viability. Notably, both compounds displayed minimal cytotoxicity even in the presence of DMSO vehicle control.

The safety profiles of NRM and RDV are well established in the literature. Numerous studies have shown that both compounds possess a broad therapeutic window, with CC_{50} values greater than 100 µM in Vero E6 cells. This indicates that they can inhibit viral replication at concentrations far below those that cause cytotoxic effects in host cells (Pruijssers *et al.*, 2020; Owen *et al.*, 2021).

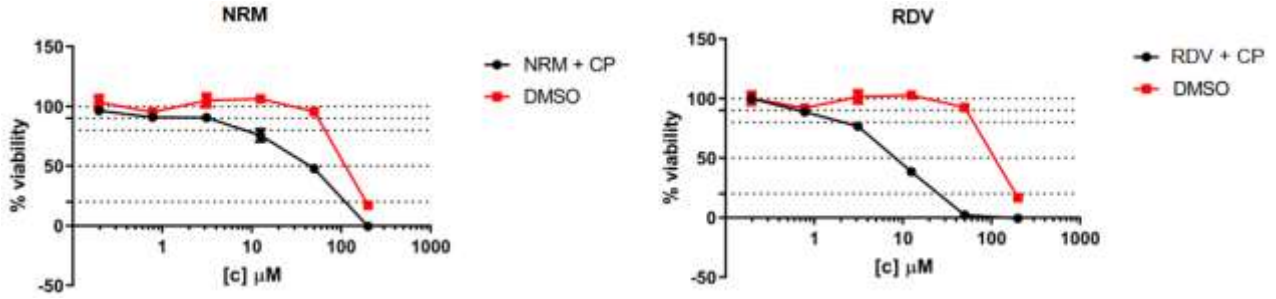

Figure 19: Cytotoxicity of NRM and RDV in combination with the P-gp inhibitor CP-100356 in VERO E6 cells.

Following cytotoxicity assessment, the antiviral efficacy of NRM and RDV was evaluated against both the SARS-CoV-2 B.1 strain and the KP.3 variant, which was emerging at the time the experiments were conducted. As shown in Figure 20, both compounds exhibited potent dose-dependent antiviral activity against both viral strains.

For the B.1 strain, the calculated IC_{50} values were 0.074 µM for NRM and 0.039 µM for RDV. Against the KP.3 variant, slightly higher IC_{50} values were observed: 0.156 µM for NRM (approximately 2-fold increase) and 0.072 µM for RDV (approximately 1.8-fold increase), indicating a modest reduction in susceptibility to both antivirals compared to the ancestral strain. Nonetheless, both compounds retained substantial antiviral potency against KP.3, with IC_{50} values remaining well within the sub-micromolar range.

The IC_{50} values determined in these assays were subsequently used as starting concentrations for the IVRS experiments, ensuring sufficient selective pressure to promote the emergence and isolation of potential resistant viral variants.

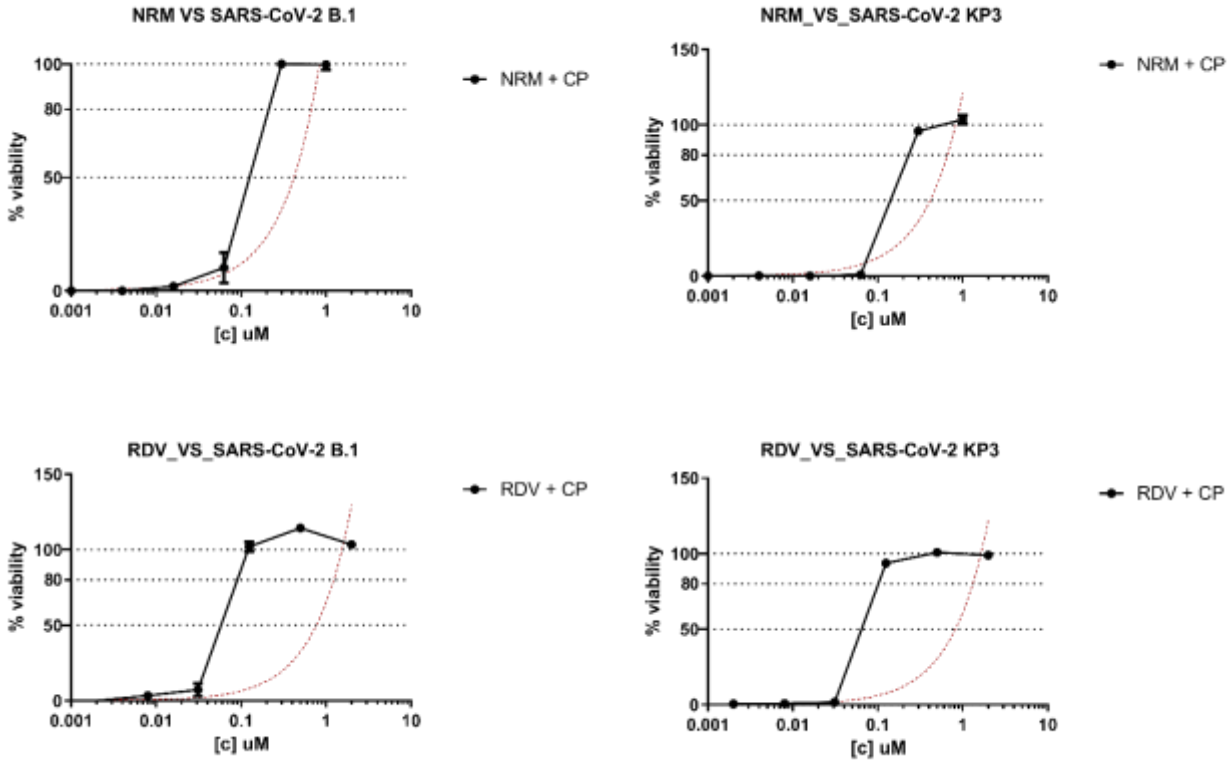

Figure 20: Antiviral activity of Nirmatrelvir (NRM) and Remdesivir (RDV) against SARS-CoV-2 B.1 and KP.3 variants. *Dose-response curves showing the antiviral activity of Nirmatrelvir (NRM) and Remdesivir (RDV) in combination with the efflux pump inhibitor CP-100356 (CP) against B.1 (wild-type) and KP.3 strains. After 72 hours of incubation, cell viability was measured and IC_{50} values were calculated.*

5.3.2.2 Mutations that emerged in IVRS experiments

IVRS experiments performed with the ancestral B.1 strain and the Omicron KP.3 variant revealed distinct patterns of resistance development under RDV and NRM monotherapy, as well as under combination therapy. As shown in figure 21, the kinetics of viral replication and the timeline of mutation emergence differed across treatment conditions. NGS analysis identified multiple amino acid substitutions in the viral RdRp and 3CLpro genes, several of which have been previously associated with reduced antiviral susceptibility.

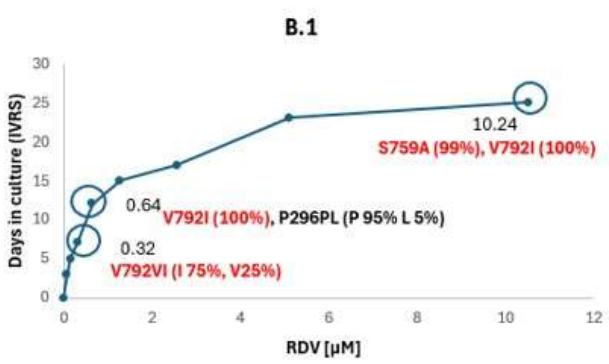
B.1
Days in culture (IVRS)
RDV [µM]
10.24
S759A (99%), V792I (100%)
0.64
V792I (100%), P296PL (P 95% L 5%)
0.32
V792VI (I 75%, V25%)

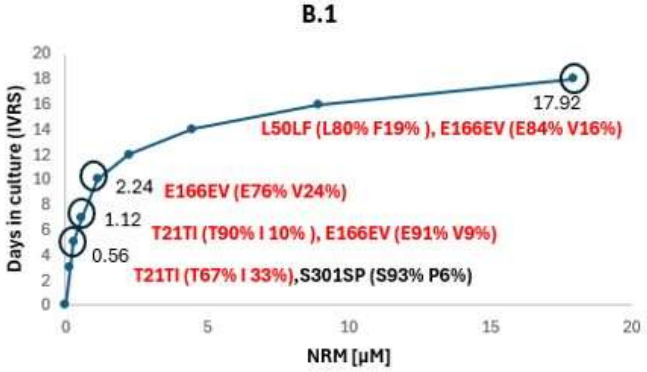
B.1
Days in culture (IVRS)
NRM [µM]
17.92
L50LF (L80% F19%), E166EV (E84% V16%)
2.24
E166EV (E76% V24%)
1.12
T21TI (T90% I 10%), E166EV (E91% V9%)
0.56
T21TI (T67% I 33%),S301SP (S93% P6%)

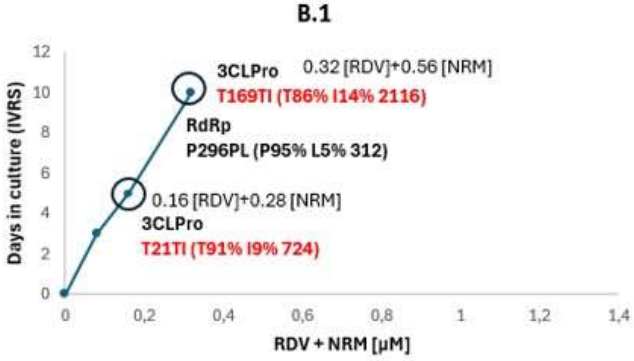
B.1
Days in culture (IVRS)
RDV + NRM [µM]
3CLPro
0.32 [RDV]+0.56 [NRM]
T169TI (T86% I14% 2116)
RdRp
P296PL (P95% L5% 312)
0.16 [RDV]+0.28 [NRM]
3CLPro
T21TI (T91% I9% 724)

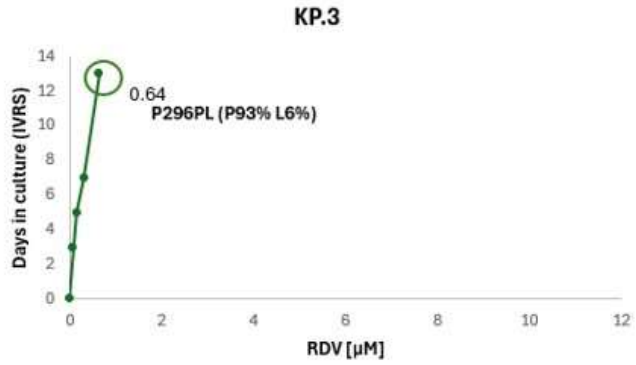
KP.3
Days in culture (IVRS)
RDV [µM]
0.64
P296PL (P93% L6%)

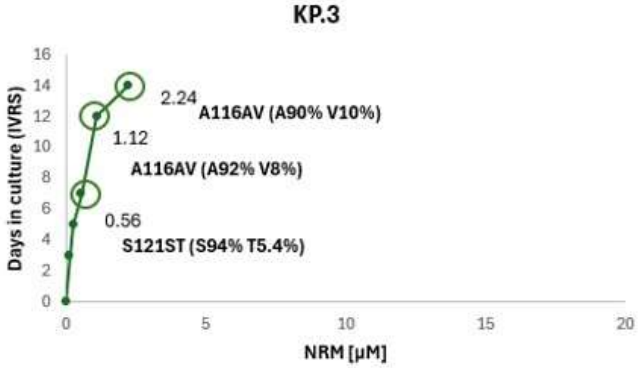
KP.3
Days in culture (IVRS)
NRM [µM]
2.24
A116AV (A90% V10%)
1.12
A116AV (A92% V8%)
0.56
S121ST (S94% T5.4%)

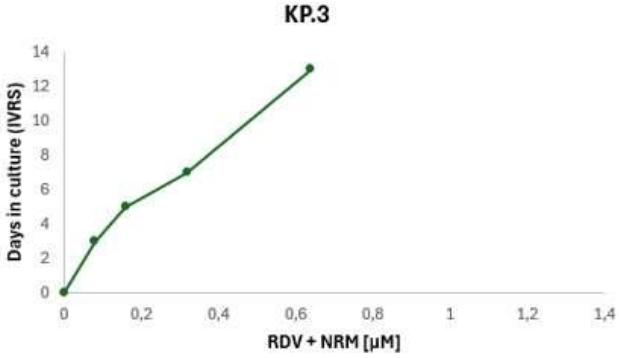
KP.3
Days in culture (IVRS)
RDV + NRM [µM]

Figure 21: IVRS mutations in the B.1 and KP.3 strains during treatment with increasing concentrations of NRM and RDV, administered individually or in combination, together with a fixed concentration of 0.5 µM CP-100356. *Each graph illustrates, over time, the stepwise increases in drug concentration following the onset of cytopathic effects induced by viral replication, as well as the corresponding emerging mutations in the respective target genes of RDV and NRM.*

Under RDV pressure, the B.1 strain progressively accumulated mutations in the RdRp gene, with V792I emerging at lower drug concentrations (0.32 µM) and reaching fixation (100% frequency) by day 15. At 0.64 µM, the P296PL substitution emerged with V792I, while at the highest concentration tested (10.24 µM), the double mutant S759A/V792I was selected after 25 days of culture. These mutations have been extensively characterized in previous studies and are known to confer resistance through distinct molecular mechanisms. The V792I substitution, located within the RdRp active site, directly impairs the incorporation kinetics of nucleotide analogs by altering the geometry of the catalytic pocket and reducing the enzyme's affinity for the triphosphate form of RDV (Stevens *et al*., 2022; Tchesnokov *et al*., 2020). In contrast, S759A operates through an allosteric mechanism, inducing conformational changes in the RdRp structure that indirectly reduce drug binding efficiency without significantly affecting polymerase activity on natural RNA substrates (Szemiel *et al*., 2021; Narayanan *et al*., 2022).

Selection with NRM led to the emergence of multiple substitutions in the 3CLpro gene. At 0.28 µM, the T21TI mutation was detected together with S301SP, although the latter remained at low frequency. By 0.56 µM (day 10), T21TI became dominant (T90% I10%) and was accompanied by the emergence of E166EV (E91% V9%). The T21I substitution replaces a polar threonine with a hydrophobic isoleucine in the S1 subsite, thereby disrupting the hydrogen bonding networks essential for NRM recognition (Ullrich *et al*., 2022; Iketani *et al*., 2022). After 18 days of culture at 17.92 µM, the T21TI substitution (T65% I35%) was lost, while L50LF mutation emerged alongside the persistent E166EV substitution. This combination is a well-characterized resistance pathway: E166V confers high-level resistance to NRM but severely impairs 3CLpro activity, requiring compensatory mutations such as L50F to restore 3CLpro function to levels allowing viral replication (Iketani *et al*., 2022). Indeed, the L50F/E166V combination is unlikely to compromise viral fitness, thereby maintaining high-level NRM resistance while preserving replicative capacity.

5.3.2.3 Phenotypic characterization of resistance mutations

To confirm that the observed genotypic changes translated into phenotypic resistance, antiviral susceptibility assays were performed on the selected viral populations (Figure 22). Resistance levels

were quantified using fold-change (FC) values, calculated as the ratio between the IC_{50} of the mutant virus and the IC_{50} of the corresponding wild-type virus.

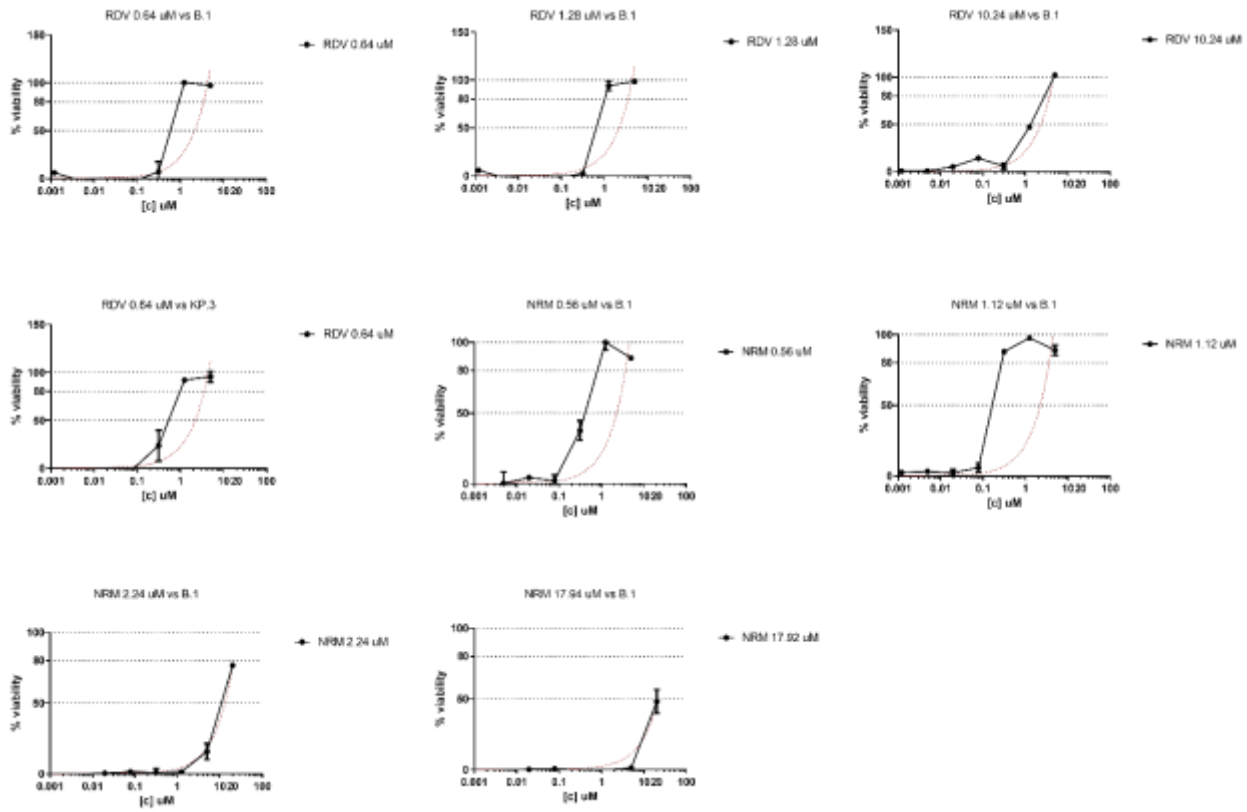

Figure 22: *Anti-SARS-CoV-2 activity of NRM and RDV in combination with 0.5 µM CP-100356 in VERO E6 cells. The compounds were tested against the resistant B.1 and KP.3 variants selected at the end of the IVRS.*

For the B.1 ancestral strain, dose-dependent increase in resistance was observed. Under RDV selection, FC values increased progressively from 4-fold at 0.32 µM to 9-fold at 0.64 µM and reached 20-fold at the highest concentration (10.24 µM). Maybe the emergence of the S759A/V792I double mutant at this stage likely contributed to the substantial increase in resistance, consistent with findings that combinations of RdRp mutations can produce synergistic effects on drug susceptibility (Gandhi *et al.*, 2022; *Velkov et al.*, 2023). Selection with NRM resulted in an even more dramatic resistance phenotype in B.1. FC values increased from 7-fold (0.56 µM) to 77-fold (1.12 µM), then escalated to 132-fold (2.24 µM) and ultimately reached 241-fold at 17.92 µM. This marked level of resistance correlates with the fixation of E166V, a mutation that has been identified as one of the most impactful single substitutions for NRM resistance across multiple SARS-CoV-2 lineages (Iketani *et al*., 2022; Zhou *et al*., 2022). The co-selection of L50F plus E166V in intermediate passages likely facilitated the survival and expansion of highly resistant variants by mitigating the fitness costs typically associated with active-site alterations (Jochmans *et al*., 2023).

In contrast, the KP.3 strain showed a much lower capacity to develop resistance. Under RDV selection, resistance emerged only modestly, with a maximum selected concentration of 0.64 µM, and a peak FC of just 4-fold. Viral extinction prevented further drug pressure escalation, unlike the B.1 strain, which tolerated concentrations up to 10.24 µM. Similarly, NRM selection in KP.3 yielded only low-level resistance, with no measurable increases in FC. The viral population exposed to 2.24 µM NRM underwent extinction, as no CPE was observed, precluding any further drug pressure escalation. This contrasts with the B.1 strain, which survived concentrations up to 17.92 µM, indicating intrinsically lower genetic flexibility in KP.3. This finding is consistent with studies suggesting that certain Omicron sublineages may exhibit reduced mutational tolerance in functionally constrained regions of RdRp and 3CLpro, potentially due to epistatic interactions arising from the extensive S protein mutations that characterize these variants (Starr *et al*., 2023; Carabelli *et al.*, 2023).

Importantly, the combination of RDV and NRM exhibited a substantially higher barrier to resistance than either drug alone. In the B.1 strain, the combined treatment suppressed viral replication at lower concentrations and, notably, resulted in the selection of fewer resistance mutations compared to monotherapy. In the KP.3 strain, the combination completely prevented the emergence of detectable resistance mutations throughout the selection period, underscoring the potential clinical value of dual DAA therapy in limiting resistance development. This combinatorial approach may be especially beneficial in high-risk populations, including immunocompromised patients, in whom prolonged viral persistence increases the likelihood of resistance emergence and therapeutic failure.

B.1	DAA [µM]	Days in culture	AA mutations in DAA target genes	IC50 [µM]	FC (Fold Change)
RDV	0.32	12	**V792I (V75% I25%)**	0.28	4
	0.64	15	P296PL (P95% L5%), **V792I** (100%)	0.58	9
	10.24	25	**S759A (99%), V792I (100%)**	1.33	20
NRM	0.56	7	**T21TI (T67% I 33%)**, S301SP (S 93% P 6%)	0.43	7
	1.12	10	**T21TI (T90% I 10%), E166EV (E91% V9%)**	5.00	77
	2.24	12	**E166EV (E76% V24%)**	11.23	132
	17.92	18	**E166EV (84%; 16%)** **L50LF (L80%; F19%)**	20.50	241
RDV + NRM	RDV 0,16 + NRM 0,28	5	3CLPro: **T21TI (T91% I9%)**	4.53	70
	RDV 0,32 + NRM 0,56	10	RdRp: P296PL (P95% L5% 312), 3CLPro:T169TI (T86% I14%)	-	-

KP.3	DAA [µM]	Days in culture	AA mutations in DAA target genes	IC_{50} [µM]	FC (Fold Change)
RDV	0.64	13	P296PL (P93% L6%)	0.43	4
NRM	0.56	7	S121ST (S 94% T 5%)	-	-
	1.12	12	A116AV (A 93% V 7%)	-	-
	2.24	-	A116AV (A90% V10%)	-	-
RDV + NRM	RDV 0,16 + NRM 0,28	5	-	-	-
	RDV 0,32 + NRM 0,56	7	-	-	-

Table 11: *The table summarizes IVRS results for B.1 and KP.3 strains exposed to increasing concentrations of RDV, NRM, or both drugs. Amino acid mutations in RdRp and 3CLpro are reported with their frequencies (in parentheses); red text highlights known resistance-associated mutations. Resistance levels are expressed as fold change (FC) in IC_{50} relative to parental strains. B.1 developed progressive resistance under monotherapy), with key mutations including V792I, S759A, and E166EV. KP.3 exhibited minimal resistance capacity. Combination therapy significantly reduced resistance emergence in B.1 and prevented it entirely in KP.3, demonstrating a higher genetic barrier to resistance.*

5.4 Conclusions

This study provides a comprehensive assessment of SARS-CoV-2's genetic barrier to resistance against RDV and NRM, integrating longitudinal genomic analyses of treated patients with systematic i*n vitro* viral selection experiments using viral strains that represent the virus's evolution over the course of the pandemic. Over five years after the pandemic began, drug-resistant strains of SARS-CoV-2 are still a real public health concern, even though the emergency phase has officially ended. The virus's intrinsic capacity to accumulate mutations has led to the emergence of VOCs, including Omicron lineages and their descendants (such as JN.1 and KP.3), which have demonstrated markedly reduced susceptibility to therapeutic monoclonal antibodies. Although DAAs like RDV and NRM remain highly effective against currently circulating variants, their prolonged use, particularly in immunocompromised patients, may increase the risk of resistance development. This underscores the need for continuous genomic surveillance. Genomic analysis of 33 patients showed that genotypic resistance to DAAs is rare *in vivo.* Resistance-associated mutations were detected in only three immunocompromised individuals receiving standard RDV treatment, where V792I and M794I substitutions in the RdRp catalytic domain reached intra-host frequencies above 20%. No 3CLpro mutations were observed in patients treated with NRM.

These findings highlight the need for additional studies in cohorts of immuno-compromised patients with prolonged infections. Such work will be essential to clarify how often DAA resistance emerges and to determine its clinical significance in contexts where the virus is able to replicate over extended periods.

IVRS experiments confirmed that both drugs have high genetic barriers, requiring prolonged selective pressure for resistant phenotypes to emerge. However, the ease of resistance development varied notably by strain. In the ancestral B.1 lineage, RDV pressure selected the V792I and S759A mutations, which conferred up to a 35-fold increase in resistance. Under NRM pressure, multiple 3CLpro mutations arose, including L50F/E166V, resulting in a 277-fold increase in resistance through compensatory changes that restored viral fitness. In contrast, the KP.3 Omicron variant showed a substantially reduced ability to acquire resistance. It reached only a 4-fold increase in RDV resistance and failed to develop any detectable NRM resistance before undergoing viral extinction. This pattern suggests that the extensive mutational load carried by highly evolved Omicron lineages may constrain their evolutionary flexibility. Such epistatic interactions likely limit the number of viable adaptive pathways in functionally within functionally essential regions of the genome.

The most encouraging result comes from the evaluation of RDV and NRM combination therapy. In the B.1 strain, the combined treatment markedly reduced the emergence of resistance mutations compared with either drug alone. Even more notably, in the KP.3 strain the combination fully suppressed detectable resistance throughout the selection period. These findings provide strong molecular support for using DAA combinations in clinical practice, particularly for immunocompromised patients or individuals with persistent infections, where the risk of selecting resistant variants is greatest.

In conclusion, our data indicates that SARS-CoV-2 still exhibits a high genetic barrier to both RDV and NRM, with clinically meaningful resistance remaining rare and primarily confined to immunocompromised patients undergoing prolonged therapy.

6 REFERENCES:

- Ackaert, C., Coates, M., Hermanns, K., Huck, S., Jonckers, T. H. M., Kraus, G., ... & Stoops, B. (2023). Safety, tolerability, and pharmacokinetics of JNJ-64281802, a novel non-nucleoside pan-serotype dengue virus inhibitor: Results of a randomized, double-blind, placebo-controlled, single- and multiple-ascending-dose first-in-human study in healthy volunteers. Clinical Infectious Diseases, 76(3), e950-e958.
- Agrawal, S., Orschler, L., & Lackner, S. (2023). Long-term monitoring of SARS-CoV-2 RNA in wastewater of the Frankfurt metropolitan area in Southern Germany. *Scientific Reports*, *13*(1), 4873.
- Akkız, H. (2022). The biological functions and clinical significance of SARS-CoV-2 variants of concern. *Frontiers in Medicine*, *9*, 849217.

- Ali, A., & Vijayan, R. (2020). Dynamics of the ACE2–SARS-CoV-2/SARS-CoV spike protein interface reveal unique mechanisms. *Scientific Reports*, *10*(1), 14214.
- Artsob, H., Lindsay, R., & Drebot, M. (2017). Arboviruses. In International Encyclopedia of Public Health (pp. 154–160). Elsevier. https://doi.org/10.1016/B978-0-12-803678-5.00023-0
- Baden, L. R., El Sahly, H. M., Essink, B., Kotloff, K., Frey, S., Novak, R., ... & Zaks, T. (2021). Efficacy and safety of the mRNA-1273 SARS-CoV-2 vaccine. *New England Journal of Medicine*, *384*(5), 403-416.
- Barzon, L. (2018). Ongoing and emerging arbovirus threats in Europe. *Journal of Clinical Virology*, *107*, 38–47. https://doi.org/10.1016/j.jcv.2018.08.007
- Bassetto, M., Ferla, S., Pertusati, F., Kandil, S., Slusarczyk, M., Tsay, S. C., Neyts, J., & Brancale, A. (2017). Design and synthesis of novel piperazine derivatives targeting the NS3 helicase of hepatitis C virus. *European Journal of Medicinal Chemistry*, *125*, 901-913. https://doi.org/10.1016/j.ejmech.2016.09.079
- Beigel, J. H., Tomashek, K. M., Dodd, L. E., Mehta, A. K., Zingman, B. S., Kalil, A. C., ... & Lane, H. C. (2020). Remdesivir for the treatment of Covid-19. *New England Journal of Medicine*, *383*(19), 1813-1826.
- Bernardo-Menezes, M. E., Medeiros, D. B. A., Silva, S. J. R., & Paiva, P. M. G. (2022). Zika virus: An updated review of competent or naturally infected mosquitoes. *PLoS Neglected Tropical Diseases*, *16*(1), e0010084.
- Bhatt, P., Sabeena, S. P., Varma, M., & Arunkumar, G. (2021). Current Understanding of the Pathogenesis of Dengue Virus Infection. Current Microbiology, 78(1), 17–32. https://doi.org/10.1007/s00284-020-02284-w
- Bhatt, S., Gething, P. W., Brady, O. J., Messina, J. P., Farlow, A. W., Moyes, C. L., Drake, J. M., Brownstein, J. S., Hoen, A. G., Sankoh, O., Myers, M. F., George, D. B., Jaenisch, T., Wint, G. R. W., Simmons, C. P., Scott, T. W., Farrar, J. J., & Hay, S. I. (2013). The global distribution and burden of dengue. Nature, 496(7446), 504–507
- Biswal, S., Reynales, H., Saez-Llorens, X., Lopez, P., Borja-Tabora, C., Kosalaraksa, P., ... & Rivera, L. (2019). Efficacy of a tetravalent dengue vaccine in healthy children and adolescents. New England Journal of Medicine, 381(21), 2009-2019.
- Boldescu, V., Behnam, M. A. M., Vasilakis, N., & Klein, C. D. (2017). Broad-spectrum agents for flaviviral infections: Dengue, Zika and beyond. Nature Reviews Drug Discovery, 16(8), 565-586.
- Brand, C., Bisaillon, M., & Geiss, B. J. (2017). Organization of the Flavivirus RNA replicase complex. Wiley interdisciplinary reviews. RNA, 8(6), 10.1002/wrna.1437.
- Brasil, P., Pereira, J. P., Jr, Moreira, M. E., Ribeiro Nogueira, R. M., Damasceno, L., Wakimoto, M., ... & Szejnfeld, J. (2016). Zika virus infection in pregnant women in Rio de Janeiro. *New England Journal of Medicine*, *375*(24), 2321-2334.

- Brès, P. (2018). Impact of Arboviruses on Human and Animal Health. In The arboviruses: (pp. 47–61). Elsevier. https://doi.org/10.1016/B978-0-12-812365-2.00004-4
- Brüssow, H., & Figuerola, J. (2025). The Spread of the Mosquito-Transmitted West Nile Virus in North America and Europe. *Microbial biotechnology*, *18*(3), e70120. https://doi.org/10.1111/1751-7915.70120
- Buitrago-Garcia, D., Ipekci, A. M., Heron, L., Imeri, H., Araujo-Chaveron, L., Arevalo-Rodriguez, I., ... & Zamora, J. (2022). Occurrence and transmission potential of asymptomatic and presymptomatic SARS-CoV-2 infections: Update of a living systematic review and meta-analysis. *PLoS Medicine*, *19*(5), e1003987.
- Cao, Y., Yisimayi, A., Jian, F., Song, W., Xiao, T., Wang, L., ... & Xie, X. S. (2022). BA.2.12.1, BA.4 and BA.5 escape antibodies elicited by Omicron infection. *Nature*, *608*(7923), 593-602.
- Cao-Lormeau, V. M., Blake, A., Mons, S., Lastère, S., Roche, C., Vanhomwegen, J., ... & Ghawché, F. (2014). Guillain-Barré syndrome outbreak associated with Zika virus infection in French Polynesia: A case-control study. *The Lancet*, *384*(9942), 531-540.
- Carabelli, A. M., Peacock, T. P., Thorne, L. G., Harvey, W. T., Hughes, J., COVID-19 Genomics UK Consortium, Peacock, S. J., Barclay, W. S., de Silva, T. I., Towers, G. J., & Robertson, D. L. (2023). SARS-CoV-2 variant biology: Immune escape, transmission and fitness. Nature Reviews Microbiology, 21(3), 162–177. https://doi.org/10.1038/s41579-022-00841-7
- Cataldo, F., Marotta, C., Koliopoulos, P., Goletti, D., & Zumla, A. (2024). Zika virus: An emerging flavivirus with implications for global health. *Journal of Infection*, *88*(1), 106086.
- Cavallaro, A., Domínguez, F., & Camacho, C. (2023). Privileged structure-based design of novel piperazine derivatives with potential antiviral activity. *Journal of Medicinal Chemistry*, *66*(12), 8831-8844. https://doi.org/10.1021/acs.jmedchem.3c00217
- Centers for Disease Control and Prevention. (2024). Dengue transmission. https://www.cdc.gov/dengue/transmission
- Centers for Disease Control and Prevention. (n.d.). Dengue clinical case management (CME course). https://www.cdc.gov/dengue/training/cme/ccm
- Cevik, M., Kuppalli, K., Kindrachuk, J., & Peiris, M. (2020). Virology, transmission, and pathogenesis of SARS-CoV-2. *BMJ*, *371*, m3862.
- Chareonviriyaphap, T., Akratanakul, P., Nettanomsak, S., & Huntamai, S. (2003). Larval habitats and distribution patterns of Aedes aegypti (Linnaeus) and Aedes albopictus (Skuse), in Thailand. The Southeast Asian journal of tropical medicine and public health, 34(3), 529–535.
- Chauhan, C., Lakshmi, P. S., & Lodha, R. (2024). Advances in the understanding of dengue pathogenesis. Journal of Clinical Virology, 174, 105–132.

- Chen, J., Wang, R., Gilby, N. B., & Wei, G. W. (2022). Omicron variant (B.1.1.529): Infectivity, vaccine breakthrough, and antibody resistance. *Journal of Chemical Information and Modeling*, *62*(2), 412-422.
- Chen, L. H., & Wilson, M. E. (2016). Update on non-vector transmission of dengue: relevant studies with Zika and other flaviviruses. Tropical diseases, travel medicine and vaccines, 2, 15.
- Chen, R. F., Yang, K. D., Wang, L., Liu, J. W., Chiu, C. C., & Cheng, J. T. (2007). Different clinical and laboratory manifestations between dengue haemorrhagic fever and dengue fever with bleeding tendency. *Transactions of the Royal Society of Tropical Medicine and Hygiene*, *101*(11), 1106–1113.
- Chen, R., & Vasilakis, N. (2011). Dengue — molecular biology and pathogenesis. Current Opinion in Virology, 1(1), 1–6.
- Choudhary, S., Sharma, K., & Silakari, O. (2022). The interplay between inflammatory pathways and COVID-19: A critical review on pathogenesis and therapeutic options. *Microbial Pathogenesis*, *150*, 104673.
- Choudhury, C., Priyadarshini, M., & Saha, A. (2021). Computational screening of piperazine-based inhibitors targeting SARS-CoV-2 main protease and RdRp. *Journal of Biomolecular Structure and Dynamics*, *39*(19), 7045-7056. https://doi.org/10.1080/07391102.2020.1850356
- Chung, S. C., Providencia, R., & Sofat, R. (2024). Association between angiotensin blockade and incidence of influenza in the United Kingdom. *New England Journal of Medicine*, *378*(16), 1543-1544.
- Clark, M. B., & Schaefer, T. J. (2023). West Nile Virus. In *StatPearls*. StatPearls Publishing.
- clinical candidate for the treatment of COVID-19. Science, 374(6575), 1586–1593. https://doi.org/10.1126/science.abl4784
- Conway, M. J., Colpitts, T. M., & Fikrig, E. (2014). Role of the Vector in Arbovirus Transmission. Annual Review of Virology, 1(Volume 1, 2014), 71–88.
- Côrtes, V. A., Santos, A. L. S., Souza, T. M. L., & Ferreira, D. F. (2023). Flavivirus infection: A complex interplay between host and viral factors. Viruses, 15(3), 745.
- Da Silva Queiroz, J. A., Botelho-Souza, L. F., & Nogueira-Lima, F. S. (s.d.). Phylogenetic Characterization of Arboviruses in Patients Suffering from Acute Fever in Rondônia, Brazil.
- Davies, N. G., Abbott, S., Barnard, R. C., Jarvis, C. I., Kucharski, A. J., Munday, J. D., ... & Edmunds, W. J. (2021). Estimated transmissibility and impact of SARS-CoV-2 lineage B.1.1.7 in England. *Science*, *372*(6538), eabg3055.
- Dejnirattisai, W., Supasa, P., Wongwiwat, W., Rouvinski, A., Barba-Spaeth, G., Duangchinda, T., & Screaton, G. R. (2015). Dengue virus sero-cross-reactivity drives antibody-dependent enhancement of infection with Zika virus. Nature Immunology, 17(9), 1102-1108.

- Del Rosario García-Lozano, M., Pagni, S., Montomoli, E., & Capobianchi, M. R. (2023). Evaluation of piperazine-derived small molecules as potential flavivirus NS3 protease inhibitors. *Viruses*, *15*(11), 2208. https://doi.org/10.3390/v15112208
- Delatte, H., Desvars, A., Bouétard, A., Bord, S., Gimonneau, G., Vourc'h, G., & Fontenille, D. (2010). Blood-feeding behavior of Aedes albopictus, a vector of Chikungunya on La Réunion. *Vector borne and zoonotic diseases (Larchmont, N.Y.)*, *10*(3), 249–258.
- Deng, Y. Q., Zhang, N. N., Li, C. F., Tian, M., Hao, J. N., Xie, X. P., ... & Cheng, G. (2016). Adenosine analog NITD008 is a potent inhibitor of Zika virus. Open Forum Infectious Diseases, 3(4), ofw175.
- Deschenes, N. M., Pérez-Vargas, J., Zhong, Z., Thomas, M., Kenward, C., Mosimann, W. A., Worrall, L. J., Waglechner, N., Li, A. X., Maguire, F., Aftanas, P., Smith, J. R., Lim, J., Young, R. N., Cherkasov, A., Farooqi, L., Moinuddin, A., Siddiqi, L., Malik, I., Lefebvre, M., … Kozak, R. A. (2025). Functional and Structural Characterization of Treatment-Emergent Nirmatrelvir Resistance Mutations at Low Frequencies in the Main Protease (Mpro) Reveals a Unique Evolutionary Route for SARS-CoV-2 to Gain Resistance. The Journal of infectious diseases, 232(5), e789–e798.
- Diani, E., Lagni, A., Turrini, F., Labbozzetta, M., Basso, M., Zagotto, G., ... & Richter, S. N. (2023). Recent advances in flavivirus drug discovery. Viruses, 15(2), 487.
- Dinata, R., Baindara, P., & Mandal, S. M. (2025). Evolution of Antiviral Drug Resistance in SARS-CoV-2. *Viruses*, *17*(5), 722.
- Donadieu, E., Bahuon, C., Lowenski, S., Zientara, S., Coulpier, M., & Lecollinet, S. (2013). Differential virulence and pathogenesis of West Nile viruses. Viruses, 5(11), 2856–2880.
- Duffy, M. R., Chen, T. H., Hancock, W. T., Powers, A. M., Kool, J. L., Lanciotti, R. S., ... & Hayes, E. B. (2009). Zika virus outbreak on Yap Island, Federated States of Micronesia. *New England Journal of Medicine*, *360*(24), 2536-2543.
- Elrefaey, A. M. (2019). Characterization of insect-specific flaviviruses and efficacy assessment of antivirals against flaviviruses.
- Epling, B. P., Rocco, J. M., Boswell, K. L., Laidlaw, E., Galindo, F., Kellogg, A., ... & Imamichi, T. (2022). Clinical, virologic, and immunologic evaluation of symptomatic coronavirus disease 2019 rebound following nirmatrelvir/ritonavir treatment. *Clinical Infectious Diseases*, *76*(3), e530-e533.
- Etymologia: Dengue. (2006). Emerging Infectious Diseases, 12(6), 893–893.
- European Centre for Disease Prevention and Control. (2024). Dengue worldwide overview. https://www.ecdc.europa.eu/en/dengue-monthly
- European Centre for Disease Prevention and Control. (2025). Communicable disease threats report — weekly updates. https://www.ecdc.europa.eu/
- European Medicines Agency. (2023). *EMA recommends against use of Evusheld for prevention of COVID-19*. https://www.ema.europa.eu

- European Medicines Agency. (2024). *COVID-19 vaccines and treatments*. https://www.ema.europa.eu
- Fall, G., Di Paola, N., Faye, M., Dia, M., Freire, C. C. M., Loucoubar, C., Zanotto, P. M. A., Faye, O., & Sall, A. A. (2017). Biological and phylogenetic characteristics of West African lineages of West Nile virus. PLoS neglected tropical diseases, 11(11), e0006078.
- Fernandez, E., Dejnirattisai, W., Cao, B., Scheaffer, S. M., Supasa, P., Wongwiwat, W., ... & Diamond, M. S. (2017). Human antibodies to the dengue virus E-dimer epitope have therapeutic activity against Zika virus infection. Nature Immunology, 18(11), 1261-1269.
- Focosi, D. (2025). Monoclonal antibodies for COVID-19 in 2025. *Drugs*, *85*, 1-15.
- Focosi, D., Quiroga, R., McConnell, S., Johnson, M. C., & Casadevall, A. (2024). Convergent evolution in SARS-CoV-2 spike creates a variant soup from which new COVID-19 waves emerge. *International Journal of Molecular Sciences*, *25*(3), 1264.
- Fong, S.-W., Kini, R. M., & Ng, L. F. P. (2018). Mosquito Saliva Reshapes Alphavirus Infection and Immunopathogenesis. Journal of Virology, 92(12), 10.1128/jvi.01004-17. https://doi.org/10.1128/jvi.01004-17
- Gandhi, S., Klein, J., Robertson, A. J., Peña-Hernández, M. A., Lin, M. J., Roychoudhury, P., Lu, P., Fournier, J., Ferguson, D., Mohamed Bakhash, S. A., Muenker, C., Srivathsan, A., Wunder, E. A., Jr., Kerantzas, C., Ott, M., Shon, J., Kudo, E., Watkins, A., Wang, W., … Iwasaki, A. (2022). De novo emergence of a remdesivir resistance mutation during treatment of persistent SARS-CoV-2 infection in an immunocompromised patient: A case report. Nature Communications, 13(1), 1547. https://doi.org/10.1038/s41467-022-29104-y
- Gao, X., Liu, Y., Zhang, W., & Zhao, H. (2023). Piperazine analogues targeting viral polymerases as broad-spectrum antiviral agents. *Molecules*, *28*(1), 160. https://doi.org/10.3390/molecules28010160
- Giraldo, M. I., Xia, H., Aguilera-Aguirre, L., Hage, A., van Tol, S., Shan, C., ... & Rajsbaum, R. (2023). Envelope protein ubiquitination drives entry and pathogenesis of Zika virus. *Nature*, *585*(7825), 414-419.
- Goethals, O., Kaptein, S., Kesteleyn, B., Bonfanti, J. F., Van Wesenbeeck, L., Van Loock, M., ... & Neyts, J. (2023). Blocking NS3-NS4B interaction inhibits dengue virus in non-human primates. Nature, 615(7950), 678-686.
- Guarner, J., & Hale, G. L. (2019). Four human diseases with significant public health impact caused by mosquito-borne flaviviruses: West Nile, Zika, dengue and yellow fever. *Seminars in Diagnostic Pathology*, *36*(3), 170-176.

- Guo, K., Barrett, B. S., Morrison, J. H., Mickens, K. L., Vladar, E. K., Hasenkrug, K. J., ... & Cam, M. (2024). Interferon resistance of emerging SARS-CoV-2 variants. *Proceedings of the National Academy of Sciences*, *121*(26), e2322739121.
- Guo, X. X., Li, C. X., Wang, J. J., Xu, Y. P., Zhang, Y. M., Qing, J., ... & Deng, Y. Q. (2022). Zika virus infections and implications of antiviral treatment in pregnancy. *Signal Transduction and Targeted Therapy*, *7*(1), 1-16.
- Guzman, M. G., & Harris, E. (2015). Dengue. The Lancet, 385(9966), 453–465. https://doi.org/10.1016/S0140-6736(14)60572-9
- Hadinegoro, S. R., Arredondo-García, J. L., Capeding, M. R., Deseda, C., Chotpitayasunondh, T., Dietze, R., ... & Tornieporth, N. (2015). Efficacy and long-term safety of a dengue vaccine in regions of endemic disease. New England Journal of Medicine, 373(13), 1195-1206.
- Haidar, G., Agha, M., Bilderback, A., Lukanski, A., Linstrum, K., Troyan, R., ... & Mellors, J. W. (2025). Prospective evaluation of sipavibart prophylaxis against SARS-CoV-2 in immunocompromised patients. *Clinical Infectious Diseases*, ciae619.
- Halstead, S. B. (2007). Dengue. The Lancet, 370(9599), 1644–1652. https://doi.org/10.1016/S0140-6736(07)61687-0
- Hammond, J., Leister-Tebbe, H., Gardner, A., Abreu, P., Bao, W., Wisemandle, W., ... & Seegobin, S. (2022). Oral nirmatrelvir for high-risk, nonhospitalized adults with COVID-19. *New England Journal of Medicine*, *386*(15), 1397-1408.
- Harvey, W. T., Carabelli, A. M., Jackson, B., Gupta, R. K., Thomson, E. C., Harrison, E. M., ... & Robertson, D. L. (2021). SARS-CoV-2 variants, spike mutations and immune escape. *Nature Reviews Microbiology*, *19*(7), 409-424.
- Hasan, S. S., Sevvana, M., Kuhn, R. J., & Rossmann, M. G. (2019). Structural biology of Zika virus and other flaviviruses. *Nature Structural & Molecular Biology*, *26*(2), 13-20.
- Heath, P. T., Galiza, E. P., Baxter, D. N., Boffito, M., Browne, D., Burns, F., ... & Munro, A. P. S. (2021). Safety and efficacy of NVX-CoV2373 COVID-19 vaccine. *New England Journal of Medicine*, *385*(13), 1172-1183.
- Hoffmann, M., Kleine-Weber, H., Schroeder, S., Krüger, N., Herrler, T., Erichsen, S., ... & Pöhlmann, S. (2020). SARS-CoV-2 cell entry depends on ACE2 and TMPRSS2 and is blocked by a clinically proven protease inhibitor. *Cell*, *181*(2), 271-280.
- Hu, Y., Lewandowski, E. M., Tan, H., Zhang, X., Morgan, R. T., Zhang, X., ... & Lemieux, M. J. (2023). Naturally occurring mutations of SARS-CoV-2 main protease confer drug resistance to nirmatrelvir. *mBio*, *14*(4), e01285-23.
- Hu, Y., Meng, X., Zhang, F., Xiang, Y., & Wang, J. (2025). SA55: A potent pan-sarbecovirus neutralizing antibody. *Cell Reports*, *44*(1), 113636.

- Iketani, S., Hong, S. J., Sheng, J., Bahari, F., Culbertson, B., Atanaki, F. F., Aditya, A., Jansen, M. O., Vera, J. C., Rao, V., Nair, M. S., Peña-Hernández, M. A., Shion, H., Zhang, X., Debnath, A., Suzuki, Y., Khandhar, A. P., Kosuri, S., Lindenbach, B. D., … Ho, D. D. (2022). Functional map of SARS-CoV-2 3CL protease reveals tolerant and immutable sites. Cell Host & Microbe, 30(9), 1354–1362.e6. https://doi.org/10.1016/j.chom.2022.08.003
- Infectious Diseases Society of America. (2024). *IDSA guidelines on the treatment and management of patients with COVID-19*. https://www.idsociety.org
- Iriyama, C., Ichikawa, T., Tamura, T., Takahata, M., Ishio, T., Ibata, M., Kawai, R., Iwata, M., Suzuki, M., Adachi, H., Nao, N., Suzuki, H., Kawai, A., Kamiyama, A., Suzuki, T., Hirata, Y., Iida, S., Katano, H., Ishii, Y., … Tomita, A. (2025). Clinical and molecular landscape of prolonged SARS-CoV-2 infection with resistance to remdesivir in immunocompromised patients. PNAS Nexus, 4(4), pgaf085. https://doi.org/10.1093/pnasnexus/pgaf085
- Istituto Superiore di Sanità. (2025a). Casi di arbovirosi in Italia: dati al 23 settembre 2025. EpiCentro – Sistema Nazionale di Sorveglianza Integrata delle Arbovirosi. Retrieved from https://www.epicentro.iss.it/febbre-dengue/aggiornamenti
- Istituto Superiore di Sanità. (2025b). Arbovirosis surveillance data, August 26, 2025 update. EpiCentro. Retrieved from https://www.epicentro.iss.it/arbovirosi/aggiornamenti
- Ji, Y., Wang, L., Zhou, R., Yang, X., Li, S., Cen, S., & Li, Y. (2024). Design, synthesis, and antiviral activity of 1-aryl-4-arylmethylpiperazine derivatives as Zika virus inhibitors with broad antiviral spectrum. *Bioorganic & medicinal chemistry*, *103*, 117682.
- Jochmans, D., Liu, C., Donckers, K., Stoycheva, A., Boland, S., Stevens, S. K., De Vita, C., Vanmechelen, B., Maes, P., Trüeb, B., Ebert, N., Thiel, V., De Wilde, A. H., Neyts, J., Breuer, J., Snoeck, R., & Andrei, G. (2023). The substitutions L50F, E166A, and L167F in SARS-CoV-2 3CLpro are selected by a protease inhibitor in vitro and confer resistance to nirmatrelvir. mBio, 14(1), e02815-22. https://doi.org/10.1128/mbio.02815-22
- Khan, K., Karim, F., Ganga, Y., Bernstein, M., Jule, Z., Reedoy, K., ... & Lessells, R. J. (2023). Omicron BA.4/BA.5 escape neutralizing immunity elicited by BA.1 infection. *Nature Communications*, *14*(1), 4686.
- Kounde, C. S., García-Sánchez, M. F., Luque-Ortega, J. R., & Torrens, F. (2017). Piperazine derivatives as dengue virus replication inhibitors targeting viral non-structural proteins. *Bioorganic Chemistry*, *73*, 76-84. https://doi.org/10.1016/j.bioorg.2017.05.013
- Krow-Lucal, E. R., Biggerstaff, B. J., & Staples, J. E. (2017). Estimated incubation period for Zika virus disease. *Emerging Infectious Diseases*, *23*(5), 841-845.

- Kumar, A., Singh, B., & Kumar, V. (2023). Piperazine derivatives disrupt spike-ACE2 interactions: Insight into potential SARS-CoV-2 entry inhibitors. *Chemico-Biological Interactions*, *382*, 110531. https://doi.org/10.1016/j.cbi.2023.110531
- Laureti, M., Narayanan, D., Rodriguez-Andres, J., Fazakerley, J. K., & Kedzierski, L. (2018). Flavivirus Receptors: Diversity, Identity, and Cell Entry. Frontiers in Immunology, 9.
- Lei, H., Alu, A., Yang, J., He, C., Hong, W., Yang, L., ... & Xu, J. (2020). Caspase-3 activation is required for efficient influenza A virus propagation. *Journal of Virology*, *94*(1), e01433-19.
- Li, M., Lou, F., & Fan, H. (2024). SARS-CoV-2 variants and COVID-19 vaccines: Current challenges and future strategies. *International Journal of Biological Sciences*, *20*(4), 1294-1314.
- Liang, Y., & Dai, X. (2024). The global incidence and trends of three common flavivirus infections (dengue, yellow fever, and Zika) from 2011 to 2021. *Frontiers in Microbiology, 15*, 1458166.
- Liang, Y., Wang, M. L., Chien, C. S., Yarmishyn, A. A., Yang, Y. P., Lai, W. Y., ... & Chiou, S. H. (2020). Highlight of immune pathogenic response and hematopathologic effect in SARS-CoV, MERS-CoV, and SARS-CoV-2 infection. *Frontiers in Immunology*, *11*, 1022.
- Lim, S. P., Noble, C. G., & Shi, P. Y. (2015). The dengue virus NS5 protein as a target for drug discovery. Antiviral Research, 119, 57-67.
- Lindenbach, B. D., Thiel, H., & Rice, C. M. (2007). Flaviviridae:The Viruses and Their Replication. Fields Virol. 5th Ed., 1101–1113.
- Ling-Hu, T., Simons, L. M., Rios-Guzman, E., Carvalho, A. M., Agnes, M. F. R., Alisoltanidehkordi, A., Ozer, E. A., Lorenzo-Redondo, R., & Hultquist, J. F. (2025). The impact of remdesivir on SARS-CoV-2 evolution in vivo. *JCI insight*, *10*(4), e182376.
- Liu, Y., & Rocklöv, J. (2021). The reproductive number of the Delta variant of SARS-CoV-2 is far higher compared to the ancestral SARS-CoV-2 virus. *Journal of Travel Medicine*, *28*(7), taab124.
- Liu, Y., Liu, J., Du, S., Shan, C., Nie, K., Zhang, R., ... & Shi, P. Y. (2017). Evolutionary enhancement of Zika virus infectivity in Aedes aegypti mosquitoes. *Nature*, *545*(7655), 482-486.
- Magalhães, B., Melo, A., & Oliveira, A. L. (2025). Immune responses to mRNA vaccines: Molecular mechanisms and clinical implications. *Vaccines*, *13*(1), 42.
- Magurano, F., Remoli, M. E., Baggieri, M., Fortuna, C., Marchi, A., Fiorentini, C., Bucci, P., Benedetti, E., Ciufolini, M. G., Rizzo, C., Piga, S., Salcuni, P., Rezza, G., & Nicoletti, L. (2012). Circulation of West Nile virus lineage 1 and 2 during an outbreak in Italy. *Clinical microbiology and infection : the official publication of the European Society of Clinical Microbiology and Infectious Diseases*, *18*(12), E545–E547.
- Markov, P. V., Ghafari, M., Beer, M., Lythgoe, K., Simmonds, P., Stilianakis, N. I., & Katzourakis, A. (2023). The evolution of SARS-CoV-2. *Nature Reviews Microbiology*, *21*(6), 361-379.

- Martinot, M., Jary, A., Fafi-Kremer, S., Leducq, V., Delagreverie, H., Garnier, M., & Bruel, T. (2022). Emerging resistance to remdesivir in SARS-CoV-2 after treatment in an immunocompromised patient: A case report. *Nature Communications*, *13*(1), 1547.
- Maucourant, C., Petitdemange, C., Yssel, H., & Vieillard, V. (2019). Control of acute arboviral infection by natural killer cells. *Current Opinion in Virology*, *34*, 113-119.
- May, F. J., Davis, C. T., Tesh, R. B., & Barrett, A. D. (2011). Phylogeography of West Nile virus: from the cradle of evolution in Africa to Eurasia, Australia, and the Americas. *Journal of virology*, *85*(6), 2964–2974. https://doi.org/10.1128/JVI.01963-10
- Mazzotta, E., Mazzoccoli, C., De Leo, A., Testa, A., Di Penta, A., & Rossi, A. (2020). Piperazine derivatives inhibit human adenovirus replication by interfering with viral gene expression in vitro. *Antiviral Research*, *176*, 104741. https://doi.org/10.1016/j.antiviral.2020.104741
- Meinhardt, J., Radke, J., Dittmayer, C., Franz, J., Thomas, C., Mothes, R., ... & Heppner, F. L. (2021). Olfactory transmucosal SARS-CoV-2 invasion as a port of central nervous system entry in individuals with COVID-19. *Nature Neuroscience*, *24*(2), 168-175.
- Miner, J. J., & Diamond, M. S. (2017). Zika virus pathogenesis and tissue tropism. *Cell Host & Microbe*, *21*(2), 134-142.
- Mlakar, J., Korva, M., Tul, N., Popović, M., Poljšak-Prijatelj, M., Mraz, J., ... & Avšič Županc, T. (2016). Zika virus associated with microcephaly. *New England Journal of Medicine*, *374*(10), 951-958.
- Moderna. (2025, January). *Moderna announces positive interim Phase 3 data for its next-generation COVID-19 vaccine candidate* [Press release]. https://investors.modernatx.com
- Moghadasi, S. A., Heilmann, E., Moraes, S. N., Kearns, F. L., Sassoon, L. J., Aamer, F., ... & Harris, R. S. (2023). Rapid resistance profiling of SARS-CoV-2 protease inhibitors. *Nature Communications*, *14*(1), 4991.
- Monath, T. P. (2012). Review of the risks and benefits of yellow fever vaccination including some new analyses. Expert Review of Vaccines, 11(4), 427-448.
- Morrison, J., Aguirre, S., & Fernandez-Sesma, A. (2012). Innate Immunity Evasion by Dengue Virus. Viruses, 4(3), Articolo 3.
- Mukhopadhyay, S., Kuhn, R. J., & Rossmann, M. G. (2005). A structural perspective of the flavivirus life cycle. Nature Reviews Microbiology, 3(1), 13–22.
- Narayanan, A., Narwal, M., Majowicz, S. A., Varricchio, C., Toner, S. A., Ballatore, C., Brancale, A., Murakami, K. S., & Jose, J. (2022). Identification of SARS-CoV-2 inhibitors targeting Mpro and PLpro using in-cell-protease assay. Communications Biology, 5(1), 169. https://doi.org/10.1038/s42003-022-03090-9
- Naveca, F. G., Pontes, G. S., Chang, A. Y., Silva, G. A. V., Nascimento, V. A., Monteiro, D. C. S., ... & Wallau, G. L. (2018). Analysis of the immunological biomarker profile during acute Zika virus

infection reveals the overexpression of CXCL10, a chemokine linked to neuronal damage. *Memórias do Instituto Oswaldo Cruz*, *113*(6), e170542.

- Neufeldt, C. J., Cortese, M., Acosta, E. G., & Bartenschlager, R. (2018). Rewiring cellular networks by members of the Flaviviridae family. Nature Reviews Microbiology, 16(3), 125–142. https://doi.org/10.1038/nrmicro.2017.170
- Ng, W. C., Soto-Acosta, R., Bradrick, S. S., Garcia-Blanco, M. A., & Ooi, E. E. (2017). The 5′ and 3′ Untranslated Regions of the Flaviviral Genome. Viruses, 9(6), Articolo 6.
- Nyberg, T., Ferguson, N. M., Nash, S. G., Webster, H. H., Flaxman, S., Andrews, N., ... & Bhatt, S. (2022). Comparative analysis of the risks of hospitalisation and death associated with SARS-CoV-2 omicron (B.1.1.529) and delta (B.1.617.2) variants in England: A cohort study. *The Lancet*, *399*(10332), 1303-1312.
- Ostrowsky, J., Diemert, D., & Gutman, J. (2025). Zika virus vaccine development: Progress and challenges. Human Vaccines & Immunotherapeutics.
- Owen, D. R., Allerton, C. M. N., Anderson, A. S., Aschenbrenner, L., Avery, M., Berritt, S., ... & Zhu, Y. (2021). An oral SARS-CoV-2 M^pro^ inhibitor clinical candidate for the treatment of COVID-19. *Science*, *374*(6575), 1586-1593.
- Painter, W. P., Holman, W., Bush, J. A., Almazedi, F., Malik, H., Eraut, N. C. J. E., ... & Painter, G. R. (2021). Human safety, tolerability, and pharmacokinetics of molnupiravir, a novel broad-spectrum oral antiviral agent with activity against SARS-CoV-2. *Antimicrobial Agents and Chemotherapy*, *65*(5), e02428-20.
- Paixao, E. S., Teixeira, M. G., Costa, M. D. C. N., & Rodrigues, L. C. (2022). Symptomatic and asymptomatic Zika virus infection and microcephaly: Systematic review and meta-analysis. *BMC Infectious Diseases*, *22*(1), 321.
- Pang, X., Zhang, R., Cheng, G. (2017). Progress towards understanding the pathogenesis of dengue virus infection. Virologica Sinica, 32(1), 16–32. https://doi.org/10.1007/s12250-016-3930-2
- Pardi, N., Hogan, M. J., Pelc, R. S., Muramatsu, H., Andersen, H., DeMaso, C. R., ... & Weissman, D. (2018). Zika virus protection by a single low-dose nucleoside-modified mRNA vaccination. Nature, 543(7644), 248-251.
- Pearce, K. (2024). AstraZeneca withdraws COVID-19 vaccine worldwide. *BMJ*, *385*, q1192.
- Pierson, T. C., & Diamond, M. S. (2020). The continued threat of emerging flaviviruses. *Nature microbiology*, *5*(6), 796–812.
- Polack, F. P., Thomas, S. J., Kitchin, N., Absalon, J., Gurtman, A., Lockhart, S., ... & Gruber, W. C. (2020). Safety and efficacy of the BNT162b2 mRNA COVID-19 vaccine. *New England Journal of Medicine*, *383*(27), 2603-2615.

- Ponlawat, A., & Harrington, L. C. (2005). Blood feeding patterns of Aedes aegypti and Aedes albopictus. Journal of Medical Entomology, 42(5), 909–918. https://doi.org/10.1603/0022-2585(2005)042[0909:BFPOAA]2.0.CO;2
- Puelles, V. G., Lütgehetmann, M., Lindenmeyer, M. T., Sperhake, J. P., Wong, M. N., Allweiss, L., ... & Huber, T. B. (2020). Multiorgan and renal tropism of SARS-CoV-2. *New England Journal of Medicine*, *383*(6), 590-592.
- Richner, J. M., Himansu, S., Dowd, K. A., Butler, S. L., Salazar, V., Fox, J. M., ... & Diamond, M. S. (2017). Modified mRNA vaccines protect against Zika virus infection. Cell, 168(6), 1114-1125.
- Robert, M. A., Stewart-Ibarra, A. M., & Estallo, E. L. (2020). Climate change and viral emergence: Evidence from Aedes-borne arboviruses. Current Opinion in Virology, 40, 41–47. https://doi.org/10.1016/j.coviro.2020.05.001
- Rodriguez-Roche, R., & Gould, E. A. (2013). Understanding the dengue viruses and progress towards their control. Biomed Research International, 2013, 690835. https://doi.org/10.1155/2013/690835
- Rouvinski, A., Guardado-Calvo, P., Barba-Spaeth, G., Duquerroy, S., Vaney, M. C., Kikuti, C. M., ... & Rey, F. A. (2017). Recognition determinants of broadly neutralizing human antibodies against dengue viruses. Nature, 520(7545), 109-113.
- Sacramento, C. Q., de Melo, G. R., de Freitas, C. S., Rocha, N., Hoelz, L. V. B., Miranda, M., ... & Tanuri, A. (2017). The clinically approved antiviral drug sofosbuvir inhibits Zika virus replication. Scientific Reports, 7(1), 40920.
- Sánchez-Céspedes, J., Guijarro, F., Jiménez, C., & Álvarez, E. (2016). Synthesis and evaluation of novel piperazine-based antiviral agents against adenoviruses. *Bioorganic & Medicinal Chemistry Letters*, *26*(3), 912-917. https://doi.org/10.1016/j.bmcl.2015.12.028
- Schurink, B., Roos, E., Radonic, T., Barbe, E., Bouman, C. S., de Boer, H. H., ... & van den Toorn, L. M. (2020). Viral presence and immunopathology in patients with lethal COVID-19: A prospective autopsy cohort study. *The Lancet Microbe*, *1*(7), e290-e299.
- Sencanski, M., Perovic, V., & Veljkovic, N. (2022). Novel piperazine-based compounds targeting SARS-CoV-2 main protease: In silico and in vitro evaluation. *Computers in Biology and Medicine*, *141*, 105168. https://doi.org/10.1016/j.compbiomed.2021.105168
- Sheikh, A., Kerr, S., Woolhouse, M., McMenamin, J., & Robertson, C. (2022). Severity of omicron variant of concern and effectiveness of vaccine boosters against symptomatic disease in Scotland (EAVE II): A national cohort study with nested test-negative design. *The Lancet Infectious Diseases*, *22*(7), 959-966.
- Sick, F., Beer, M., Kampen, H., & Wernike, K. (2019). Culicoides Biting Midges—Underestimated Vectors for Arboviruses of Public Health and Veterinary Importance. Viruses, 11(4), 376.

- Silva-Pilipich, N., Cobo-Gaspar, T., Vanrell, L., & Smerdou, C. (2024). Self-amplifying RNA vaccines: Mode of action, design, development and optimization. *Vaccines*, *12*(1), 35.
- Sinha, S., Singh, K., Ravi Kumar, Y. S., Roy, R., Phadnis, S., Meena, V., Bhattacharyya, S., & Verma, B. (2024). Dengue virus pathogenesis and host molecular machineries. Journal of biomedical science, 31(1), 43.
- Smithburn, K. C., Hughes, T. P., Burke, A. W., & Paul, J. H. (1940). A neurotropic virus isolated from the blood of a native of Uganda. American Journal of Tropical Medicine and Hygiene, 20, 471–492.
- Soriano, J. B., Murthy, S., Marshall, J. C., Relan, P., & Diaz, J. V. (2024). A clinical case definition of post-COVID-19 condition by a Delphi consensus. *The Lancet Infectious Diseases*, *24*(4), e254-e262.
- Starr, T. N., Greaney, A. J., Hannon, W. W., Loes, A. N., Hauser, K., Dillen, J. R., Ferri, E., Farrell, A. G., Dadonaite, B., McCallum, M., Matreyek, K. A., Corti, D., Veesler, D., Snell, G., & Bloom, J. D. (2023). Shifting mutational constraints in the SARS-CoV-2 receptor-binding domain during viral evolution. Science, 377(6604), 420–424. https://doi.org/10.1126/science.abo7896
- Stevens, L. J., Pruijssers, A. J., Lee, H. W., Gordon, C. J., Tchesnokov, E. P., Gribble, J., George, A. S., Hughes, T. M., Lu, X., Li, J., Perry, J. K., Porter, D. P., Cihlar, T., Gotte, M., Denison, M. R., & Sheahan, T. P. (2022). Mutations in the SARS-CoV-2 RNA-dependent RNA polymerase confer resistance to remdesivir by distinct mechanisms. Science Translational Medicine, 14(656), eabo0718. https://doi.org/10.1126/scitranslmed.abo0718
- Szemiel, A. M., Merits, A., Orton, R. J., MacLean, O. A., Pinto, R. M., Wickenhagen, A., Lieber, G., Turnbull, M. L., Wang, S., Mair, D., Filipe, A. D. S., Willett, B. J., Wilson, S. J., Patel, A. H., Thomson, E. C., Palmarini, M., Kohl, A., & Stewart, M. E. (2021). In vitro selection of remdesivir resistance suggests evolutionary predictability of SARS-CoV-2. PLOS Pathogens, 17(9), e1009929. https://doi.org/10.1371/journal.ppat.1009929
- Tay, M. Z., Poh, C. M., Rénia, L., MacAry, P. A., & Ng, L. F. P. (2020). The trinity of COVID-19: Immunity, inflammation and intervention. *Nature Reviews Immunology*, *20*(6), 363-374.
- Taylor, P. C., Adams, A. C., Hufford, M. M., de la Torre, I., Winthrop, K., & Gottlieb, R. L. (2021). Neutralizing monoclonal antibodies for treatment of COVID-19. *Nature Reviews Immunology*, *21*(6), 382-393.
- Tchesnokov, E. P., Feng, J. Y., Porter, D. P., & Götte, M. (2020). Mechanism of inhibition of Ebola virus RNA-dependent RNA polymerase by remdesivir. Viruses, 12(11), 1337. https://doi.org/10.3390/v12111337
- Tegally, H., Wilkinson, E., Giovanetti, M., Iranzadeh, A., Fonseca, V., Giandhari, J., ... & de Oliveira, T. (2021). Detection of a SARS-CoV-2 variant of concern in South Africa. *Nature*, *592*(7854), 438-443.

- Tricou, V., Sáez-Llorens, X., Yu, D., Rivera, L., Jimeno, J., Villarreal, A. C., ... & Borkowski, A. (2024). Safety and immunogenicity of a tetravalent dengue vaccine in children aged 4-16 years: A randomised, placebo-controlled, phase 2 trial. The Lancet, 395(10234), 1423-1433.
- Tseng, H. F., Ackerson, B. K., Luo, Y., Sy, L. S., Talarico, C. A., Tian, Y., ... & Qian, L. (2023). Effectiveness of mRNA-1273 against SARS-CoV-2 omicron and delta variants. *Nature Medicine*, *29*(4), 1016-1022.
- U.S. Food and Drug Administration. (2022). *FDA updates on Evusheld* [Press release]. https://www.fda.gov
- U.S. Food and Drug Administration. (2024). *Emergency use authorization for PEMGARDA*. https://www.fda.gov
- Ullrich, S., Ekanayake, K. B., Otting, G., & Nitsche, C. (2022). Main protease mutants of SARS-CoV-2 variants remain susceptible to nirmatrelvir. Bioorganic & Medicinal Chemistry Letters, 62, 128629. https://doi.org/10.1016/j.bmcl.2022.128629
- Van Den Elsen, K., Quek, J., Schreurs, E., & Watterson, D. (2021). Flavivirus cell entry and membrane fusion. Viruses, 13(4), 537.
- Vangeel, L., Chiu, W., De Jonghe, S., Maes, P., Slechten, B., Raymenants, J., & Jochmans, D. (2021). Remdesivir, molnupiravir and nirmatrelvir remain active against SARS-CoV-2 Omicron and other variants of concern. *Antiviral Research*, *198*, 105252.
- Varasi, I., Lai, A., Fiaschi, L., Bergna, A., Gatti, A., Caimi, B., Biba, C., Della Ventura, C., Balotta, C., Riva, A., Zehender, G., Zazzi, M., & Vicenti, I. (2023). Neutralizing antibodies response to novel SARS-CoV-2 omicron sublineages in long-term care facility residents after the fourth dose of monovalent BNT162b2 COVID-19 vaccination. *The Journal of infection*, *87*(3), 270–272.
- Vicenti, I., Boccuto, A., Giannini, A., Dragoni, F., Saladini, F., & Zazzi, M. (2018). Comparative analysis of different cell systems for Zika virus (ZIKV) propagation and evaluation of anti-ZIKV compounds in vitro. Virus Research, 244, 64-70.
- Vicenti, I., Boccuto, A., Giannini, A., Dragoni, F., Saladini, F., & Zazzi, M. (2018). Comparative analysis of different cell systems for Zika virus (ZIKV) propagation and evaluation of anti-ZIKV compounds in vitro. Virus research, 244, 64–70.
- V'kovski e, A. R., Abdulle, A. E., Timens, W., Hillebrands, J. L., Navis, G. J., Gordijn, S. J., ... & van Goor, H. (2020). Angiotensin-converting enzyme 2 (ACE2), SARS-CoV-2 and the pathophysiology of coronavirus disease 2019 (COVID-19). *The Journal of Pathology*, *251*(3), 228-248.
- V'kovski, P., Kratzel, A., Steiner, S., Stalder, H., & Thiel, V. (2021). Coronavirus biology and replication: Implications for SARS-CoV-2. *Nature Reviews Microbiology*, *19*(3), 155-170.

- Wang, Q. Y., Bushell, S., Qing, M., Xu, H. Y., Bonavia, A., Nunes, S., ... & Shi, P. Y. (2009). Inhibition of dengue virus through suppression of host pyrimidine biosynthesis. Journal of Virology, 83(9), 4072-4083.
- Weaver, S. C., & Barrett, A. D. T. (2004). Transmission cycles, host range, evolution and emergence of arboviral disease. Nature Reviews Microbiology, 2(10), 789–801.
- Weaver, S. C., & Vasilakis, N. (2009). Molecular evolution of dengue viruses: Contributions of phylogenetics to understanding the history and epidemiology of the preeminent arboviral disease. Infection, Genetics and Evolution, 9(4), 523–540.
- Weaver, S. C., Costa, F., Garcia-Blanco, M. A., Ko, A. I., Ribeiro, G. S., Saade, G., ... & Vasilakis, N. (2016). Zika virus: History, emergence, biology, and prospects for control. *Antiviral Research*, *130*, 69-80.
- Wilder-Smith, A., Lindsay, S. W., Scott, T. W., Ooi, E. E., Gubler, D. J., & Das, P. (2020). The Lancet Commission on dengue and other Aedes-transmitted viral diseases. *Lancet (London, England)*, *395*(10241), 1890–1891.
- Winkler, G. (2024). Flavivirus NS3 protease: Structure, function, and implications for antiviral drug design. *Frontiers in Virology*, *3*, 145-157. https://doi.org/10.3389/fviro.2024.014515
- World Health Organization Solidarity Trial Consortium. (2022). Repurposed antiviral drugs for COVID-19—Interim WHO solidarity trial results. *New England Journal of Medicine*, *384*(6), 497-511.
- World Health Organization Technical Advisory Group on COVID-19 Vaccines. (2024). *Statement on the antigen composition of COVID-19 vaccines*. https://www.who.int
- World Health Organization. (2016). *WHO statement on the first meeting of the International Health Regulations (2005) (IHR 2005) Emergency Committee on Zika virus and observed increase in neurological disorders and neonatal malformations*. WHO.
- World Health Organization. (2020). *WHO Director-General's opening remarks at the media briefing on COVID-19 - 11 March 2020*. https://www.who.int
- World Health Organization. (2022). *Tracking SARS-CoV-2 variants*. https://www.who.int
- World Health Organization. (2024). *Clinical management of COVID-19: Living guideline*. https://www.who.int
- World Health Organization. (2024). Dengue and severe dengue – Key facts. https://www.who.int/news-room/fact-sheets/detail/dengue-and-severe-dengue
- World Health Organization. (2024). Dengue and severe dengue. WHO Fact Sheet. Retrieved from https://www.who.int/news-room/fact-sheets/detail/dengue-and-severe-dengue
- World Health Organization. (2024). *Post COVID-19 condition (Long COVID)*. https://www.who.int
- Xiao, F., Tang, M., Zheng, X., Liu, Y., Li, X., & Shan, H. (2020). Evidence for gastrointestinal infection of SARS-CoV-2. *Gastroenterology*, *158*(6), 1831-1833.

- Yan, R., Zhang, Y., Li, Y., Xia, L., Guo, Y., & Zhou, Q. (2020). Structural basis for the recognition of SARS-CoV-2 by full-length human ACE2. *Science*, *367*(6485), 1444-1448.
- Young, P. R. (2018). Arboviruses: A family on the move. In R. Hilgenfeld & S. Vasudevan (Eds.), Dengue and Zika: Control and antiviral treatment strategies (Advances in Experimental Medicine and Biology, Vol. 1062). Springer. https://doi.org/10.1007/978-981-10-8727-1_1
- Yu, X.-J., & Cheng, G. (2022). Global epidemiology and clinical burden of dengue: A review. Infectious Diseases of Poverty, 11, 95.
- Zhou, Y., Gammeltoft, K. A., Ryberg, L. A., Pham, L. V., Tjørnelund, H. D., Binderup, A., Duarte Hernandez, C. R., Fernandez-Antunez, C., Offersgaard, A., Fahnøe, U., Peters, G. H. J., Ramirez, S., & Bukh, J. (2022). Nirmatrelvir-resistant SARS-CoV-2 variants with high fitness in an infectious cell culture system. Science Advances, 8(51), eadd7197.